Thermo-chemotherapeutic effects of magnetic nanoparticles on cancer cells

A Thesis Submitted in fulfilment of the requirement for the award of the degree of

DOCTOR OF PHILOSOPHY

IN

BIOTECHNOLOGY

NEHA SRIVASTAVA

(Registration No. 901700003)

Under the supervision of

Dr Manoj Baranwal
(Professor)

Dr B N Chudasama
(Professor)

Department of Biotechnology

Thapar Institute of Engineering and Technology,

Patiala, Punjab

September, 2024

CERTIFICATE

Certified that the thesis entitled "**Thermo-chemotherapeutic effects of magnetic nanoparticles on cancer cells**", which is being submitted by Mrs. Neha Srivastava, in fulfilment of the requirement for the award of the degree of Doctor of Philosophy in Biotechnology, Thapar Institute of Engineering & Technology, Patiala, India is a record of candidate's own independent and original research work carried out by her under our supervision and guidance. The matter embodied in this thesis has not been submitted in part or full to any other University or Institute for the award of any degree.

(Dr. Manoj Baranwal)

Supervisor

Professor
Department of Biotechnology
Thapar Institute of Engineering & Technology,
Patiala-147004,
Punjab, India

(Dr. B N Chudasama)

Supervisor

Professor
School of Physics and Materials Science
Thapar Institute of Engineering &
Technology,
Patiala-147004,
Punjab, India

Place: Patiala

Date: September 30, 2024

DECLARATION

I hereby declare that the work which is being presented in this thesis "**Thermo-chemotherapeutic effects of magnetic nanoparticles on cancer cells** " submitted by me for the award of the degree of Doctor of Philosophy in the Department of Biotechnology, Thapar Institute of Engineering & Technology, Patiala, India, is true and original record of my own independent and original research work carried out under the supervision of Dr. Manoj Banarwal, Professor, Department of Biotechnology and Dr. B N Chudasama, Professor, School of Physics and Materials Science, Thapar Institute of Engineering & Technology, Patiala, India. The matter embodied in this thesis has not been submitted in part or full to any other University or Institute for the award of any degree in India or abroad.

Place: Patiala

Date: September 30, 2024

Neha Srivastava

(Neha Srivastava)

This work is dedicated to my family:

Father – Dr. Devesh Chandra Srivastava

Mother – Smt. Shashi Srivastava

Husband – Mr. Prashanth Vudanti

ACKNOWLEDGEMENT

While the acknowledgements in my thesis are a small token of appreciation, they hardly convey the deep gratitude I feel for the many individuals who have shaped my life. It is a genuine pleasure to thank all those who, in countless ways, contributed to my doctoral work and made this journey truly unforgettable.

It is with immense joy and heartfelt gratitude that I express my deepest appreciation to my supervisor, **Dr. Manoj Baranwal**, Professor in the Department of Biotechnology (DBT) at Thapar Institute of Engineering & Technology (TIET), Patiala, for his unwavering support and invaluable mentorship throughout this journey. I extend my sincere thanks and deep respect to my co-supervisor, **Dr. B.N. Chudasama**, Professor in the School of Physics and Materials Science (SPMS) at TIET, Patiala. Their profound knowledge in their respective fields and their continuous encouragement through insightful feedback have been a source of inspiration. I feel truly privileged to have been associated with them, and their guidance will forever remain a guiding light in my life.

I would like to thank the members of my Doctoral committee **Dr. N. Das, Dr. Sanjay Saxena** and **Dr. Bonamali Pal** for examining the progress reports and encouraging me to make my work better. I express my sincere thanks to **Dr. M. S. Reddy**, Head, Department of Biotechnology, TIET, Patiala, for support and encouragement.

It has been a privilege to pursue my postgraduate studies at this prestigious institution. My sincere thanks go to **Dr. Prof. Padmakumar Nair** (Director, TIET), Dr. **N. Tejo Prakash** (Dean of Research and Sponsored Projects), **Prof. Inderveer Chana** (Dean of Student Affairs), and **Dr. Prof. Maninder Singh** (Dean of Academic Affairs) for providing this exceptional opportunity.

Sincere thanks to **Dr. Manoj Baranwal**, Professor, Department of Biotechnology (DBT), Thapar Institute of Engineering & Technology (TIET), for the support in laboratory and experimental work. I am also thankful to SAIF, IIT Bombay and SAIF Punjab University for for extending characterization facilities. My gratitude also extends to **Dr. Diptiman Choudhury**, Associate Professor at the School of Chemistry and Biochemistry, Thapar Institute of Engineering & Technology (TIET), along with his lab members, **Sunidhi** and **Komal**, for their invaluable support in conducting experiments in their lab.

I would like to offer my gratitude to colleagues of Research Lab-3 and Nanomedicine Lab for their help and support in the completion of this work. I am thankful to Lab assistants (**Mr. Ram Newal, Surinder Pal, Lalan ji and Phool chand ji**) for their support.

I am deeply grateful to my seniors, **Sahil Jain** and **Purnima Sharma**, for their invaluable guidance, and I extend my heartfelt thanks to my lab mates and friend **Yogita Kautish, Neha Kaushal**, **Ajay**, **Baneet, Mamta, Yashpreet, Garima**, and **Tania** for their constant support and cheerful presence throughout this journey. Their advice has been instrumental in my achievement. A special note of thanks goes to **Pratima** for dedicating her time and support during the final submission process.

I am filled with immense joy as I thank my husband **Prashanth Vudanti**, who has always proved to be a shoulder to lean on whenever stressful situations invaded during the course of this work and his companionship will be acknowledged till the last breath. I may be short of words to pay the debt of recognition towards the person who have always been a source of strength for me, my father, **Dr. Devesh Chandra Srivastava**.

Last but not the least; I would like to pay high regards to almighty God for giving me skills, wisdom, knowledge and ability to work hard to reach where I am today. Moreover, I thank God for the blessings and support He has showered on me through my family, friends, professors and colleagues. Without His blessings and support, this thesis would have never been possible.

Neha Srivastava

(Neha Srivastava)

LIST OF PUBLICATIONS

Published

1. Srivastava, N., Baranwal, M., & Chudasama, B. (2023). Evaluation of Magnetic Hyperthermia Efficiency of PEG-Coated Fe3O4 Nanoparticles. *Nano*, *18*(12), 2350094. (SCI, IF=1.0)
2. Srivastava, N., Chudasama, B., & Baranwal, M. (2022). Advancement in magnetic hyperthermia-based tagged therapy for cancer treatment. *Biointerphases*, *18*(6). (SCI, IF=1.6)

Revision Submitted

In-vitro assessment of Polyethylene Glycol-coated iron oxide nanoparticles integrating Luteinising Hormone Releasing-Hormone targeted magnetic hyperthermia and doxorubicin for Lung and Breast cancer cells

WORKSHOP

Self-sponsored online 2nd Faculty Development Program/Short-Term Course (FDP/STC) on "Recent Advancement in Biomaterials and Nanotechnology for Biomedical Applications" at DBRA NIT Jalandhar from 28th September-2nd October 2023.

Abstract

Magnetic nanoparticle-based hyperthermia has garnered significant attention as a promising approach in cancer treatment. This study presents the synthesis and comprehensive evaluation of polyethylene glycol (PEG)-coated Fe_3O_4 nanoparticles, designed specifically for magnetic hyperthermia applications. The Fe_3O_4 nanoparticles were synthesized using the chemical coprecipitation method, followed by surface modification with PEG coating to enhance their biocompatibility and stability in biological systems. To characterize the synthesized nanoparticles, various advanced techniques were employed. X-ray powder diffraction (XRD) confirmed the crystalline structure of the Fe_3O_4 nanoparticles, revealing an inverse-spinel configuration with a crystallite size of 9.1 nm. Fourier-transform infrared spectroscopy (FTIR) further confirmed the successful coating of the nanoparticles with PEG, as evidenced by characteristic absorption bands. The magnetic properties were analysed by vibrating sample magnetometer (VSM), which indicated that both the uncoated Fe_3O_4 nanoparticles and the PEG-coated variants exhibited superparamagnetic behaviour, a key attribute for magnetic hyperthermia. The physical size of the uncoated Fe_3O_4 nanoparticles was determined using high-resolution transmission electron microscopy which showed an average size of 9.5 ± 0.12 nm. Upon PEG coating, dynamic light scattering (DLS) measurements revealed that the hydrodynamic size of the PEG-coated nanoparticles increased to 118 ± 0.25 nm from 87 ± 0.31 nm (bare Fe_3O_4), reflecting the successful addition of the PEG layer and its impact on particle size in solution.

The magnetic hyperthermia efficiency of PEG-coated Fe_3O_4 nanoparticles was systematically evaluated by varying several key parameters: magnetic field frequency (ranging from 162 to 935.6 kHz), field strength (from 5 to 12 mT), and nanoparticle concentration (between 1 to 100 mg/mL). To assess their performance, the temperature rise in an aqueous dispersion of the nanoparticles as monitored over a 20 minutes time period. This temperature increase reflects the nanoparticle's ability to generate heat when subjected to an alternating magnetic field, a critical factor for effective hyperthermia treatment in cancer therapy. The specific loss power (SLP), a measure of the nanoparticle's heat-generating capacity, was calculated by using the corrected slope method. The analysis revealed a clear relationship between the SLP values and the tested parameters. Specifically, the SLP of the PEG-coated Fe_3O_4 nanoparticles increased linearly with both the frequency and strength of the magnetic field, meaning that higher frequencies and stronger fields led to greater heat generation. Conversely, the SLP values

decreased exponentially as the concentration of nanoparticles increased, indicating that more diluted nanoparticle dispersions were more efficient at converting electromagnetic energy into heat.

The conditions for magnetic hyperthermia efficiency were identified at a magnetic field frequency of 580.8 kHz, a field strength of 10 mT, and a nanoparticle concentration of 25 mg/mL. These findings demonstrate that the synthesized PEG-coated Fe_3O_4 nanoparticles exhibit strong potential as candidates for magnetic hyperthermia-based cancer treatment. Their ability to efficiently convert electromagnetic energy into heat under optimal conditions makes them promising for use in targeted, localized hyperthermia therapy, where precise heat delivery is essential for effective tumour cell destruction without harming surrounding healthy tissue.

Magnetic nanoparticle-based hyperthermia, combined with chemotherapy, represents a promising and innovative strategy for cancer treatment. In this study, a targeted drug delivery system was developed, consisting of a doxorubicin (DOX)-loaded magnetic core, coated with polyethylene glycol (PEG), and functionalized with the targeting ligand [D-Trp6] luteinizing hormone-releasing hormone (LHRH) or Triptorelin. This system was designed to enhance the effectiveness of cancer therapy by selectively delivering DOX to cancer cells while simultaneously employing magnetic hyperthermia to further induce cell death. Fourier-transform infrared (FTIR) spectroscopy confirmed the successful conjugation of the LHRH ligand to the PEG-coated magnetite (Fe_3O_4) nanoparticles, as evidenced by characteristic peaks in the spectrum. The drug loading efficiency of the LHRH-targeted PEG-coated Fe_3O_4 nanoparticles was analysed using UV–vis spectroscopy, revealing a 66 % loading efficiency for DOX, indicating that a substantial amount of the drug was successfully incorporated into the nanoparticles.

To assess the therapeutic potential of these synthesized nanoparticles, their effects were tested on human lung cancer cells (A549) and human breast cancer cells (MCF-7) using an MTT cell viability assay. The LHRH-targeted PEG-coated Fe_3O_4 nanoparticles, loaded with DOX, were evaluated for cytotoxicity under three different treatment conditions: thermotherapy (magnetic hyperthermia), chemotherapy (DOX alone), and a combination of thermotherapy and chemotherapy (thermo-chemotherapy). In the A549 lung cancer cells, thermo-chemotherapy where both DOX and magnetic hyperthermia were applied resulted in an 88 % reduction in cell viability at the highest DOX concentration tested (10 μg/mL). This was a notable improvement over chemotherapy alone, which reduced cell viability of 62 %, and thermotherapy alone,

which caused a 47 % reduction. A similar trend was observed in MCF-7 breast cancer cells, where thermo-chemotherapy led to a 91 % reduction in cell viability at highest DOX concentration (8 μg/mL), surpassing chemotherapy (57%) and thermotherapy (45 %) when used as standalone treatments.

In addition to assessing cell viability, the study also explored the immune response generated by the treatment, specifically focusing on the production of interferon-gamma (IFN-γ), a cytokine known for its role in immune-mediated cancer cell inhibition. IFN-γ production was measured in A549 lung cancer cells using both targeted and non-targeted drug-loaded nanoparticle conjugates, with and without the application of an alternating magnetic field. The findings demonstrated that the use of targeted, DOX-loaded magnetic nanoparticles led to a significant increase in IFN-γ production, regardless of magnetic field application, compared to non-targeted nanoparticles. This suggests that the targeted delivery of DOX, coupled with the magnetic hyperthermia, not only enhances direct cell killing but may also stimulate a more robust immune response against the cancer cells.

Overall, this study highlights the potential of targeted magnetic hyperthermia approach in combination with chemotherapy to significantly enhance the effectiveness of cancer treatment. The dual action of the therapy inducing direct cancer cell death through hyperthermia while delivering cytotoxic drugs like DOX along with the stimulation of an immune response through increased IFN-γ production, provides a compelling case for the use of this strategy in treating cancers such as lung and breast cancer. By leveraging the advantages of magnetic fields to focus treatment on tumour cells and increase drug efficacy, this combined thermo-chemotherapy approach could offer a promising and more effective method for combating cancer.

TABLE OF CONTENTS

Chapter 1: Introduction ……..…….. **1 - 5**

Chapter 2: Review of Literature …… **6 - 30**

2.1 Lung Cancer ……. 6

2.2 Breast cancer ……...…. 7

2.3 Conventional cancer treatments ……...10

2.4 Hyperthermia ……... 11

2.5 Magnetic hyperthermia …….……... 13

2.6 Magnetic hyperthermia combined with conventional chemotherapy …….. 16

2.7 Drug targeting methods …… 19

a) Passive targeting
b) Active targeting

2.8 Biological targeting receptors combined with magnetic hyperthermia …… 22

2.9 Luteinizing hormone-releasing hormone (LHRH) targeted magnetic hyperthermia ……. 26

Chapter 3: Materials and Methods ……..…. 31 - 38

3.1 Materials ……..……. 31

3.2 Synthesis of Fe_3O_4 nanoparticles …….…. 31

3.3 Surface modification of Fe_3O_4 nanoparticles with PEG ……..…….. 32

3.4 Characterization of Fe_3O_4 and PEG-coated Fe_3O_4 nanoparticles ……..... 33

3.5 Materials ……..…….. 34

3.7 Drug loading into LHRH- tagged PEG-coated Fe_3O_4 …….…….. 34

3.8 Materials ……. 35

3.9 Magnetic hyperthermia measurement of PEG-coated Fe_3O_4 nanoparticles …... 35

3.10 Cell cultures (*In-vitro* analysis) …… 36

3.11 Cytokine Analysis ……. 38

3.12 Statistical analysis ……. 38

Chapter 4: Results ……..…. **39 - 63**

4.1 Drug loading ……. 48

4.2 Drug loading efficiency …… 48

4.3 Magnetic hyperthermia of PEG-coated Fe_3O_4 nanoparticles ……..... 49

4.4 Cell viability Assessment ……. 54

4.5 Morphological study ……..... 59

4.6 Cytokines Estimation …… 62

Chapter 5: Discussion ……..... **64 - 74**

Chapter 6: ……... **75 - 78**

6.1 Summary …….. 75

6.2 Scope for future work …….. 77

References ……. **79 - 101**

LIST OF FIGURES

Figure	Description	Page No.
2.1	Subtypes of lung cancer	**7**
2.2	Subtypes of breast cancer	**9**
2.3	Active and passive targeting approach	**20**
2.4	Mechanism of receptor mediated endocytosis of nanoparticle-drug conjugate to the tumour site	**22**
2.5	Luteinizing hormone-releasing hormone (LHRH) mode of action (32)	**27**
3.1	Flow diagram illustrating the synthesis protocols utilised for the preparation of Fe_3O_4	**32**
4.1	XRD pattern of as-synthesized Fe_3O_4 nanoparticles	**39**
4.2	(a) Transmission electron micrograph (b) lattice fringe image and (c) specific area electron diffraction pattern of Fe_3O_4 nanoparticles	**40**
4.3	Size distribution histogram of Fe_3O_4 nanoparticles obtained from HR-TEM micrograph	**41**
4.4	Fe_3O_4 nanoparticles dispersed in water. Histograms are fitted with log normal distribution function (Eq. 4.2)	**42**
4.5	FTIR spectra of (a) Fe_3O_4, (b) PEG-600 and (c) PEG-coated Fe_3O_4 nanoparticles measured in the spectral range of 4000 – 500 cm^{-1}	**43**
4.6	Magnetization (M) versus applied magnetic field (H) plots of (−) bare Fe_3O_4 and (−) PEG-coated Fe_3O_4 nanoparticles. Inset shows the magnified view of M-H curves in the field range of -100 Oe to + 100 Oe	**45**
4.7	Magnetization (M) versus applied magnetic field (H) data of a) Fe_3O_4 and b) PEG-coated Fe_3O_4 nanoparticles fitted with modified Langevin function [Eq. 3]	**45**

4.8	FTIR spectra of (a) bare Fe_3O_4, (b) PEG and (c) PEG-coated Fe_3O_4 (d) LHRH and (e) LHRH conjugated PEG-coated Fe_3O_4 nanoparticles. Measurement was performed in the spectral range of 4000 – 500 cm^{-1}	**47**
4.9	UV–visible absorption spectrum of aqueous solution of (a) free doxorubicin (geen color) and (b) DOX loaded LHRH tagged PEG-coated Fe_3O_4 nanoparticles (black color). The spectrum was recorded at 25 °C with HPLC grade water as reference	**49**
4.10	Temperature – time profiles of as-synthesized PEG-coated Fe_3O_4 nanoparticles measured as a function of (a) magnetic field frequency (b) magnetic field strength and (c) nanoparticle concentration	**50**
4.11	$\Delta\theta$ vs time plots of PEG-coated Fe_3O_4 nanoparticles measured as a function of (a) magnetic field frequency (b) magnetic field strength and (c) nanoparticle concentration, which are fitted with box-Lucas model (Eq. 4.5).	**51**
4.12	Effect of magnetic field frequency field strength, and nanoparticle concentration on the SLP of PEG-coated Fe_3O_4 nanoparticles	**53**
4.13	a) Cell viability of A549 cells in the absence and presence of magnetic field after treatment with different concentrations of PEG-coated Fe_3O_4. b) Cell viability of MCF-7 cells in the absence and presence of magnetic field after treatment with different concentrations of PEG-coated Fe_3O_4.. Unpaired t-tests were used for comparisons, *P<0.05, **P<0.01, ***P<0.001	**55**
4.14	a) Cell viability of A549 cells in the absence and presence of magnetic field after treatment with different concentrations of LHRH tagged PEG-coated Fe_3O_4. b) Cell viability of MCF-7cells after treatment with different concentrations of PEG-coated Fe_3O_4. Unpaired t-tests were used for comparisons, *P<0.05, **P<0.01, ***P<0.001	**56**
4.15	a) Cell viability of A549 cells in the absence of magnetic field after treatment with: free DOX, DOX loaded PEG-coated Fe_3O_4 and DOX loaded LHRH tagged PEG-coated Fe_3O_4., b) Cell viability of MCF-7 cells in the absence of magnetic field after treatment with: free DOX, DOX loaded PEG-coated Fe_3O_4 and DOX loaded LHRH tagged PEG-coated Fe_3O_4., Unpaired t-tests were used for comparisons, *P<0.05, **P<0.01, ***P<0.001	**57**

4.16 a) Cell viability of A549 cells in the presence of magnetic field after treatment with: free DOX, DOX loaded PEG-coated Fe_3O_4 and DOX loaded LHRH tagged PEG-coated Fe_3O_4., b) Cell viability of MCF-7 cells in the absence of magnetic field after treatment with: free DOX, DOX loaded PEG-coated Fe_3O_4 and DOX loaded LHRH tagged PEG-coated Fe_3O_4., Unpaired t-tests were used for comparisons, *P<0.05, **P<0.01, ***P<0.001 **58**

4.17 Cellular morphology of A549 cells under alternating magnetic field (AMF) a) untreated A549 cells. b) LHRH tagged PEG-coated Fe_3O_4 (25 µg/mL) treated A549 cells. c) DOX loaded LHRH tagged PEG-coated Fe_3O_4 (DOX concentration: 1.25 µg/mL) treated A549 cells. d) DOX loaded LHRH tagged PEG-coated Fe_3O_4 (DOX concentration: 2.5 µg/mL) treated A549 cells, e) DOX loaded LHRH tagged PEG-coated Fe_3O_4 (DOX concentration: 5 µg/mL) treated A549 cells and f) DOX loaded LHRH tagged PEG-coated Fe_3O_4 (DOX concentration: 10 µg/mL) treated a549 cells were viewed using inverted microscope. Red arrow (➔) shows cell shrinkage while black arrow (➔) pointed at the suspension of dead cells. Magnification: x40; **60**

4.18 Cellular morphology of MCF-7 cells under alternating magnetic field (AMF) a) untreated MCF-7 cells, b) LHRH tagged PEG-coated Fe_3O_4 (25 µg/mL) treated MCF-7 cells, c) DOX loaded LHRH tagged PEG-coated Fe_3O_4 (DOX concentration: 1µg/mL) treated MCF-7 cells, d) DOX loaded LHRH tagged PEG-coated Fe_3O_4 (DOX concentration: 2µg/mL) treated MCF-7 cells ,e) DOX loaded LHRH tagged PEG-coated Fe_3O_4 (DOX concentration: 4µg/mL) treated MCF-7 cells and f) DOX loaded LHRH tagged PEG-coated Fe_3O_4 (DOX concentration: 8µg/mL) treated MCF-7 cells were viewed using inverted microscope. Red arrow (➔) shows cell shrinkage while black arrow (➔) pointed at the suspension of dead cells. Magnification: x40; **61**

4.19 Secretion levels of IFN-γ in response to free DOX, DOX loaded PEG - coated Fe_3O_4 and DOX loaded LHRH tagged PEG-coated Fe_3O_4 against A549 cells a) in the absence of magnetic field and b) in the presence of magnetic field. Unpaired t-tests were used for comparisons, *P<0.05, **P<0.01, ***P<0.001 **63**

4.20 Secretion levels of IFN-γ in response to free DOX, DOX loaded PEG - coated Fe_3O_4 and DOX loaded LHRH tagged PEG-coated Fe_3O_4 against MCF-7 cells
a) in the absence of magnetic field and
b) in the presence of magnetic field. Unpaired t-tests were used for comparisons, *P<0.05, **P<0.01, ***P<0.001 **63**

LIST OF TABLES

Figure	Description	Page No.
2.1	Magnetic nanoparticles conjugates exhibiting magnetic hyperthermia in different cancer cell lines	**19**
2.2	Magnetic nanoparticles conjugated with different biological receptors used in magnetic hyperthermia against different cancer cell lines	**25**
4.1	Band interpretations of FTIR spectra of Fe_3O_4, PEG and PEG-coated Fe_3O_4 nanoparticles	**43**
4.2	Saturation magnetization (M_S), mean cluster size (D_m), polydispersity (σ), magnetic moment (μ), and susceptibility (χ) of Fe_3O_4 and PEG-coated Fe_3O_4 nanoparticles obtained by fitting M-H curve with modified Langevin function	**46**
4.3	Band interpretations of ATR-FTIR spectra of Fe_3O_4, PEG, and PEG-coated Fe_3O_4 and LHRH tagged PEG-coated Fe_3O_4 nanoparticles	**47**
4.4	Table. Fitting parameters ($\Delta\theta_s$ and k) of empirical box-Lucas model, specific loss power (SLP) and intrinsic loss power (ILP) measured as a function of magnetic field frequency, field strength, and nanoparticle concentration.	**53**

LIST OF ABBREVIATIONS

BSA	Bovine serum albumin
PEG-600	Polyethylene glycol
$FeCl_3.6H_2O$	Ferric chloride
$FeSO_4.7H_2O$	Ferrous sulphate heptahydrate
HCl	Hydrochloric acid
NaOH	Sodium hydroxide
RPMI 1640	Roswell Park Memorial Institute
D_H	Hydrodynamic particle size
DMEM	Dulbecco's modified eagle's medium
DMSO	Dimethyl sulfoxide
DOX	Doxorubicin hydrochloride
EDTA	Ethylenediamine tetraacetic acid
et al.	And others
etc.	And other things
eV	Electron volt
FBS	Fetal Bovine serum
gm	Gram
H2O2	Hydrogen peroxide
emu	Electromagnetic units
Oe	Oersted
Fe_3O_4	Magnetite
MTT	(3-(4,5-dimethylthiazol-2-yl)-2,5-diphenyltetrazolium bromide)
mV	Millivolts
OA	Oleic acid
NCCS	National Centre for Cell Culture
nm	Nanometer
OD	Optical density
EDC	1-Ethyl-3-(3-dimethylaminopropyl)carbodiimide
PBS	Phosphate buffer saline
ILP	Intrinsic loss power
TMB	3,3′,5,5′-Tetramethylbenzidine
rpm	Revolution per minute
SLP	Specific loss power

TEM	Transmission electron microscopy
WHO	World Health Organization
ELISA	Enzyme-linked immunosorbent assay
µg/mL	Microgram per milliliter
µL	Microliter
µM	Mircomolar
IFN-γ	interferon-gamma

Chapter 1

Introduction:

Cancer stands as a significant global health challenge, impacting individuals worldwide and responsible for one in every six deaths globally (1,2). In 2022, around 20 million new cancer cases were identified, and close to 9.7 million people lost their lives (3). Cancer is a multifaceted and progressive collection of illnesses characterized by the gradual loss of control over cellular growth in the body. Breast and lung cancers are prominently ranked as one of the top prevalent and life-threatening cancer types. During the year 2022, lung cancer had the highest number of new cases, with 2.5 million diagnoses, making up 12.4% of all new cancer cases. Breast cancer followed closely, with 2.3 million new cases, representing 11.6% of the total cases (4).

Lung cancer stands out as the leading contributor to cancer-related deaths worldwide, surpassing the combined mortality of pancreas, colon, and prostate cancers. A mere 15% of individuals diagnosed with lung cancer manage to survive for five years or more (5). The classification of lung cancer into small cell lung cancer and non-small cell lung cancer (NSCLC) also revealed that NSCLC comprises a significant 85% of every case. The primary approach to treating lung cancer involves multi-drug therapy, with chemotherapy being the favoured option. However, the harsh side-effects associated with chemotherapy highlight the urgency for exploring alternate treatment methods (6).

Breast cancer remains a substantial health issue in women. It is positioned as the second leading reason for death in cancer patients. It is the foremost frequently diagnosed cancer among women, representing 25% of total cancer cases. It is also the main contributor to cancer deaths, resulting into 14.7% of overall cancer deaths worldwide. With its high mortality rate, breast cancer is a pressing issue that requires greater efforts to improve its prevention, early detection, and treatment. Due to its prevalence, much attention has recently been given to its treatment. The most common breast cancer treatment currently involves surgery supplemented with radiation therapy, systemic adjuvant chemotherapy, and hormonal therapy (7).

The development of more efficient and safer anticancer drugs is crucial. Among therapeutic modalities, chemotherapy stands out as a method capable of impeding cancer cell proliferation

by targeting rapidly dividing cells. However, its impact extends beyond cancer cells, affecting various normal cell populations, including hair, hematopoietic stem cells, and those within the central nervous system and mucous membranes (8). This non-specificity leads to heightened systemic inflammation and notable side-effects, encompassing hair loss, gastrointestinal disturbances, and increased susceptibility to infections in liver, kidney, etc. (6). Consequently, it is imperative to develop efficacious and targeted cancer treatments, capable of minimizing collateral damage to normal cells while effectively combating cancer. A fundamental challenge associated with chemotherapeutic agents lies in their lack of specificity and selectivity, primarily arising from subtle metabolic disparities between tumour cells and the normal cells (9). Hence, the successful implementation of chemotherapy requires the administration of high doses of chemotherapeutic drugs. However, recent breakthroughs in cancer therapy have revolutionized cancer treatment. Substantial strides have been achieved in understanding the intricate pathways involved in cancer progression, leading to more effective ways to target them. The advancements made have opened avenues for novel strategies, such as the utilization of drugs, biomolecules, and immune-mediated therapies. These interventions are now being applied, even in situations where conventional treatments have proven insufficient in significantly reducing the mortality rates or extending the survival of individuals with metastatic cancer.

In recent time, hyperthermia has emerged and regarded as a potential alternative within the realm of cancer therapy. This therapeutic approach involves the application of heat, either localized or throughout the entire body, with the specific goal of raising temperatures to 40-45 °C within cancerous cells (10,11). Tumours, characterized by leaky vasculature, exhibit limited heat dissipation and disrupted blood flow, while healthy tissues benefit from vasodilation, facilitating enhanced blood flow and heat conduction. Hyperthermia has proven effective in eliminating cancer cells, especially within the acidic and hypoxic environment found in the cores of solid tumours. It also enhances blood flow in tumour regions. Various clinical methods are utilized for hyperthermia, including local, regional, and whole-body approaches (12,13). The key challenges impeding the clinical adoption of hyperthermia include the difficulty in consistently depositing heat into the tumour mass and the complexity of measuring temperatures in both the tumour mass and its surrounding tissues. Moreover, their efficacy in treating deep-seated tumours is limited (14). Magnetic nanoparticle-mediated hyperthermia has come to be a promising approach to overcome these challenges. Nanotechnology offers a groundbreaking platform for cancer therapy, with extensive research focused on developing

nanoparticles with therapeutic capabilities (15,16). In this domain, magnetic nanoparticles (MNPs) have garnered substantial attention over the past few years for their potential applications in cancer detection and treatment (17). In magnetic hyperthermia, cancerous tissues are targeted for destruction through elevated temperatures from magnetic energy losses. MNPs possess the ability to convert electromagnetic energy into heat, presenting the potential to eliminate tumor cells by raising their temperature to the apoptosis threshold. When exposed to temperatures beyond 42 °C, cancerous cells undergo apoptosis due to the disruption of their natural enzymatic processes (18,19). The major challenge in developing successful magnetic hyperthermia therapy is availability of magnetic nanostructures capable of regulating magnetic energy losses within the prescribed therapeutic temperature window (42-45 °C). Without suitable mechanism to control these energy losses in magnetic hyperthermia, there is a risk of unabated elevation in body temperature, which could eventually result in the detriment of healthy cells as temperature may exceed the critical threshold of 45 °C. Amongst magnetic nanomaterials iron oxide nanoparticles are suitable for this application, Nanoparticles of iron oxide represent prominent candidate for the magnetic hyperthermia therapy as they are the only magnetic nanoparticles which are authorized through the US Food and Drug Administration regarding *in vivo* use. Nevertheless, these bare iron oxide magnetic nanoparticles exhibit poor stability in biological environment (20). Hence, innovative approaches have been explored to enhance their solubility, bioavailability, and targeted delivery to the diseased site.

In addition to addressing the specificity challenges in magnetic hyperthermia, there is a growing focus on targeted approaches to improve its effectiveness in cancer treatment. The successful adoption of magnetic nanoparticles (MNPs) conjugate for drug administration systems relies on their targeted delivery to tumour tissues. The combination of magnetic hyperthermia and targeted chemotherapy exhibits a synergistic effect in cancer treatment (21). Two primary approaches, passive and active targeting, are employed for effective MNP-based drug delivery. Both approaches aim to accumulate MNPs in metastatic and highly porous tumour environment. They differ in the mechanisms of anchoring MNPs to the targeted tumour site (22).

Passive targeting depends on the difference in physicochemical properties of caner tissue and healthy tissue. When MNPs are introduced intravenously, they tend to stay in the bloodstream for a prolonged duration in contrast with the free drug. MNPs can efficiently penetrate the fenestrated structure of blood vessels found in angiogenic tissues. This results in significant concentration of the MNPs at the site of the disease, which is facilitated by slow lymphatic

system drainage. This occurrence is labelled as the enhanced permeability and retention (EPR) effect and is supported by compelling data from numerous studies on MNPs (23).

On the contrary, active targeting relies on a biological interaction between ligands upon the surface of MNPs and the target cell. Such ligands promote a uptake of targeted MNPs via receptor-mediated endocytosis, increasing its collection inside cancer cells, whereas reducing absorption through healthy tissues. (24). In recent years, targeted magnetic hyperthermia has gained attention as an adjuvant therapy to conventional cancer treatments (11,21). Previous comprehensive reviews have provided valuable insights into magnetic nanoparticle hyperthermia and drug targeting methods (25-27).

The use of active targeting ligands specific to cancer cell receptors in magnetic hyperthermia holds promise for delivering nanoparticles and / or anticancer drugs directly to the tumour site while minimizing damage to healthy cell. Combining targeted magnetic hyperthermia with conventional cancer treatments has synergistic impact on cancer treatment (11,28). By harnessing this approach, there is potential for improved outcomes, as it can selectively target and treat cancer cells while minimizing the effect on surrounding healthy tissue (10,18,21).

In this study, the ligand chosen for nanoparticle conjugation is the (LHRH) agonist, also known as Triptorelin (Pyr-His-Trp-Ser-Tyr-Gly-Leu-Arg-Pro-Gly-NH2) is a synthetic decapeptide analogs of gonadotropin-releasing hormone (GnRH) and acts as an activator of [D-Trp6] Luteinizing Hormone-Releasing Hormone (LHRH) receptors (28,29). LHRH receptors are exhibited in a variety of cancer cell types, such as breast, prostate, ovarian, endometrial, bladder, lung, and lymphoma. Notably, approximately 50% of the breast tumours, particularly those that are estrogen receptor-positive (ER+), exhibit an upregulation of LHRH receptors (30-32). This upregulation presents an opportunity for targeted therapy using LHRH analogs like Triptorelin, which can specifically bind to these overexpressed receptors. While LHRH is primarily known for its role in reproductive processes, recent evidence indicates its potential involvement in various non-reproductive tissues and cancers (29). However, there is a lack of comprehensive documentation regarding the indication of LHRH among A549 cancer cells, which are widely studied adenocarcinoma cells of the human lung. Non-small cell lung cancer (NSCLC) exhibits n upregulation of the Luteinizing hormone-releasing hormone (LHRH) (6).

This study aims to synthesize targeted magnetic drug delivery system consisting of a doxorubicin (DOX) as chemotherapeutic drug, targeting [D-Trp6] luteinizing Hormone-Releasing Hormone (LHRH) (Triptorelin) as ligand, and a PEG-coated magnetite nanoparticles as core. This targeted drug delivery platform further used to determine the cytotoxic effects of

the delivered DOX under conditions with and without an alternating magnetic field (AMF) by using MTT-based cell viability assays in LHRH-positive cancer cells (MCF-7 and A549). Additionally, interferon-gamma (IFN-γ) secretion levels using sandwich enzyme-linked immunosorbent assay (ELISA) was measured in A549 and MCF-7 to understand the effect of a targeted magnetic drug delivery system.

Chapter 2

Review of literature:

Cancer is an intricate and pervasive disease exemplified by the unchecked proliferation and spread of anomalous cells, which is a major contributing factor to the high mortality rates globally (33). It is a complex challenge that poses significant obstacles to healthcare systems and to the society at large. The hallmark of cancer encompasses a range of distinctive features, including uncontrolled cellular replication, a compromised ability to respond to growth signals leading to the cessation of cell division, persistent angiogenesis, resistance to apoptosis, and the capability to infiltrate adjacent tissues (34).

2.1 Lung cancer

Lung cancer, identified as the foremost contributor to cancer-related fatalities globally, constitutes a heterogeneous group of exceptionally aggressive malignant tumors affecting the lower respiratory tract. Recent data disseminated by the American Cancer Society underscores the profound impact of lung cancer, eclipsing the combined mortality associated with pancreatic, colorectal, prostate, and breast cancers (35). The intricate landscape of lung cancer is demarcated into two principal categories: small cell lung cancer (SCLC) and non-small cell lung cancer (NSCLC). This nomenclature of SCLC is derived from the diminutive size of its cancer cells, representing a relatively smaller fraction, approximately 10-15 %, of total lung cancer cases. In stark contrast, NSCLC dominates the lung cancer panorama, comprising a substantial 80-85 % of all instances and exhibiting a diverse composition with at least three histological subtypes—squamous cell carcinoma, adenocarcinoma, and large cell carcinoma (36,37). Squamous cell tumors predominantly manifest in the bronchi, while adenocarcinoma predominantly arises in the peripheral regions of lung tissue, encompassing the terminal bronchioles and alveoli (38,39). Conversely, large-cell carcinoma, characterized by heightened anaplasiais intricately associated with rapid metastasis, often initiating peripherally and subsequently spreading centrally within the lungs (40). The intricate classification of lung cancer subtypes underscores the complexity of the disease, requiring specialized diagnostic and treatment approaches tailored to their unique characteristics (Fig. 2.1). Estrogen has been documented as a factor that promotes the onset and development of various human cancers. A growing body of scientific data implies that the majority of human lung tumors exhibit estrogen receptor expression (41). Irrespective of gender among the different isoforms of estrogen receptors (ERα, ERβ, mERs), ERβ stands out by being highly expressed in nearly 90% of non-

small cell lung cancer (NSCLC) human tumors . In contrast, ER-α is typically low in lung cancer cells (42).

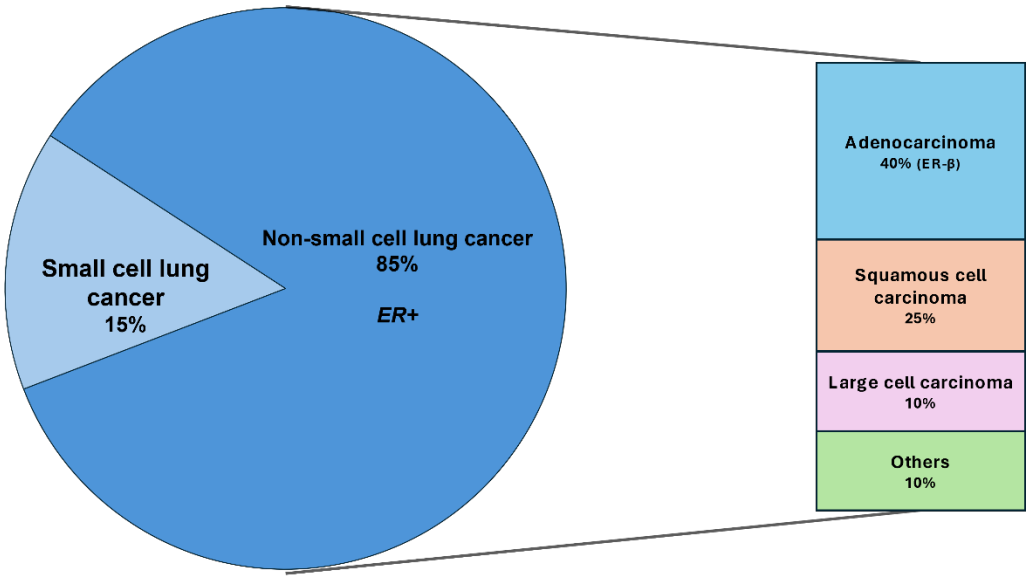

Fig 2.1: Subtypes of lung cancer

Scientific investigations have elucidated that estrogen is crucial in stimulating the proliferation of NSCLC cells and the subsequent growth of tumors. Notably, studies have shown that the application of anti-estrogen treatment strategies can yield significant benefits, leading to reductions in tumor size, growth rate, and cellular proliferation (43,44). These outcomes hold the promise of contributing to enhanced patient outcomes, representing a potential avenue for therapeutic intervention in the context of NSCLC. The association between estrogen and small cell lung cancer (SCLC) has been scarcely examined and is mostly obsolete.

2.2 Breast cancer

Breast cancer, a prevalent and highly diverse disease in women worldwide, exhibits distinct subtypes classified on the basis of immunohistochemical expression of hormone receptors (45,46). These subtypes are primarily characterized by the occurrence or non-occurrence of specific biomarkers, notably human epidermal growth factor receptor 2 (HER2) and hormone receptors (HR), which play pivotal role in the pathogenesis of malignancy. These subtypes include progesterone receptor positive (PR+), estrogen receptor-positive (ER+), triple-negative breast cancer (TNBC) and human epidermal growth factor receptor positive (HER2+), which are distinguished by the absence of ER, PR, and HER2 expression (Fig. 2.2).

The primary subtypes include Luminal A (47). This subtype is distinguished by the presence of hormone receptors (HR-positive) and the absence of overexpression of HER2 (HER2-negative). Luminal A breast cancers are characterized by a relatively low proliferation rate and are often correlated with a more positive outcome. This subtype is specifically denoted through the presence of receptor estrogen (ER) and/or progesterone (PR) (48). Hormones such as estrogen and progesterone contribute to the growth of ER and/or PR-positive cancers, and therapeutic interventions involving the reduction in these hormones have displayed efficacious in treating such type of breast cancer. Moreover, Luminal A tumors are characterized by being HER2-negative, where HER2 denotes human epidermal growth factor receptor-2—a type of protein inherent in the body that plays crucial contribution to cell proliferation and healing in healthy breast cells. A patient with a normal HER2 protein level is classified as having HER2-negative. Conversely, Luminal B Breast cancer is marked by the expression of hormone receptors (HR-positive) coupled with overexpression of HER2 (HER2-positive). This subtype exhibits a higher proliferation rate as compared to Luminal A and may require more aggressive clinical course (49-51).

Triple-negative subtype lacks expression of both hormone (HR-negative) and HER2 (HER2-negative) (52). Triple-negative breast cancer is associated with distinct molecular features and tends to be more aggressive, posing challenges in terms of targeted therapeutic options while HER2-positive subtype is defined by the overexpression of HER2, irrespective of hormone receptor status. Breast cancers classified as HER2-positive usually show increased aggressiveness, though targeted therapies such as anti-HER2 agents have proven effective in improving outcomes for patients with this subtype (45,53).

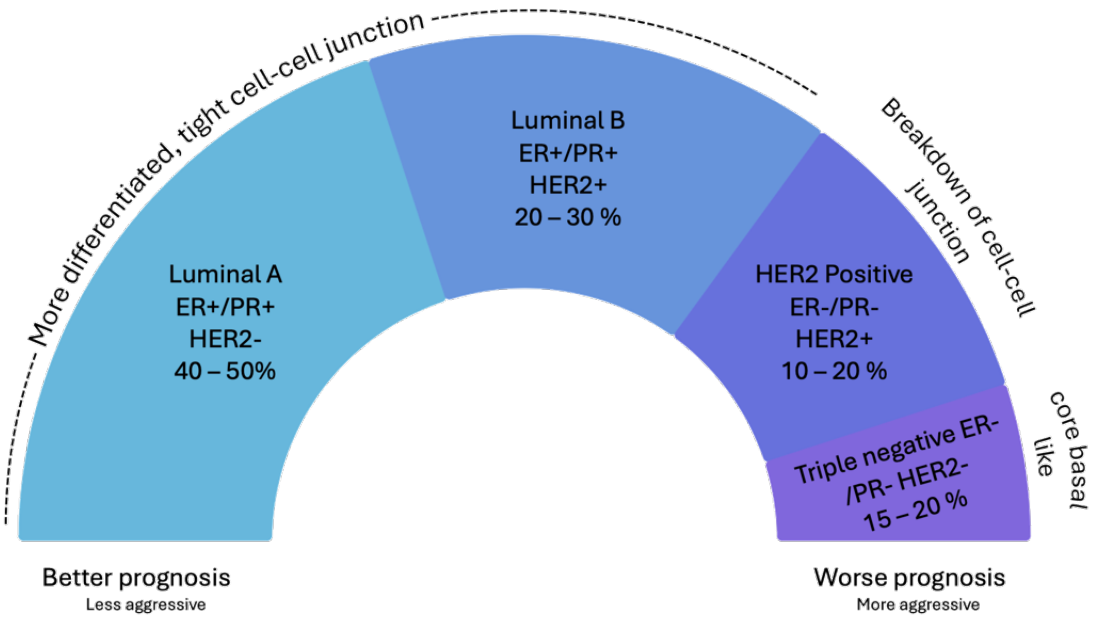

Fig 2.2: Subtypes of breast cancer

Estrogen receptor (ER) assumes a pivotal role in the diagnostic landscape, with approximately 70–75 percent of cases of invasive breast carcinomas demonstrating high ER expression (54,55). The expression Progesterone receptor (PR), observed in more than 50% of ER-positive patients, and occasionally in those exhibiting ER-negative breast cancer, is intricately regulated by ER, offering perspectives on the functional ER pathway through physiological PR values. Both ER and PR are not only abundant in breast cancer cells but also serve as critical diagnostic and prognostic biomarkers for the disease. Conversely, lower PR levels are indicative of a more aggressive course of disease, leading to poor reoccurrence and prognosis. This complex network of hormone receptor interactions underscores the intricate nature of breast cancer, emphasizing the indispensable role of ER and PR as crucial indicators for comprehending its clinical trajectory and prognostic implications (56).

In the spectrum of breast cancer subtypes, luminal A tumors stand out for having the most favorable prognosis, indicating a relatively more optimistic outlook for patients diagnosed with this specific subtype. On the other hand, luminal B, HER2-enriched, and basal subtypes are characterized by associations with poor clinical outcomes, suggesting a greater complexity and potentially more challenging treatment trajectories for individuals diagnosed with these particular categories of breast cancer. The recognition of such distinctions among breast cancer subtypes acts as a crucial position in tailoring and optimizing treatment approaches,

contributing to more informed and personalized strategies for patients based on the unique characteristics of their cancer subtype.

2.3 Conventional cancer treatments

The present array of therapeutic interventions for cancer encompasses a diverse spectrum of methodologies. Conventional treatment modalities, comprising surgical procedures, radiation therapy, and chemotherapy, are routinely employed. Additionally, a repertoire of nonconventional or complementary approaches exists, exemplified by hormone therapy, immunotherapy, nano-therapy, and other innovative strategies (57,58). While these well-established therapeutic interventions effectively target tumors, exerting inhibitory or decelerating effects on cellular growth, their efficacy falls short of conferring comprehensive protection. Current cancer treatments have limitations and side-effects that can be distressing for patients (59). As a result, there is continuous search for more effective therapies. The goal is to address the shortcomings of current treatments and improve the overall therapeutic options for those suffering from this challenging disease.

Conventional chemotherapeutic strategies fundamentally hinge on the disruption of cellular replication, a hallmark feature of neoplastic cells. This approach, however, lacks specificity, and the consequence is the indiscriminate targeting of both cancerous and healthy, rapidly dividing cells, such as those present in the bone marrow, macrophages, digestive tract, and hair follicles. The deficiency in selectivity characterizing conventional chemotherapy manifests as a key limitation, leading to an array of frequently observed adverse effects associated with chemotherapeutic agents (60).

Among the prominent challenges inherent in conventional chemotherapy is its failure to execute targeted actions exclusively within cancerous tissue. This deficiency necessitates compromises in treatment, involving dose reductions, delays, or even cessation due to the emergence of intolerable side-effects. Solid tumors pose a particular conundrum, where the quiescence of cell division in the proximity to the tumor center diminishes the responsiveness of neoplastic cells to chemotherapeutic drugs.

Further complexities arise from the inadequate penetration of these agents into the core regions of solid tumors, resulting in a suboptimal eradication of cancerous cells. Compounding these issues is the proclivity of chemotherapeutic agents to be rapidly sequestered by macrophages, culminating in swift clearance from the circulation (61). This accelerated clearance curtails the

temporal window during which these agents can interact with cancer cells, thereby substantially compromising the effectiveness of the therapy.

Additionally, the suboptimal solubility of conventional chemotherapy drugs emerges as a significant impediment, hindering their ability to traverse biological membranes effectively. This compromise in bioavailability represents a formidable challenge in achieving therapeutic concentrations at the target site, further attenuating the overall efficacy of conventional chemotherapy (62). In the pursuit of more precise and efficacious cancer therapies, these multifaceted challenges underscore the imperative for advancements in therapeutic modalities that can surmount the limitations inherent in traditional chemotherapeutic approach.

Doxorubicin (DOX) is a widely used anthracycline antibiotic and a key player in chemotherapy for various human cancers. Despite its effectiveness, particularly in treating breast cancer, its clinical application is hampered by two main challenges: the imposition of strict maximum dosage limits and the frequent development of resistance to treatment. The mechanism by which DOX operates involves its interaction with DNA through intercalation and the inhibition of macromolecular biosynthesis. This leads to the triggering of apoptotic pathways, ultimately resulting in the death of cancer cells. However, despite its therapeutic benefits, DOX is noted for its side effects, which can be severe and cumulative over time (63).

2.4 Hyperthermia

Compared to the well-organized vascular network in healthy tissues, tumour vasculature is chaotically arranged, lacking smooth muscle control and often hypoxic. Mild hyperthermia (37 °C – 42 °C) promotes local vasodilation in tumours, increasing oxygen delivery and mitigating inflammation. Above 42 °C, this chaotic nature becomes a liability. Heat directly damages tumour vasculature, increasing permeability leading to the fluid build-up, further compromising perfusion. Simultaneously, heat activates mechanisms for direct tumour cell death, inhibiting growth and proliferation (64,65,28). Additionally, exceeding 37 °C disrupts tumour cell membrane fluidity, impacting essential functions like movement and signalling, hindering metastasis potential. This multi-pronged approach makes hyperthermia a promising strategy for tumour vulnerabilities with direct anti-tumour effects and improved oxygenation, highlighting its potential for future cancer treatment advancement.

Numerous researchers have gravitated towards investigating the integration of hyperthermia with other therapeutic modalities. However, temperature and heating duration are pivotal factors in hyperthermia therapy (28). Therefore, it is imperative to implement real-time

temperature control for the optimized treatment. Different clinical techniques are used for hyperthermia, such as local, regional, as well as whole-body methods.

Local hyperthermia is suitable for solid tumours and employs external or intraluminal modalities to elevate temperatures in superficial or deep-seated subcutaneous tumours, like those in the rectum or esophagus. Thermal ablation, involving extremely high temperatures, results in irreversible damage to cells. Heat sources such as radio waves, microwaves, ultrasound are utilized in hyperthermia (66,67). Regional hyperthermia uses heat to large sections, such as organs, limbs, or hollow body spaces, often combined with chemotherapy or radiation therapy. Techniques like regional perfusion, continuous hyperthermic peritoneal perfusion, and hyperthermic intraperitoneal chemotherapy (HIPEC) have been explored. In perfusion methods, blood is temporarily extracted, externally heated, and then reintroduced to elevate internal temperature. HIPEC, on the other hand, administers heated chemotherapy drugs directly into the peritoneal cavity during surgery to cure peritoneum cancer (67-69). Whole-body hyperthermia (WBH) entails raising the overall body temperature and can synergize with chemotherapy or radiation therapy in treating metastatic cancers. Whole-body hyperthermia can be achieved by using hot water bath or radiant heat. Traditional hyperthermia treatments with laser or microwave applicators may cause invasive damage to superficial tissues and discomfort during therapy. Nevertheless, mainstream medicine has historically overlooked this cancer therapy.

Landon et al. (70) demonstrated that hyperthermia at 43 °C acts synergistically with cisplatin (cPt) in bladder cancer cells, leading to enhanced cPt uptake and increased cytotoxicity. This underscores the potential of hyperthermia to augment cisplatin-based chemotherapy, particularly in regional applications like HIPEC or HIVEC. Furthermore, Choi et al. (71) observed hyperthermia-induced apoptosis in retinoblastoma cells, suggesting its therapeutic potential in combination with carboplatin for human retinoblastoma treatment. Additionally, Zhang et al. (72) elucidated the synergistic promotion of apoptosis in prostate cancer cells through therapy combining hyperthermia and cisplatin.

Chae et al. (73) investigated the synergy between systemic doxorubicin and pulsed high-intensity, focused ultrasound-induced mild hyperthermia (HIFU-HT) *in vitro* and *in vivo*. They found that at 42 °C, HIFU-HT enhanced nuclear penetration of doxorubicin compared to 37 °C, leading to increased cytotoxicity over time. Moreover, the combined treatment exhibited superior inhibition of squamous cancer cell growth *in vivo*. Their study aimed to enhance

systemic doxorubicin efficacy using HIFU-induced hyperthermia, focusing on intranuclear doxorubicin uptake in squamous cell carcinoma (SCC)-7 cells. Tang et al. (74) showed that increasing the heating rate maximizes hyperthermia's enhancing effect on chemotherapy. The study employed two hyperthermia techniques, specifically rapid heating through a near-infrared laser and gradual heating via a cell culture incubator, to prompt cellular necrosis and apoptosis, correspondingly. The results demonstrated that the concurrent administration of doxorubicin and hyperthermia effectively overcame multidrug resistance in a uterine cancer cell line. These findings suggest that combining chemotherapy with hyperthermia might signify a promising process for curing of drug-resistant cancers. The integration of hyperthermia alongside chemotherapy is prevalent during clinical settings and has continued to be extensively evaluated in the context of soft tissue sarcoma (STS). The EORTC 62961 phase-III trial examined the effect of incorporating regional hyperthermia into chemotherapy regimens to assess its influence on local tumor control after macroscopically complete resection of high-risk abdominal or retroperitoneal sarcomas (75). Results partly suggest the efficacy of combining hyperthermia with other therapies According to Klimanov et al. (76), adding regional moderate hyperthermia to chemotherapy may have the ability to improve outcomes for treating patients with breast cancer and multiple liver metastases. Although hyperthermia is broadly adopted in clinical practice, there are significant challenges in accurately targeting the treatment area, achieving precise temperatures, and optimizing treatment methods, which require further exploration.

2.5 Magnetic hyperthermia

Magnetic hyperthermia utilizes elevated temperatures produced by MNPs to eliminate cancerous tissues. MNPs can convert electromagnetic energy transmuted into heat, presenting the power to eradicate tumour cells by heating them to their apoptosis threshold (77). This technique relies on the pertaining to the use of an alternating magnetic field (AMF) to induce heat generation through the rotation of magnetic vectors or physical rotation of the NPs themselves. Once the magnetic field ceases, MNPs accumulated passively within the tumour are cleared by the body, minimizing their long-term presence (78). Compared to conventional thermal therapies, magnetic hyperthermia offers superior safety by causing minimal heating of healthy tissues, reducing side-effects through targeted action, and enabling precise temperature control within tumour. Further, advancements promise even better targeted heating at the molecular level, potentially revolutionizing cancer treatment with remarkable precision and

minimal collateral damage. In essence, magnetic hyperthermia offers a safe, non-invasive, and highly effective approach to eradicate tumours, making it a promising treatment of cancer.

The concept of magnetic hyperthermia was initially discovered by Gilchrist et al. in 1957, who injected magnetic iron oxide nanoparticles (ranging from 20 to 100 nm in size) into lymphatic channels to heat cancer cells under an AMF (79). By subjecting the NPs to high-frequency magnetic field, magnetic energy is dissipated as thermal energy through mechanisms such as hysteresis loss and relaxation processes. Hysteresis loss occurs mainly in multi-domain NPs, where the movement of domain walls leads to the heat loss. In single domain MNPs, heat loss is predominantly caused by relaxation mechanisms, namely, Neel and Brownian relaxations (80-82).

The heating potential of MNPs is often measured as watts per gram (W/g). Specific loss power (SLP), stated as specific absorption rate (SAR), stands for the heating efficiency, which is the power converted into heat per unit mass of MNPs per unit time. SLP measures the hyperthermic response of the MNPs, considering factors like the amplitude and frequency of the applied external field. The heat production is influenced by various characteristics of MNPs, including size, shape, composition, surface functionalization, saturation magnetization, magnetic susceptibility, and magnetic anisotropy. Size and shape particularly affect the magnetic anisotropy, which defines the maximum achievable SAR. Increasing magnetization or magnetic anisotropy and modifying the nanoparticle shape can enhance the relative heating efficiency (83-86).

The desired temperature range for magnetic hyperthermia typically falls between 42 and 44 °C. Tumour cells, being hypoxic, are generally more sensitive to heat within this range compared to healthy cells (87. The use of nanoparticles in magnetic hyperthermia must fulfil two main requirements: (i) they should possess enough heating capacity, and (ii) they should possess good stability that prevents the aggregation of nanoparticles (88). Among various nanoparticles, Iron oxide nanoparticles (IONPs) are extensively studied as heat mediators in magnetic hyperthermia applications because of their ease of synthesis, self-heating under applied an alternating magnetic field, tenable magnetic properties, and good biocompatibility. Additionally, IONPs are authorised through the United States Food and Drug Administration intended for human *in vivo* studies (20,82,89).

Among various synthesis processes, the coprecipitation method is broadly adopted aimed at synthesizing iron oxide nanoparticles due to its simplicity, mild reaction conditions, and

feasibility for easy scale-up. This technique involves simultaneous precipitation of ferric (Fe^{3+}) and ferrous ions (Fe^{2+}) under basic conditions (90). To maintain colloidal stability, nanoparticles are coated with suitable biocompatible surfactants (91). Surface functionalization of MNPs is significant in their biological applications. It ensures stability of their physicochemical properties in different mediums, accounting for factors such as pH changes, hydrophobicity/hydrophilicity, etc. Modifying the surface of MNPs is essential to prevent their engulfment by phagocytic immune cells like macrophages and neutrophils. Therefore, surface reconstruction is necessary to minimize nanoparticle agglomeration in cellular environment. Surface modification of IONPs can be achieved with polymers such as dextran, chitosan, alginate, polyethylene glycol (PEG), polyvinyl alcohol (PVA), polydopamine (PDA), polysaccharides, polyethyleneimine, polyvinylpyrrolidone (PVP), polyacid polyetherimide, polyamidoamine (PAMAM), oleic acid (OA), etc. Among these, PEG is widely used due to its good biocompatibility in magnetic hyperthermia applications (92).

In phospholipid–PEG-coated Fe_3O_4 nanoparticles and in oleic acid (OA)-coated Fe_3O_4 nanoparticles, a temperature rise up to 42 °C at low-nanoparticle concentration was reported (93). In an alternative study, superparamagnetic IONPs coated with phospholipid–PEG were loaded with doxorubicin (94). These nanoparticles generate adequate heat to increase the local temperature up to 43 °C, which was adequate kill HeLa cells. Belyanina et al. (95) reported that for magnetic hyperthermia, IONPs should be superparamagnetic and should form stable dispersion in physiological media. Sudame et al. (96) and Vassallo et al. (97) highlighted that enhanced colloidal stability of magnetic nanoparticles leads to the better hyperthermic response. In one of the studies, researchers reported that magnetic hyperthermia-mediated heating efficacy varied with different surface coatings such as glutamic acid, citric acid, PEG, polyvinylpyrrolidone, ethylene diamine and cetyl-trimethyl ammonium bromide on Fe_3O_4 nanoparticles at fixed frequency (316 kHz) and field strength (450 Oe) (98). In another study, Pluronic-coated Fe_3O_4 nanoparticles showed hyperthermic response against HeLa cancer cells by applying an AC magnetic field of 4.0–20 kA/m at 210 kHz frequency (99).

According to Maity et al. (100), the viability of cells using *in vitro* analysis on human breast cancer cells (MCF-7) confirmed the cytocompatibility of triethylene glycol-coated magnetite NPs and demonstrated their efficient cellular uptake and impressive magnetic hyperthermia performance.

Studies reported that retinoblastoma cells (Y79) display heightened susceptibility to thermal damage, consistent with the sensitivity observed in other cancer cells. The magnetic hyperthermia, utilizing dextran-coated iron NPs, selectively eradicates retinoblastoma cells in a manner contingent on dosage and duration in-vitro, while preserving nontumor cells. This process induces apoptotic cell death in Y79 cells predominantly via the intrinsic pathway activated by TNF-α signalling (109). Given recent advancements in intravitreal chemotherapeutic injections for retinoblastoma management, magnetic hyperthermia employing dextran-coated iron oxide NPs presents a promising therapeutic avenue. In most of these studies, the hyperthermic response of nanoparticles was measured at certain magnetic field strength, field frequency, or nanoparticle concentration. Since the hyperthermic response of nanoparticles strongly depends on these parameters, they need to be optimized for optimal performance of magnetic nanoparticles in magnetic hyperthermia therapy.

2.6 Magnetic hyperthermia combined with conventional chemotherapy

The field of nanotechnology has emerged as a prospective basis for advancing cancer therapy (102-106). Numerous studies have centered on the development of nanoparticles (NPs) with therapeutic capabilities, and magnetic nanoparticles (MNPs) have particularly garnered attention for their potential in cancer detection and treatment. Researchers have explored the encapsulation of DOX within nanocarriers to address these issues and minimize the adverse effects on patients. This approach allows targeted drug delivery specifically to cancerous tissues while reducing its dispersion in healthy tissues. Among various nanocarriers investigated, superparamagnetic iron oxide nanoparticles (SPIONs), particularly those composed of Fe_3O_4, have emerged as promising candidates. These nanoparticles possess biocompatibility, and unique superparamagnetic characteristics, making them attractive for magnetic hyperthermia (107,108). Overall, the development of magnetic nanocarrier-based delivery systems offers a possible solution to boost the treatment efficacy of chemotherapeutic drugs like DOX while minimizing its adverse effects, thereby improving the overall outcome of cancer treatment. Simultaneous application of magnetic hyperthermia and chemotherapy holds promising approach in anticancer therapy (11). Various magnetic nanoparticle conjugates have been utilized in magnetic hyperthermia to effectively deliver chemotherapeutic drugs to cancer site (Table 2.1). In a study conducted by Christopher et al. (93), phospholipid-polyethylene glycol-coated superparamagnetic IONPs were designed to deliver doxorubicin

(DOX) to cancer tumours. Notably, these MNPs acted as dual-functionality platforms, serving as both drug carriers and heat generators when exposed to AMF. Through *in-vitro* analysis, it was found that the combined impact of DOX and magnetic hyperthermia had a profound effect on inducing cell death.

Another innovative approach involved development of multifunctional polymeric micelles that encapsulated SPIONs and the chemotherapeutic drug DOX, with drug release triggered by a pH-dependent mechanism (109) One advantage of multifunctional NPs is that the encapsulation of DOX and SPIONs within the hydrophobic micelle cores can prevent potential exposure of hydrophobic SPION surfaces and the adsorption of blood proteins, thus reducing nonspecific absorption by the reticuloendothelial system. In this context, polypyrrole-coated IONPs facilitated the delivery of DOX to tumour cells when an AMF was applied (110). This magnetic core-shell nanocomposite served as vehicle for magnetic hyperthermia-mediated chemotherapy. Biocompatible superparamagnetic porous sub-micron vaterite particles exhibited high drug loading capacity and demonstrated anticancer activities in murine colon carcinoma (CT26) and murine fibroblast (NIH3T3) cell lines upon exposure to an AMF (111).

In another study, PEG-PCL (poly (ethylene glycol)-b-poly(ε-caprolactone)) conjugated cobalt- and manganese-doped IONPs, were inhibit the growth of subcutaneous ovarian tumour in nude mice (112). A magneto-thermally responsive nanocarrier / DOX was used as a thermo-chemotherapeutic strategy for liver cancer (Huh-7) (113). In this study, through magnetic targeting, drug can be effectively concentrated at the tumour site, resulting in enhanced uptake and retention by Huh-7 cells. They exhibited notable magnetothermal effects both *in vitro* and *in vivo*. One of the studies highlights the effectiveness of magnetic targeting in concentrating nanocarriers precisely at the tumour site. This localization is facilitated by the utilization of AMF, which not only heats the targeted area but also enables controlled release of the therapeutic drug. By employing this approach, Wust et al (2006), successfully achieved the spatial-temporal synchrony of thermo-chemotherapy (114). In another study, researchers utilized a dual targeting strategy, combining AMF with an external magnetic field, to efficiently transport MNPs across the blood-brain barrier for therapeutic delivery (115). Pluronic-glycine-coated Fe_3O_4 MNPs conjugates exhibited targeted cytotoxicity and anti-cancer activity in breast cancer cells (MCF7 and MDAMB231) when tagged with cinnamaldehyde. The response to radiofrequency waves for magnetic hyperthermia therapy demonstrated dose-dependent cell killing (116). Coating MNPs with dendrimer macromolecules offers a promising alternative as it prevents aggregation and provides multiple surface functionalities. The degradation products

of PAMAM exhibit significant toxicity, limiting their use in biological systems. To address this, peptide-coated dendrimer-based MNPs have been employed, displaying good potency for drug release. The effectiveness of the DOX-loaded PAMAM-based NPs was assessed using HeLa cells. The synergistic effects of the DOX-loaded formulations in combination with AMF were also evaluated to assess their potential for combinatorial therapy against HeLa cells (117). Prior studies have shown that combining cisplatin with ferucarbotran (resovist)/AMF-induced hyperthermia boosts cisplatin's anticancer effects without changing the cell cycle, offering potential for oral cancer treatment (OSC-19 and HSC-3). This combination, already used clinically, has potential for early application, allowing reduced cisplatin dosage and minimizing side-effects (118). The application of PEG modification on mesoporous $MgFe_2O_4$ magnetic nanoassemblies (MMNs) enhances their resistance to plasma protein adsorption, ensuring prolonged blood circulation. These MMNs exhibit exceptional colloidal stability in phosphate buffer saline and minimal cell-killing effect in mouse fibroblast (L929) and cervical cancer (HeLa) cells (119). Moreover, in-vitro studies confirm their potential as a versatile nanosystem for transfer of drug and magnetic hyperthermia.

Table 2.1 Magnetic nanoparticles conjugates exhibiting magnetic hyperthermia in different cancer cell lines.

Magnetic nanoparticle conjugates	Chemotherapeutic drug	Cancer cell lines	References
Phospholipid-polyethylene glycol-coated superparamagnetic iron oxide nanoparticles	Doxorubicin	*Human cervical cancer cells*	93
Polypyrrole-coated iron oxide nanoparticles	Doxorubicin	*Human hepatocellular liver carcinoma cell*	110
Superparamagnetic porous sub-micron vaterite particles	Doxorubicin	*Murine colon carcinoma & Murine fibroblast*	111
Cobalt- and manganese-doped iron oxide nanoparticles		*Human ovarian carcinoma*	112
Manganese-and zinc-doped ferrites	Doxorubicin	*Human liver cancer cells*	113
Pluronic glycine coated magnetic nanoparticles	Cinnamaldehyde	*Human breast cancer cells*	116
Polyamidoamine based nanoparticles	Doxorubicin	*Human cervical cancer cells*	117
Ferucarbotran	Cisplastin	*Human oral cancer cells*	118
Mesosporous magnetic nanoassembilies	Doxorubicin	*Mouse fibroblast & cervical cancer cells*	119

2.7 Drug targeting methods

The successful application of MNPs conjugates as drug delivery systems relies on their targeted delivery to tumour sites (120,121) The combination of magnetic hyperthermia and targeted chemotherapy exhibits a synergistic effect in cancer treatment. Two primary approaches, namely, passive and active targeting, are employed for effective MNP-based drug delivery. Both approaches aim to accumulate MNPs in metastatic and highly porous areas of the tumour, but they differ in strategies of anchoring the MNPs at the tumour site.

a) Passive targeting

Passive targeting, relies on the features of the nanoconjugates (e.g., size, circulation time, etc.) and the leaky vasculature of the tumour, which is a result of poor alignment of endothelial cells and defective lymphatic drainage in the hypoxic tumour environment. This process, named the effect known as enhanced permeability and retention (EPR), allows for easier retention of nanoparticle conjugates in tumour cells (121). However, passive targeting is limited by the size constraints of tumour fenestrations, which can lead to unstable transport of MNP conjugates in the bloodstream (Fig. 2.3). Additionally, not all types of tumours exhibit the same level of EPR effect. Active targeting serves as a supportive approach to passive targeting by enhancing the targeting capability of MNPs and increasing their retention at the tumour site (122). Hydrophilic groups on the surface of MNPs enhance their time of circulation and prevent acceptance by the mononuclear phagocyte system (10).

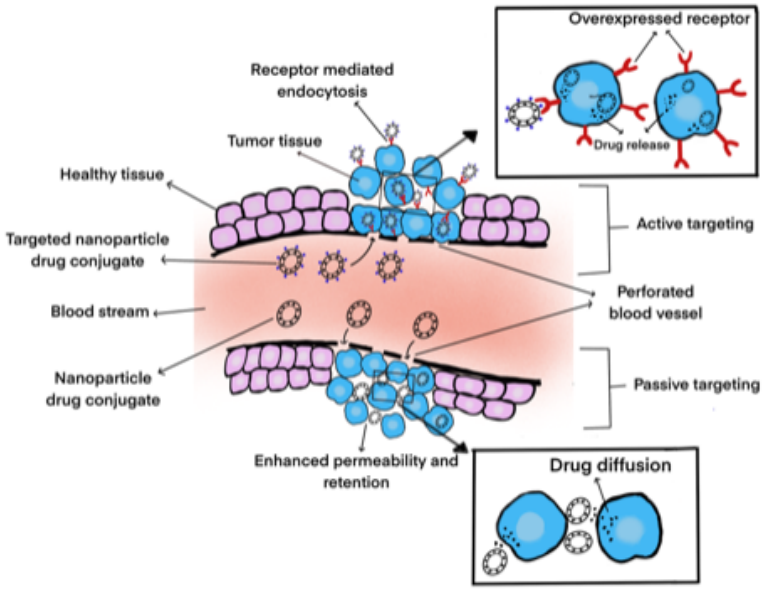

Fig 2.3: Active and passive targeting approach

b) Active targeting

Active targeting of MNPs, in conjunction with hyperthermia under an AMF, offers a highly selective delivery of drugs to tumour sites through firm adhesion across the surface of nanoparticle and specific target structures in the region of tumour. Active targeting takes

advantage of the fact that tumour cells overexpress certain biological receptors on their surface compared to the healthy cells. By conjugating MNPs with targeting ligands such as peptides, antibodies, or small organic molecules, active targeting facilitates the delivery of therapeutic agents (10,120). These targeting ligands exhibit higher affinity toward cell surface antigens (receptors) that are overexpressed on cancer cells. The interaction between the targeting ligand and tumour biomarkers, either through ligand receptor or antigen-antibody interactions (Fig. 2.4), guides the MNP conjugates to the tumour sites while avoiding nonspecific accumulation of the delivering agents at the healthy tissues. These two targeting approaches differ in process of MNP retention at the tumour site. Compared to the passive approach, active targeting achieves a higher accumulation of MNP-conjugated drug at the tumour site through target-specific binding and internalization in specific cells. This lowers the unnecessary systemic exposure of cytotoxic drugs to the healthy cells, thus improving the therapeutic outcome. Active targeting operates through receptor-mediated endocytosis, enabling the binding between ligands on the surface of nanoparticle-drug conjugates and receptors that are overexpressed on the tumour cells. This binding interaction facilitates the internalization of MNPs at the tumour site (123). The binding of ligands to receptors triggers receptor activation and subsequent internalization of the ligand-receptor complex within a vesicle, which is illustrated in Fig.4. This vesicle then undergoes fusion with an endosome and subsequently with a lysosome. Within the lysosome, acidic enzymes with a pH range of 4.0–6.0 promote enzymatic degradation, releasing the drug-conjugated nanoparticle at the tumour site.

The magnetic nanoparticles based hyperthermia by means of active targeting offers the distinct benefit of selectively accumulating within the tumour cells, facilitated by a strong binding affinity across the nanoparticle surface and specific target structures on the tumour. This process resembles hyperthermia by means of passive targeting, wherein the magnetic material accumulates primarily in the tumour's interstitial space surrounding highly vascularized regions. Consequently, retention of nanoparticle at the tumour site is influenced by the drainage of lymphatic system and target-affinity binding and internalization within particular cells. The active targeting mechanism is expected to result in proportionally higher nanoparticle levels within target cells than passive targeting methods (124).

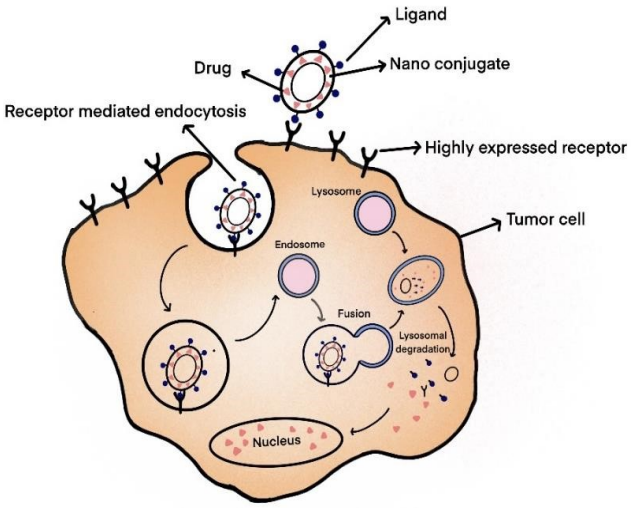

Fig 2.4: Mechanism of receptor mediated endocytosis of nanoparticle-drug conjugate to the tumour site

2.8 Biological targeting receptors combined with magnetic hyperthermia

Numerous receptors have been identified, and their corresponding ligands have been synthesized and studied extensively both *in-vitro* and *in-vivo*. These receptors have the capacity to facilitate active targeting due to their potent ligand/receptor binding properties. Table 2.2 presents list of different biological receptors that have been conjugated with MNPs to increase the potency of cancer therapy when used in conjunction with magnetic hyperthermia.

RGD can be used as targeting ligand for integrin αvβ3, which is a marker of tumour angiogenesis (125). Targeted PEG-functionalized Mn-Zn ferrite NPs have improved retention at the tumour site and have been used in MRI contrast imaging for diagnostic purposes. These targeted nanocrystals exhibit high heating potential and can induce apoptosis in tumour cells. Targeting integrins represents a promising strategy for selectively killing cancer cells. By conjugating PLGA-coated SPIONs with RGD and the drug paclitaxel (PTX), a potential targeting strategy for delivering PTX to the GBM site can be achieved in the presence of a magnetic field (126).

Cancer stem cells (CSCs) in tumours like head and neck squamous cell carcinoma are targeted using hyaluronic acid (HA) coated superparamagnetic iron oxide nanoparticles (SPIONs). These HA-PEG-coated SPIONs, when showing to an alternating magnetic field (AMF), destroy CSCs through hyperthermia, inhibiting tumour growth significantly in mice models (127). Similarly, CD20-targeted silica-coated Fe_3O_4 nanoparticles (CD20-HSPI & Fe_3O_4@SiNPs) deliver a heat shock protein inhibitor to lung CSCs under AMF, showcasing

effective targeted drug delivery (128,129). Moreover, nanoparticles targeting CD133-expressing CSCs enhance chemotherapy and hyperthermia efficacy in colorectal cancer, demonstrating superior anticancer effects in both lab and animal studies (130).

Human epithelial growth factor receptor 2(HER2) targeting has been central to various cancer treatments. Trastuzumab (Herceptin), an FDA-approved monoclonal antibody, inhibits cancer cell proliferation by binding to HER2 receptors. Conjugating trastuzumab with Au- Fe_3O_4 nanoconjugates selectively targets HER2-positive gastric cancer cells, facilitating oxaliplatin delivery with reduced side-effects (131). Similarly, trastuzumab-based therapy delivers holmium (III) doped IONP conjugates to HER2-positive breast cancer cells for magnetic hyperthermia applications (132). Additionally, HER2 antibody serves as a targeting ligand with dextranspermine MNPs, inducing magnetic hyperthermia-mediated cytotoxicity in breast cancer cells. A novel nanocarrier system combining HER2 with fluorescent IONPs and encapsulating gemcitabine shows promise for pancreatic cancer treatment, regulating apoptosis and the cell cycle both in-vitro and in-vivo. This multifunctional tactic holds potential as targeted therapeutic strategy for pancreatic cancer (133).

A combined approach of active targeting and chemo-hyperthermia delivers temozolomide (TMZ) to glioblastoma (GBM) sites under an alternating magnetic field (AMF). Magnetite nanoparticles conjugated with folic acid (FA) achieve this, boasting a high SAR of 530 W/g, ideal for magnetic hyperthermia. This method precisely delivers TMZ to GBM sites, enhancing treatment efficacy while minimizing side-effects (134). Another study develops a multifunctional drug delivery system incorporating DOX and folate onto alginate coated Fe_3O_4 nanoprticles. Folate enhances tumour cell targeting and retention, leading to improved survival outcomes in mice with lung cancer, particularly when the folate ligand is present (135).

In a recent study, researchers targeted the overexpressed folate receptor (FR) and transferrin receptor (TfR) in MCF-7 and glial cells (G1). Their findings strongly support the effectiveness of combining curcumin and 5-fluorouracil (5FU) within PLGA nanoparticles, resulting in improved uptake, increased cellular accumulation, and enhanced cytotoxicity against cancer cells. Furthermore, they investigated the potential of magnetic hyperthermia therapy, which demonstrated remarkable efficacy in rapidly destroying cancer cells and inducing enhanced apoptosis. This synergistic effect was achieved by combining MNPs with the dual-drug therapy of curcumin and 5FU (136).

In other research studies, scientists have introduced a novel method for overcoming the blood-brain tumour barrier (BBTB) by modulating its permeability using redox-responsive

nanocarriers delivering fingolimod. Fingolimod regulates blood-brain barrier integrity and was encapsulated within polymeric nanocarriers. These carriers were surface-conjugated with Plerixafor (AMD3100) for recognizing CXCR4, a chemokine receptor highly expressed on tumour vessels and cells. The resulting nanocomplexes demonstrated efficient modulation of BBTB permeability. Additionally, codelivery of ZnCoFe nanocrystals and an HSP70 inhibitor, post-BBTB modulation, achieved synergistic treatment, utilizing magnetic hyperthermia effects as a result of an alternating current magnetic field at the glioblastoma site (GL261 and U87) (137).

In cancer, the upregulation of vascular endothelial growth factor (VEGF) is due to expression of oncogene, several growth factors, and, oxygen deprivation making it a central mediator of tumour-related angiogenesis (138). VEGF, a homo- dimeric glycoprotein, plays a crucial role in angiogenesis, binding to VEGF receptor-1 and VEGF receptor-2 on vascular endothelial cells. Scientists have developed core-shell Zn^{2+} doped Zn-$CoFe_2O_4$@Zn-$MnFe_2O_4$ SPIONs (ZCMF) with precise magnetic hyperthermia properties. When modified with the VEGF antibody, these NPs exhibited enhanced uptake by liver cancer (HepG2) cells. Mild magnetic hyperthermia with MNPs effectively inhibited HepG2 cell growth by suppressing key proteins and activating innate immunity. In mouse models, targeted mild hyperthermia not only halted tumour growth but also prolonged survival, indicating its potential as a safe and promising treatment for liver cancer in the future (139). Additionally, another study has shown that modifying NPs with a VEGFR-2-targeting peptide enhances their specificity for endometriosis. In mouse experiments, these targeted MNPs efficiently accumulate in endometriotic lesions after a low-dose intravenous injection. When exposed to external AMF, they selectively elevate the temperature within lesions above 50 °C, completely eradicating them in a single treatment. (140).

Table 2.2 Magnetic nanoparticles conjugated with different biological receptors used in magnetic hyperthermia against different cancer cell lines

Magnetic nanoparticle conjugates	**Receptor/antigen**	***Cancer cell lines***	**References**
Superparamagnetic iron Oxide nanoparticles	CD44	*Human and neck squamous cell carcinoma*	126
Mn-Zn ferrite nanoparticles	Integrin	*RAW264.7 macrophage cells, Murine mammary carcinoma cells & Human umbilical vein endothelial cell*	127
Heat Shock Protein Inhibitor-loaded Silica-coated Fe_3O_4 nanoparticles	CD20	*Lung cancer stem cells*	128,129
Magnetite based nanoparticles	CD133	*Colorectal cancer cells*	130
Holmium (III)doped Iron oxide nanoparticles	Human epithelial growth factor receptor 2	*Breast cancer cells*	132
Magnetite nanoparticles	Folate receptor	*Glioblastoma cells*	134
Alginate coated magnetite nanoparticles	Folate receptor	*Lung cancer cells*	135
(PLGA)-coated Superparamagnetic Iron Oxide Nanoparticles	Folate receptor, transferrin receptor	*Breast and glial cancer cells*	136
ZnCoFe nanocrystal	CXCR4	*Glioblastoma cells*	137
Zn^{+2}doped Superparamagnetic Iron Oxide Nanoparticles	Vascular endothelial growth factor	*Liver cancer cells*	139
Polyethylene glycol coated magnetic nanoparticles	Luteinizing hormone-releasing hormone	*Ovarian cancer cells*	157
Chitosan-poly (methyl vinyl ether maleic acid) magnetic nanoparticles	Luteinizing hormone-releasing hormone	*Breast Cancer cells*	160

2.9 Luteinizing hormone-releasing hormone (LHRH) targeted magnetic hyperthermia

Incorporating targeting ligands into the design of drug-encapsulated nanoparticles offers a sophisticated means of directing these nanoparticles to specific cells or even subcellular locations. By precisely guiding the delivery of therapeutic agents to their intended targets, this strategy mitigates the risk of unintended systemic exposure to cytotoxic drugs. Consequently, including targeting ligands enhances the therapeutic efficacy of drug-loaded nanoparticles while minimizing off-target effects, thereby improving the safety and precision of drug delivery systems.

The receptor known as Luteinizing hormone-releasing hormone (LHRH) also indicated as gonadotropin-releasing hormone (GnRH), plays a crucial role in regulating reproductive functions. It is a peptide hormone having ten amino acids linked together by a peptide bond. LHRH is released by the hypothalamic neurons, exerting profound effects on endocrine regulation and reproductive functions. Operating in a pulsatile manner, LHRH is released from the median eminence into the portal vein system, subsequently reaching the anterior pituitary gland. Upon arrival, it stimulates the secretion of two key gonadotropin hormones: follicle-stimulating hormone (FSH) and luteinizing hormone (LH). These hormones are vital in gametogenesis and steroid production, thus influencing fertility and reproductive health (Fig. 2.5). Notably, the secretion of LHRH is intricately regulated by gonadal steroids, which bind to specific receptors displayed on hypothalamic neuronal cells within the pituitary gland (32). This intricate feedback mechanism ensures precise control over reproductive processes and hormonal balance within the body. Overexpression of LHRH receptor has been observed in cancers that are hormone-dependent, such as breast, endometrial, ovarian, as well as prostate cancer (141-144). Additionally, its overexpression has been detected in hormone-independent cancers such as pancreatic, lung, melanoma, and glioblastoma (145-148). LHRH agonists were initially incorporated into cancer treatment regimens targeting sensitive cancers for endocrine, such as prostate and premenopausal breast cancers. Over time, they have become indispensable elements in the armamentarium of endocrine therapies, serving as essential components in managing both early-stage and advanced cancers.

LHRH agonists, decapeptides such as goserelin, triptorelin, buserelin, and leuprolide share a alike structure to natural GnRH and exhibit high affinity for GnRH receptors. One effective targeting approach involves the utilization of the peptide Triptorelin. This 10-amino acid peptide, structurally resembling to a protein, serves as an analogs to the hormone GnRH. Notably, it exhibits high specificity towards cancers characterized by the overexpression of the

GnRH receptor (149). Consequently, the avidity of human breast cancer cells for Triptorelin makes it a valuable tool for targeting these cells. Triptorelin functions as GnRH receptor agonist with the sequence pGlu-His-Trp-Ser-Tyr-D-Trp-Leu-Arg-Pro-Gly-NH2. The peptide contains an arginine at position 8 (Arg8), which is crucial for its binding to the mammalian receptor (150).

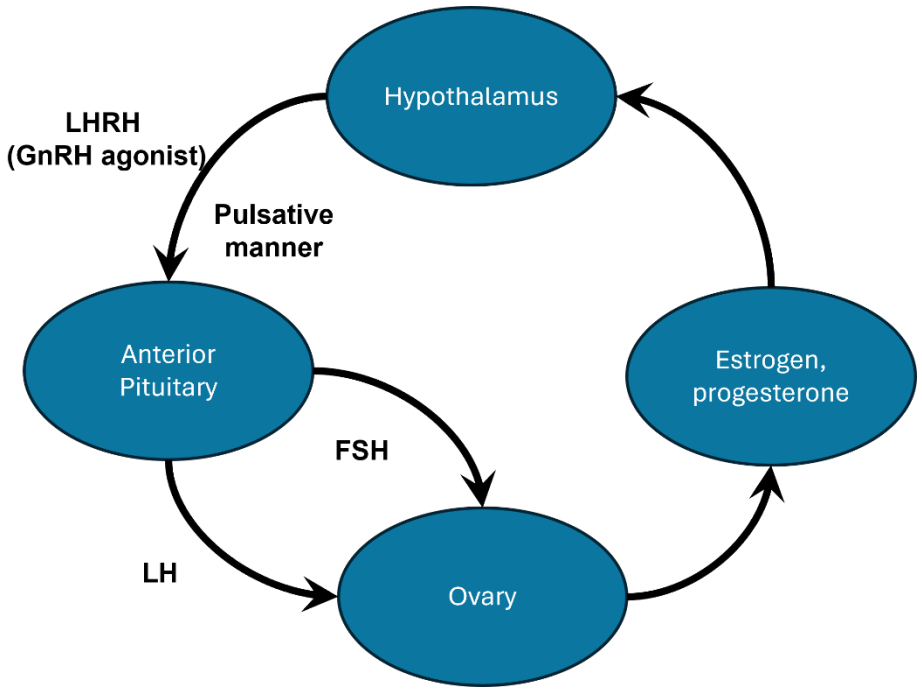

Fig 2.5: Luteinizing hormone-releasing hormone (LHRH) mode of action (32)

Triptorelin, classified as a gonadotropin-releasing hormone agonist, has obtained approval within the European Union for its use as an adjuvant endocrine therapy. The initial clinical evidence highlighting the effectiveness of triptorelin was observed in the context of monotherapy for treating endocrine-sensitive metastatic breast cancer (151,152). Seeking to achieve more potent suppression of estrogen, researchers explored the combination of triptorelin with formestane, which belongs to the first generation of aromatase inhibitors. These investigations revealed promising results, demonstrating the feasibility of this treatment approach and its ability to suppress estradiol levels effectively (153). Specifically, it is employed in conjunction with Tamoxifen to address endocrine-responsive, early-stage breast cancer. This combination therapy represents a significant advancement in the handling of breast cancer, offering patients a comprehensive treatment approach that targets hormone-sensitive tumours. This therapeutic approach involves blocking the action of estrogen in estrogen receptor-positive (ER+) breast cancer cells or inhibiting estrogen production in affected

patients. The efficacy and benefits of incorporating triptorelin as adjuvant therapy have been rigorously investigated through randomized, open-label, phase III clinical trials. These trials aim to comprehensively assess Triptorelin's impact on patient outcomes, including its ability to improve survival rates, reduce the risk of cancer recurrence, and enhance overall quality of life (154,155). The above-mentioned research sheds light on the potential of combining triptorelin with other agents to optimize estrogen suppression in the management of breast cancer, offering new avenues for enhancing therapeutic outcomes.

Few findings have discovered the application of LHRH-targeted nanoparticles in cancer treatment, yielding significant findings. For instance, researchers synthesized an LHRH-targeted PEGylated PLGA nanoparticle system to encapsulate and transport the docetaxel and Quercetin drugs specifically to the site of prostate cancer (156,157). Previous studies have also proposed the development of LHRH-targeted DOX-loaded mesoporous silica nanoparticles for the treatment of lung cancer, with encouraging experimental results confirming the drug delivery system's effectiveness in treating non-small cell lung carcinoma (158).

Drug-loaded LHRH-functionalized polyethylene glycol (PEG)-coated magnetic nano systems exhibit a high SAR value of 271 W/g, indicating their efficacy in magnetic hyperthermia treatment (159). The utilization of synthesized nanocarrier based on IONPs proved to be a highly efficient vehicle for delivering DOX to A2780/AD multidrug resistant ovarian cancer cells. Furthermore, this nanocarrier demonstrated the remarkable capability to remotely induce mild hyperthermia (40 °C) in ovarian cancer cells when exposed to AMF. This synergistic effect of mild hyperthermia, generated by IONPs in response to the AMF, significantly enhanced the cytotoxicity of DOX delivered by the nanocarrier to the cancer cells. Accordingly, the developed IONP-based delivery system exhibits immense potential for effectively treating the ovarian cancer through a combinatorial approach.

The use of LHRH-targeted DOX-loaded NPs coupled with a magnetic field yielded the most significant inhibitory effect on cell growth, particularly in MCF-7 cells. These findings highlighted the promising possibility of the layer-by-layer NPs [chitosan-poly (methyl vinyl ether maleic acid) (PMVMA)], which were designed to specifically aim LHRH receptors. By utilizing a magnetic field to guide the MNPs, they achieved dual tumor targeting in MCF-7 cells. This innovative approach has important implications as it could potentially lead to a decline the required dosage of DOX, thereby minimizing the adverse side-effects associated with the drug (160).

Many researchers have also used magnetic hyperthermia in conjunction with other conventional therapies and have shown that combination therapy has a better outcome. While numerous preclinical studies have been conducted, only a limited number successfully progress to the pivotal third and final phase of clinical trials (161). The world's first magnetic nanoparticle-based therapy, known as NanoTherm® therapy, has undergone extensive preclinical studies for the treatment of GBM and prostate cancer in Europe (MagForce Nanotechnologies AG, Berlin, Germany). Recently, clinical phase 2a has been completed to assess the efficacy of magnetic hyperthermia therapy individually or together with radiation therapy. The NoCanTher project has reached an important milestone as it has commenced the final clinical trials for the advanced pancreatic ductal adenocarcinoma treatment (162,163). These trials signify a significant step forward in evaluating the effectiveness of the proposed treatment approach and bring hope for improved outcomes in patients with this challenging condition. Magnetic hyperthermia has a significant impact on the tumour immune microenvironment, which can be leveraged for immunotherapy. Immunotherapy reactivates the immune system to resist and remove tumour cells, offering promising results. Unlike conventional methods, immunotherapy uses cytokines, chemokines, and immune cells to reshape the tumour microenvironment, ensuring powerful effects and reducing the risk of recurrence (164). In a recent study, researchers explored the potential of using OVA (ovalbumin) combined with iron oxide nanoparticles as a candidate for delivering vaccines. They examined how this nanoparticle-based delivery system impacted the expression of pro-inflammatory cytokines such as TNF-α, IFN-γ, and IL-6 in DC2.4 murine dendritic cells and RAW264.7 macrophage cells, and its effect on inhibiting tumour growth in mice. The findings suggest that this approach holds significant promise as a versatile platform for developing cancer vaccines (165). In another study using mouse models of cancer, scientists investigated the use of magnetic nanoparticles coated with dimercaptosuccinic acid (DMSA) in delivering the anti-tumorigenic cytokine IFN-γ to the tumour site by employing an external magnetic field. The nanoparticles demonstrated efficient accumulation at the tumour site and successful delivery of IFN-γ, leading to increased infiltration of immune cells and exhibiting anti-angiogenic effects (166). In a research study, scientists explored the impact of oral administration of garlic-derived nanoparticles (GNPs) on the expansion and activation of Gamma-delta (γδ) T cells in mice with B16 tumours. GNPs promoted the growth and induction of γδ T cells in the intestine, resulting in increased production of interferon-γ (IFN-γ). This transfer of γδ T cells and IFN-γ from the intestine to tumours changed the tumour's immune environment and triggered strong antitumor immunity in mice (167).

Gaps in the study

The synthesis of functionalized iron oxide nanoparticles, which are both biocompatible and capable of exhibiting a hyperthermic response, remains a significant challenge. There is a need to expedite research in the development of active targeting ligands, such as triptorelin, to elevate the targeted drug administration to specific cancer sites. To achieve optimal magnetic hyperthermia performance, it is essential to determine the most effective magnetic field strength, frequency, and nanoparticle concentration. However, previous studies have predominantly focused on using either higher field strength or longer exposure time, leaving room for further exploration and optimization. The existing literature on cytokine profiling of conjugated magnetic nanoparticles on different cancer cell lines is currently limited and inconclusive. Additional investigation is essential to provide a comprehensive insight of the potential impact and effectiveness of these nanoparticles. In order to meet this, the subsequent objectives have been outlined for this project.

Objectives

1. Preparation and characterization of functionalized magnetic nanoparticles (MNPs)
2. Conjugation of functionalized MNPs with Luteinizing Hormone-Releasing Hormone and anticancer drug Doxorubicin
3. To study the hyperthermic effect of conjugated MNPs on growth and cytokine release of cancer cells

Chapter 3

Materials and Methods:

Objective 1: Preparation and characterization of functionalized magnetic nanoparticles (MNPs)

Magnetic nanoparticles (MNPs) were synthesized by chemical process. The nanoparticle system proposed for the current investigation is iron oxide. From literature survey, it has been found that the magnetic properties of the synthesis of iron oxide nanoparticles through the co-precipitation method is affected by factors such as reaction temperature, pH of the suspension, and initial molar concentration.Synthesized magnetic nanoparticles were further functionalized with biocompatible and thermo responsive polymeric shell (PEG). Synthesized MNPs were characterized by various physical, chemical and microscopic techniques such as X-ray diffraction, Fourier-transform infrared spectroscopy, vibrating sample magnetometer, dynamic light scattering and transmission electron microscopy.

3.1 Materials

Ferric chloride ($FeCl_3.6H_2O$) (97%), ferrous sulphate heptahydrate ($FeSO_4.7H_2O$) (99%), polyethylene glycol (PEG-600) and sodium hydroxide (NaOH) were purchased from Sigma-Aldrich and hydrochloric acid (HCl), from Loba Chemicals Pvt. Ltd. All aqueous solutions were prepared in Milli-Q ultrapure water (ρ = 18.2 MΩ).

3.2 Synthesis of Fe_3O_4 nanoparticles

The coprecipitation reduction is the method to synthesize Fe_3O_4 nanoparticles (168,169). A stoichiometric solution of iron (II) sulphate heptahydrate (5 mM) and Iron (III) chloride hexahydrate (10 mM) were prepared in *3 neck* round-bottom *flask.* The pH of the solution was set to < 1.5 with diluted HCl. To this, aqueous solution of sodium hydroxide (80 mM) was added under continuous mechanical stirring at 60 °C. Addition of sodium hydroxide converts metal salts (Fe^{2+}/Fe^{3+}) into their hydroxides. The pH of the solution was held at 11. Following continuous stirring for 20 minutes at 60 °C, metal hydroxides get converted into oxides and black precipitates of Fe_3O_4 were formed. Fe_3O_4 nanoparticles were extracted from the aqueous medium by magnetic decantation. Prepared Mixture was then undergoing several washes with warm distilled water to get rid of water soluble impurities. After wash, water-wet slurry of

nanoparticles were split evenly into two portions. One portion was subject to acetone wash followed by oven drying overnight at 50 °C. Dried Fe_3O_4 nanoparticles were grinded with mortal-pestle into fine powder and stored at room temperature for further studies (Fig. 3.1).

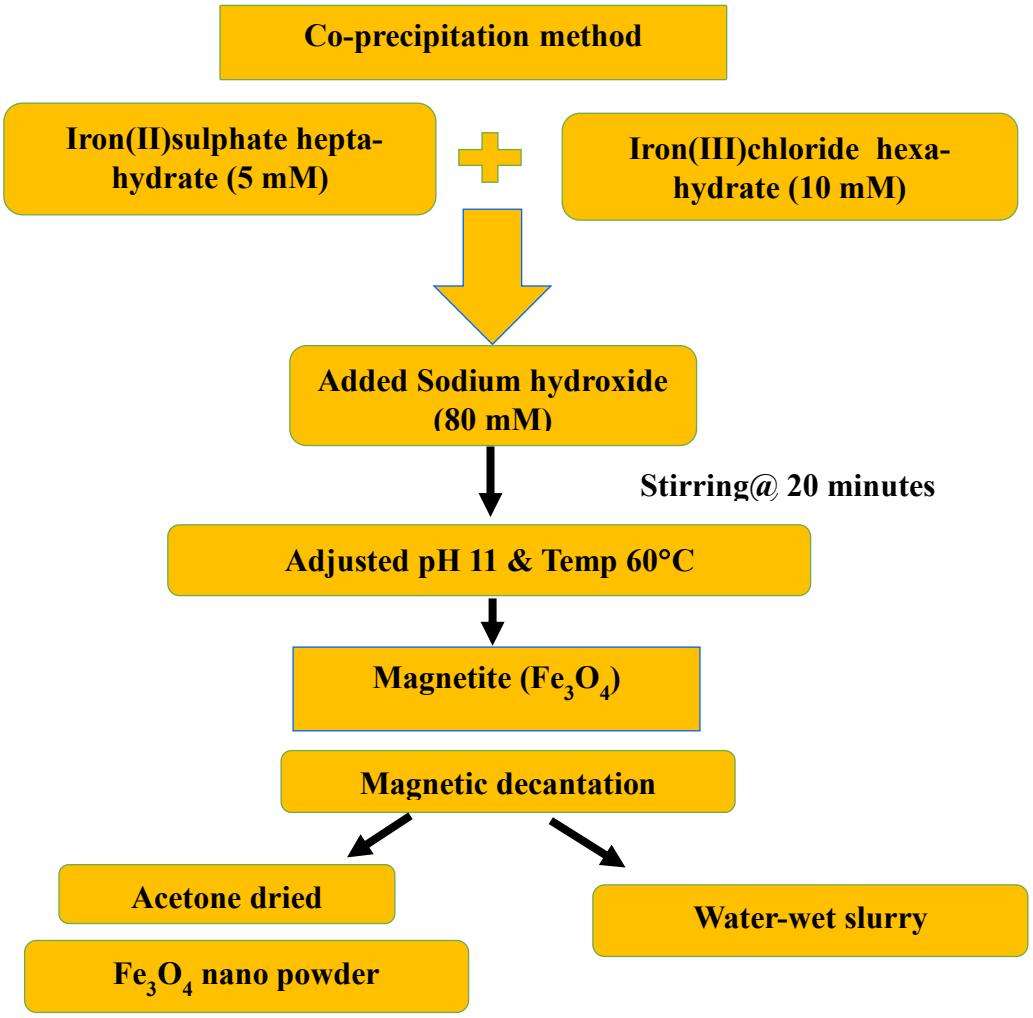

Fig 3.1: Flow diagram illustrating the synthesis protocols utilised for the preparation of Fe_3O_4

3.3 Surface modification of Fe_3O_4 nanoparticles with PEG

Second portion of water wet slurry of as-synthesized Fe_3O_4 nanoparticles were used for PEG coating. To prepare PEG-coated Fe_3O_4 magnetic nanoparticles water wet slurry of Fe_3O_4 nanoparticles was stirred and heated at 60 °C followed by addition of PEG solution. PEG to Fe_3O_4 weight ratio was optimised as 20:100. After that the solution was maintained at pH 11

and stirring was continued for another 30 minutes. PEG-coated Fe_3O_4 nanoparticles were extracted from the medium by magnetic decantation. In order to remove any free PEG and other water-soluble impurities, PEG-coated Fe_3O_4 nanoparticles were subjected to multiple washes with warm distilled water. (170). PEG-coated Fe_3O_4 nanoparticles thus obtained were allowed to remain at room temperature for future analysis.

3.4 Characterization of Fe_3O_4 and PEG-coated Fe_3O_4 nanoparticles

X-ray diffraction pattern of as-synthesized Fe_3O_4 nanoparticles was recorded on PANalytical X'Pert Pro powder X-ray diffractometer ran at 45 kV and 40 mA by means of monochromatic CuKα radiation (λ = 1.54056 nm). To assess the structure of as-synthesized Fe_3O_4 nanoparticles, High-resolution transmission electron micrograph (HR-TEM) images were recorded on JEOL (model JEM 2100F) transmission electron microscope worked at 200 kV. Functionalization of magnetite nanoparticles with PEG was verified by Fourier transform infrared spectroscopy (FTIR). FTIR spectra of bare and PEG-coated Fe_3O_4 nanoparticles were captured on Spectrum GX (Perkin Elmer) single beam spectrophotometer. The readings were undertaken in 4,000 – 400 cm^{-1} spectrum range analysed through the KBr pellet method for Fe_3O_4 nanoparticles, while for PEG-coated Fe_3O_4 nanoparticles, the measurement was carried out in the spectral range of 4,000–500 cm^{-1} with an ATR attachment. Hydrodynamic size and polydispersity index of bare and PEG-coated Fe_3O_4 nanoparticles were measured by photon correlation spectroscopy. The Dimensions were executed on Brookhaven 90 plus particle size analyser at 25 °C. Magnetization measurements of bare and PEG-coated Fe_3O_4 nanoparticles were executed on LakeShore 7404 vibrating sample magnetometer (VSM) at 25 °C. M-H loops were captured across the field range of -10 kOe to + 10 kOe.

Objective 2: Conjugation of functionalized MNPs with Luteinizing Hormone-Releasing Hormone and anticancer drug Doxorubicin

PEG-coated iron oxide nanoparticles were further tagged with cancer specific biomarker Triptorelin as a ligand to luteinizing Hormone-Releasing Hormone (LHRH) receptor. LHRH is over-expressed by most of the cancer cells including breast and lung cancer cells. The presence of ligands on these core shell nanostructures will provide them the active targeting capabilities and transport of anti-cancer drugs specifically doxorubicin to the target site.

3.5 Materials

Doxorubicin hydrochloride (DOX) was acquired from Khandelwal Ltd in India. Triptorelin as the LHRH ligand (Pyr-His-Trp-Ser-Tyr-Gly-Leu-Arg-Pro-Gly-NH_2) was purchased from **Geno Biosciences Pvt. Ltd.** 1-Ethyl-3-(3-dimethylaminopropyl)carbodiimide (EDC) was sourced from Himedia. Sterilized Milli-Q ultrapure water (R = 18.2 MΩ) was used to prepare all aqueous solutions.

3.6 Conjugation of luteinizing Hormone-Releasing Hormone ligand on synthesized PEG-coated Fe_3O_4 nanoparticles

In the present study, the LHRH ligand [D-Trp6] was conjugated to the synthesized PEG-coated iron oxide nanoparticle by carbodiimide reduction reaction (171). Here, 25 mg/mL of synthesized PEG-coated iron oxide nanoparticles were taken from stock (100 mg/mL) and redispersed in water by sonication for 10 minutes. The carbodiimide solution (30 mg in 1 mL of water) was promptly added before sonication. The mixture was subsequently cooled to 4 °C before the addition of a solution containing LHRH (3 mg in 1 mL of water). The reaction was sustained at 4 °C for 2 hours, with occasional swirling of the conical flask. Functionalized nanostructures are extruded from the reaction medium of magnetic decantation.

3.7 Drug loading into LHRH- tagged PEG-coated Fe_3O_4

To evaluate the drug loading into LHRH tagged PEG-MNPs, doxorubicin (DOX) acted as a chemotherapeutic drug. In this research, DOX was solubilized in Milli-Q water at a concentration of 2 mg/mL. 30 mg LHRH tagged PEG-MNP were combined with doxorubicin solution and stirred in a rotary shaker (200 rpm) overnight at 26 °C in dark. Afterward, the mixture was separated using a permanent magnet and concentration of free DOX was determined by optical density measurement of supernatant at 486 nm (168,172). After that magnetic nanoparticles were redispersed in Milli-Q water. The drug loading (%) was evaluated by the following equation:

$$\text{Drug loading } (\%) = \frac{(W1-W2)}{W1} X100 \quad (3.1)$$

where, W1 represents total weight of drug and W2 represents weight of free drug in supernatant.

Objective 3: To study the hyperthermic effect of conjugated MNPs on growth and cytokine release of cancer cells

The magnetic heating effect of nanoparticle conjugates was determined through magnetic hyperthermia study by using the nanoTherics magneTherm hyperthermia setup. The outcome of targeted chemotherapy and magnetic hyperthermia on the overall efficiency of the magnetic nanoparticle conjugates was assessed on human cancer cell lines A549 and MCF-7 by MTT (3-4,5 dimethylthiazolyl-2-2-5, diphenyltetrazolium) based calorimetric assay. This cell viability assay was used to measure the cytotoxicity of MNPs and MNPs loaded drug. All the *in-vitro* experiments were performed in a biological safety cabinet maintained at 37 °C. The supernatant collected from conjugates treated with human cancer cells MCF-7 and A549 were used for the analysis of IFN- cytokines. The cytokines release in the culture supernatant was assessed by sandwich ELISA (Enzyme linked immunosorbent assay) in 96-well plate as specified by the manufacture.

3.8 Materials

Dulbecco's modified eagle's medium (DMEM), RPMI (Roswell Park Memorial Institute) 1640 medium, 2.5 µg/mL amphotericin B (antifungal), antibiotic solution 100X (100 IU/mL penicillin and 100 µg/mL streptomycin), fetal bovine serum (FBS), phosphate buffer saline (PBS 1X), trypsin-EDTA and 2, 5- diphenyltetrazoliumbromide (MTT) salt, and trypan blue were purchased from Himedia. Dimethyl sulfoxide (DMSO) was supplied by Sigma-Aldrich. All liquid solutions were made using sterilized Milli-Q ultrapure water (R = 18.2 MΩ). 96-well ELISA plate (Nunc MaxiSorp®) purchased from Essence Life Sciences, Human IFN-γ Mini 3,3′,5,5′-Tetramethylbenzidine (TMB) ELISA Development Kit from PeproTech USA, TMB as the Liquid Substrate Solution obtained from KPL, Tween 20 was purchased from sigma, and Phosphate saline (PBS) was purchased from Himedia,Tecan Infinite microplate reader was applied to measure the cell viability by MTT assay.

3.9 Magnetic hyperthermia measurement of PEG-coated Fe_3O_4 nanoparticles

Heating capacity of PEG-coated Fe_3O_4 nanoparticles were determined by magnetic hyperthermia study. For this purpose, temperature-time profiles of PEG-coated Fe_3O_4 nanoparticles were conducted on nanoTherics magneTherm hyperthermia setup. 1.0 mL aqueous solution of PEG-coated Fe_3O_4 nanoparticles was added into the test vial and heating

profiles were recorded under variable magnetic field frequencies (162-935.6 kHz), field strength (5 mT, 10 mT and 12 mT) and nanoparticle concentrations (1− 100 mg/mL) (170). Three channel optical Fiber thermometers were used to measure the temperature rise in the colloidal solution of PEG-coated Fe_3O_4 nanoparticles.

3.10 Cell cultures (*In-vitro* analysis)

Human lung adenocarcinoma cells A549 and Human breast cancer cells MCF-7 were acquired from National Centre for Cell Culture (NCCS), Pune, India. The MCF-7 cells were cultured in DMEM growth medium, while the A549 cells were cultured in RPMI 1640 growth media. Both growth media were added with 10 % fetal bovine serum, 2.5 µg/mL amphotericin, and 1 % antibiotic solution (containing 100 IU/mL penicillin and 100 µg/mL streptomycin). The cells were kept in a cell culture incubator at 37 °C with 5% CO2. Once they reached 80-90% confluence, the cells were rinsed with 1X phosphate-buffered saline (PBS) and subsequently trypsinized. Appropriate cell density suspensions were prepared following cell counting. Cells were counted with the help of a hemocytometer utilizing trypan blue exclusion procedure. Briefly, 10 µL of cell sample was integrated with 10 µL 0.4% Trypan Blue solution and the final volume was raised to 100 µL with the help of complete media. From this preparation, 25 µL was dispensed onto the hemocytometer and was examined right away under a microscope (Nikon Eclipse E100-LED) at 40X magnification. Unstained viable cells were enumerated in all four corner squares. The viable cell count in the original cell suspension was determined using the following formula (173):

$$\text{Number of viable}\,\frac{\text{cells}}{\text{mL}} = \frac{\text{Number of unstained cells x } 10^4 \text{ x dilution factor}}{4} \qquad (3.2)$$

where dilution factor = 10 and number of unstained cells = total cells present in four corner squares.

For *in-vitro* cell viability experiments, 1×10^6 exponentially growing cancer cells were taken in 2 mL sterile Eppendorf vials for each conjugate and centrifuged at 1500 rpm for 5 minutes to obtain a cell pellet. Then, the cells were resuspended in a 1 mL complete DMEM media and treated with different conjugates which were PEG-coated Fe_3O_4 , LHRH tagged PEG-coated Fe_3O_4, DOX loaded PEG-coated Fe_3O_4 and DOX loaded LHRH tagged PEG-coated Fe_3O_4..The concentrations used for the first and second conjugates were 5, 10, 20 and 25 mg/mL, while those for the third and fourth conjugates PEG-coated Fe_3O_4 and LHRH tagged

PEG-coated Fe_3O_4 conjugates were kept at a constant concentration of 25 mg/mL while DOX concentration was varied between (1.25 to 10 µg/mL for A549 cells and 1 to 8 µg/mL for MCF-7 cells) and Untreated cells were used as control. Experiments were performed both in the absence and occurrence of alternating magnetic field.

For *in-vitro* magnetic hyperthermia study, the respective vials were subjected AMF at a frequency of 580.8 kHz and a field strength of 10 mT. The thermal rise of the cell suspension was checked using the optical fibre-based temperature probe for 20 minutes.

After AMF exposure, cells were centrifuged and resuspended in fresh media and seeded in 96 well plates at a cell density of 1×10^4 per well followed by incubation in a 5 % CO_2 incubator, for 24 hours. Finally, the MTT assay was accomplished to determine cell cytotoxicity (175).

The MTT assay serves as a highly sensitive technique for measuring cell viability and the inhibition of cell growth, which is reliant on mitochondrial respiration occurring outside the inner mitochondrial membrane. This process utilizes NADH and NADPH-dependent pathways, ultimately resulting in cell inhibition (176,177). MTT, or 3-(4,5-dimethylthiazol-2-yl)-2,5-diphenyltetrazolium bromide, is a colorimetric assay involving the reduction of tetrazolium salt into formazone, a blue compound generated by the action of mitochondrial dehydrogenases in living cells. The insoluble formazan produced during the assay was dissolved in DMSO. To perform the MTT assay, 20 µL of MTT was dispensed to each well of a 96-well plate and subjected to incubation for 4 hours. After incubation, 170 µL of media was carefully taken from each well without displacing the crystals that had formed. Following this, 100 µL of DMSO was incorporated to dissolve the formazan crystals. Finally, the absorbance was measured using an ELISA plate reader at wavelengths of 570 and 630 nm. For each conjugates concentrations; the absorbance of treated wells (media + cells + conjugates) was adjusted by deducting the corresponding absorbance of wells containing media and conjugates. This removes the conjugates involvement to the absorbance. All experiments were replicated three times. The cell viability (%) was derived by adopting the following equation (176-178):

$$\% \text{ Cell viability} = \frac{\text{Mean OD (sample)}}{\text{Mean OD (control)}} \text{X}100 \qquad (3.3)$$

Here, Mean OD (control) denotes the mean absorbance of negative control (wells with media and untreated cells) and Mean OD (sample) denotes mean absorbance of treated wells (media + cells + conjugates)

3.11 Cytokine Analysis

After incubating the cells with conjugates for 24 hours, we extracted the supernatant and analysed the secretion of IFN-γ using sandwich ELISA in accordance with the manufacturer's guidelines (179,180). The sandwich ELISA was executed on a 96-well ELISA plate.(Nunc MaxiSorp®). To begin with, 100 µL of capture antibody (1 µg/mL in PBS) was dispensed into each well of the ELISA plate and left to incubate overnight at ambient conditions. The wells underwent four wash cycles with 300 µL of wash buffer (0.05% Tween-20 in PBS) per well. Following the final wash, residual buffer was removed and 300 µL of blocking buffer (1% BSA in PBS) was integrated to each well. The plate was then incubated for 1 hours at room temperature to prevent non-specific binding. After rinsing the plate four times with wash buffer, 100 µL of the test sample and the IFN-γ standard were dispensed into each well. The plate was then incubated for 2 hours at room temperature to allow the IFN-γ molecules to bind to the capture antibody. Next, the plate underwent four washes, and 100 µL of detection antibody (1 µg/mL in sample diluent buffer) was introduced into each well of the ELISA plate, allowing for incubation at room temperature for an additional 2 hours. The detection antibody binds to the IFN-γ molecules captured by the capture antibody. After another four washes, 100 µL diluted streptavidin-HRP conjugate (1:2000) in sample diluent was added and incubated for 30 minutes. Streptavidin-HRP binds to the detection antibody, which in turn binds to the IFN-γ molecules, amplifying the signal. The plate was again washed four times and 100 µL of TMB substrate solution was added to each well. The TMB substrate reacts with the HRP, causing a color change. The plate was wrapped in foil and incubated at 25 °C for 20 minutes to allow the color to develop. Finally, 100 µL of 1M HCl stop solution was dispensed to each well, which stopped the reaction and turned the color yellow. Absorbance was then inscribed at 405 nm with wavelength correction configured to 650 nm using an ELISA plate reader (Tecan, Austria).

3.12 Statistical analysis

The experiments were conducted in triplicates and the MTT outputs and ELISA results were analysed using GraphPad Prism software. An unpaired t-test was executed, considering p-values under 0.05 as significant.

Chapter 4:

Results:

Objective 1: Preparation and characterization of functionalized magnetic nanoparticles (MNPs):

To study crystal structure of as-synthesized Fe_3O_4 nanoparticles, powder X-ray diffraction was performed. X-ray diffractogram (XRD) of Fe_3O_4 nanoparticles recorded in the 2θ range of 20°-80° is shown in Fig. 4.1. This X-ray diffractogram is indexed well with the face centred cubic (FCC) inverse spinel lattice and consistent with the JCPDS card No. 19-0629. The lattice parameter of Fe_3O_4 nanoparticles determined from the highest intense (311) peak is 0.837 nm. This value matches well with that reported in JCPDS data base (card No. 19-0629). The average crystallite size (d) of Fe_3O_4 nanoparticles was calculated by using the classical Scherrer's equation

$$d = \frac{0.9\,\lambda}{\beta cos\theta} \tag{4.1}$$

where λ stands for the wavelength of X-rays, β refers to full-width half maximum (FWHM) of the highest intense peak (311) and θ is the angle of diffraction of the highest intense peak. FWHM of the highest intense peak was resolved by fitting it with the pseudo-voigt peak function. The average crystallite size attained from Eq. (4.1) is 9.1 nm.

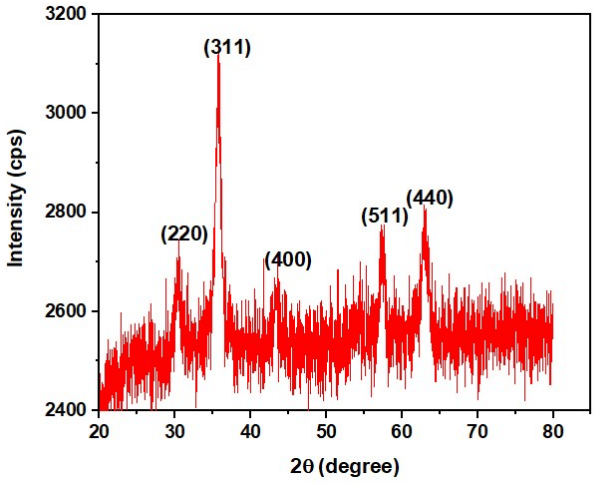

Fig 4.1: XRD pattern of as-synthesized Fe_3O_4 nanoparticles

To examine the morphology of Fe_3O_4 nanoparticles, high-resolution transmission electron microscopy (HR-TEM) was employed. Micrographs are presented in Fig. 4.2. Aggregated nanoparticles with near spherical morphology are visible in the micrograph. Inset (b) of Fig. 2 shows a lattice fringe image of Fe_3O_4 nanoparticles. Inter planner spacing is 0.49 nm, corresponding to (111) plane of the inverse spinel lattice of Fe_3O_4 nanoparticles. Inset (c) of Fig. 4.2 represents the selected area electron diffraction (SAED) pattern of nanoparticles. Diffraction fringes in the SAED pattern in Fig. 4.2(c) are indexed well with the inverse spinel structure of Fe_3O_4 nanoparticles and corroborate well with the X-ray diffractogram reported in Fig. 4.1.

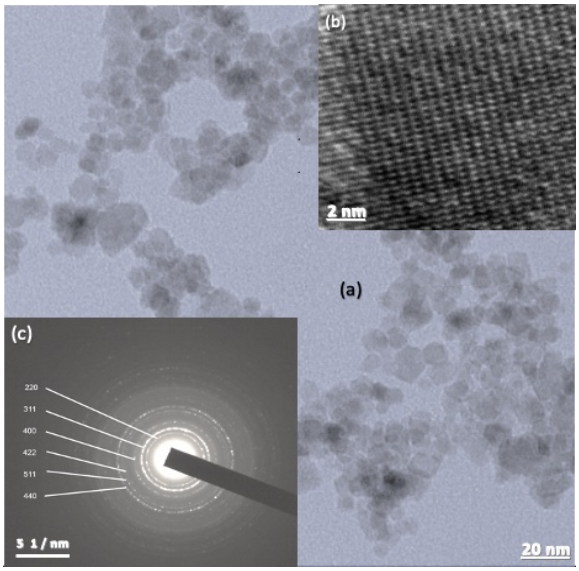

Fig 4.2: (a) Transmission electron micrograph **(b)** lattice fringe image and **(c)** specific area electron diffraction pattern of Fe_3O_4 nanoparticles

Size distribution histogram of Fe_3O_4 nanoparticles obtained from the TEM micrograph is shown in Fig. 4.3. This histogram depicting size distribution was prepared through the measurement of the diameter of 37 nanoparticles with the help of Carl Zeiss AxioVision software. This size distribution histogram is fitted with the log-normal particle size distribution function. The average physical size of the nanoparticles thus obtained from the fit is 9.5 ± 0.12 nm, which corresponds closely to the crystallite size of the nanoparticles, indicating each nanoparticle is single grain.

Hydrodynamic particle size (D) and polydispersity (σ) of as-synthesized Fe_3O_4 and PEG-coated Fe_3O_4 nanoparticles were determined by photon correlation spectroscopy.

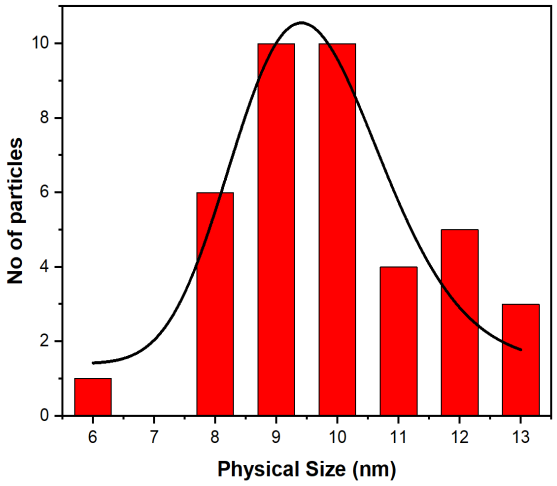

Fig. 4.3 Size distribution histogram of Fe_3O_4 nanoparticles obtained from HR-TEM micrograph

Hydrodynamic particle size distribution histograms of Fe_3O_4 and PEG coated Fe_3O_4 nanoparticles are diplayed in Fig. 4.4. Each histogram is fitted with log-normal particle size distribution function:

$$P(\mathrm{D}) = \frac{1}{(\mathrm{D}\sigma\sqrt{2\pi})} \exp\left[-\frac{\left(\ln\left(\frac{\mathrm{D}}{\mathrm{D}_0}\right)\right)^2}{2\sigma^2}\right] \tag{4.2}$$

Here, σ is the polydispersity, D signifies the hydrodynamic particle size and ln D_0 stands for the mean of ln D. From the best fits, hydrodynamic particle size and polydispersity of Fe_3O_4 and PEG-coated Fe_3O_4 nanoparticles were determined. The hydrodynamic size of Fe_3O_4 and PEG-coated Fe_3O_4 nanoparticles are 87 nm and 118 nm, respectively. The polydispersity index of Fe_3O_4 and PEG-coated Fe_3O_4 nanoparticles are 0.31 and 0.25, respectively.

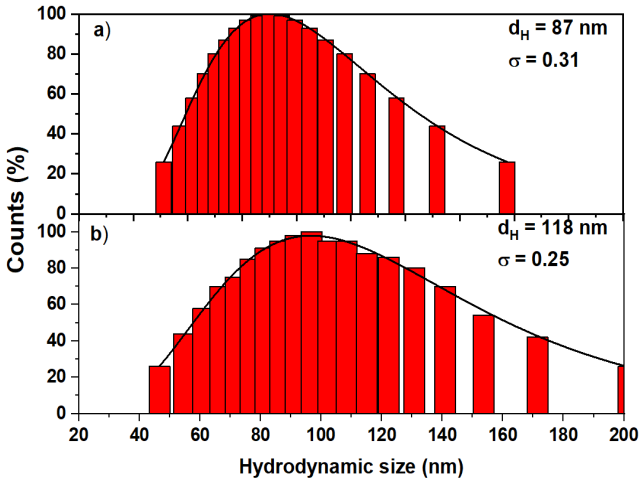

Fig 4.4: Hydrodynamic particle size distribution histograms of **(a)** Fe_3O_4 and **(b)** PEG-coated Fe_3O_4 nanoparticles dispersed in water. Histograms are fitted with log normal distribution function (Eq. 4.2)

To confirm PEG-coating on Fe_3O_4 nanoparticles, FTIR spectroscopy was used. FTIR spectra of bare Fe_3O_4 nanoparticles, PEG-coated Fe_3O_4 nanoparticles, and PEG-600 are displayed in Fig. 4.5. Various vibrational bands depicted in Fig. 4.5 are outlined in Table 4.1. The presence of absorption bands at 559 cm^{-1} and 640 cm^{-1} is due to Fe–O stretching vibrations of Fe_3O_4. In the case of PEG-coated Fe_3O_4, the vibrational band originally observed at 559 cm^{-1} shifts to a higher wavelength, which corresponds to a wavenumber of 540 cm^{-1}. The vibrational band initially at 640 cm^{-1} shifts to a lower wavelength, corresponding to a wavenumber of 665 cm^{-1}. Further, a strong absorption band at 989 cm^{-1} was observed in the FTIR spectra of PEG 600. This band shifts to a lower wavelength corresponding to 1121 cm^{-1} in the case of PEG-coated Fe_3O_4. This band is ascribed to the C–O–C stretching vibrations of PEG. These shifts in the band positions of Fe–O stretching vibrations and C–O–C stretching vibrations in PEG-coated Fe_3O_4 nanoparticles suggest that PEG is chemi-adsorbed on the surface of Fe_3O_4 nanoparticles.

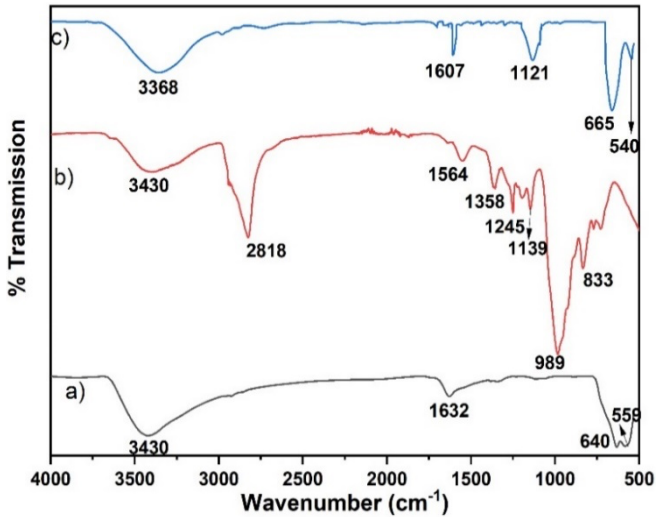

Fig 4.5: FTIR spectra of **(a)** Fe_3O_4**, (b)** PEG-600 and **(c)** PEG-coated Fe_3O_4 nanoparticles measured in the spectral range of 4000 – 500 cm^{-1}

Table 4.1. Band interpretations of FTIR spectra of Fe_3O_4, PEG and PEG-coated Fe_3O_4 nanoparticles

Sample	IR bands (cm^{-1})	Description
Fe_3O_4	559	Stretching vibration of Fe–O
	640	Stretching vibration of Fe–O
	1632	-OH stretching
	3430	-OH stretching
PEG-600	833	C-H bending
	989	C-O-C stretching vibration of PEG
	1139	C-O stretching
	1245	C-H twisting
	1358	C-H bending
	1564	$–CH_3$
	2818	m_s (–CH)
	3430	-OH stretching
PEG-coated Fe_3O_4	540	Stretching vibration of Fe–O
	665	Stretching vibration of Fe–O
	1121	C-O-C stretching vibration of PEG
	1607	-OH stretching
	3368	-OH stretching

These M-H loops are presented in Fig. 4.6. As evident from these hysteresis loops, both bare and PEG-coated Fe_3O_4 nanoparticles are superparamagnetic. A magnified view of M-H loops from −100 Oe to 100 Oe, for bare and PEG-coated Fe_3O_4 nanoparticles, shows that the coercivity of bare nanoparticles reduces from 32.42 Oe to 3.56 Oe and remanence drops from

1.78 emu/g to 0.159 emu/g, confirming the reduction in the clustering of magnetic nanoparticles post surface functionalization with PEG. This was also evident in the reduction in polydispersity index measured by photon correlation spectroscopy (Fig. 4.4). Saturation magnetization (M_S) of bare and PEG-coated Fe_3O_4 nanoparticles is 53.36 emu/g and 46.89 emu/g, correspondingly. Magnetization (M) versus the magnetic field (H) of bare and PEG-coated Fe_3O_4 nanoparticles recorded in the top right quadrant (Fig. 4.6) are also fitted with the modified Langevin function:

$$M = M_s \int_0^\infty f(D) L\left(\frac{\mu(H)}{k_B T}\right) dD + \chi H \quad (4.3)$$

where Ms corresponds to the saturation magnetization of nanoparticles and L(α) denotes Langevin function. The Langevin parameter, $\alpha = \mu(H)/k_BT$, where μ signifies the magnetic moment of individual spin clusters, H is the applied external magnetic field, k_B is the Boltzmann constant, and T stands for absolute temperature.

$$f(\mathrm{D})\mathrm{dD} = \frac{1}{(\sqrt{2\pi}\mathrm{D})} \exp\left[-\frac{\ln\left(\frac{D}{D_m}\right)^2}{2\sigma^2}\right] dD \quad (4.4)$$

here, f(D)dD denotes log-normal cluster size distribution function with mean cluster size D_m, polydispersity σ. χ corresponds to susceptibility of paramagnetic component of nanoparticles. The fitted graph is shown in Fig. 4.7 derived from the most suitable fits, mean cluster size (D_m), saturation magnetization (M_s) and polydispersity (σ) are evaluated, and presented in Table 4.2.

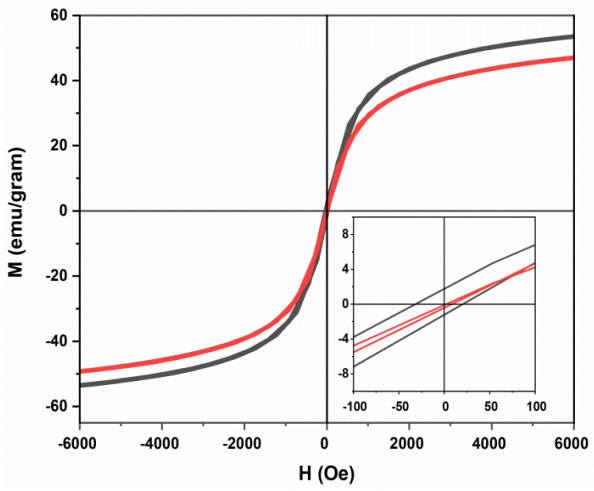

Fig 4.6: Magnetization (M) versus applied magnetic field (H) plots of (—) bare Fe_3O_4 and (—) PEG-coated Fe_3O_4 nanoparticles. Inset shows the magnified view of M-H curves in the field range of -100 Oe to + 100 Oe

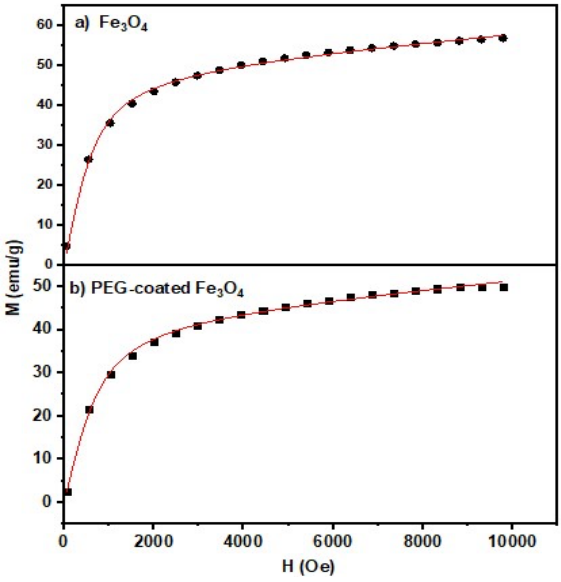

Fig 4.7: Magnetization (M) versus applied magnetic field (H) data of **a)** Fe_3O_4 and **b)** PEG-coated Fe_3O_4 nanoparticles fitted with modified Langevin function [Eq. 3]

The findings from fitting the M-H curve with the modified Langevin function include several key parameters, as shown in Table 4.2. The reduction in the polydispersity index from 0.18 for Fe_3O_4 to 0.12 for PEG-coated Fe_3O_4 indicates that the particles are more uniform in size, which can enhance their magnetic properties. The mean cluster size influences the magnetic

behaviour, particularly the superparamagnetic properties. The magnetic moment provides insight into the strength of the magnetic properties of individual nanoparticles, while higher susceptibility indicates a stronger response to the magnetic field.

Table 4.2. Saturation magnetization (M_S), mean cluster size (D_m), polydispersity (σ), magnetic moment (μ), and susceptibility (χ) of Fe_3O_4 and PEG-coated Fe_3O_4 nanoparticles obtained by fitting M-H curve with modified Langevin function

Sample	Saturation Magnetization (emu/gm)	Polydispersity	Mean cluster size (nm)	Magnetic moment x μ_B	Susceptibility x 10^{-5}
Fe_3O_4	56	0.18	6.2	16000	1.25
PEG-coated Fe_3O_4	46	0.12	7.8	15999	1.25

Objective 2: Conjugation of functionalized MNPs with Luteinizing Hormone-Releasing Hormone and anticancer drug Doxorubicin:

To confirm LHRH conjugation on PEG-coated Fe_3O_4, ATR-FTIR spectroscopy was used. ATR-FTIR spectra of LHRH tagged PEG-coated Fe_3O_4, LHRH, PEG-coated Fe_3O_4 and Fe_3O_4 nanoparticles are exhibited in Fig 4.8. Various vibrational bands observed are summarised in Table 4.3. The appearance of absorption bands at 559, and 640 cm^{-1} is due to Fe-O stretching vibrations of bare Fe_3O_4. In case of PEG-coated Fe_3O_4, vibrational band at 559 cm^{-1} red shift to 540 cm^{-1} and 640 cm^{-1} blue shifts to 665 cm^{-1}. Further, a strong absorption band at 989 cm^{-1} was observed in the FTIR spectra of PEG 600. This band red shifts to 1121 cm^{-1} in case of PEG-coated Fe_3O_4. This band is ascribed to the C-O-C stretching vibrations in PEG. These consequences confirm the chemi-adsorption of PEG-600 on the surface of Fe_3O_4 nanoparticles. The ATR-FTIR spectra of LHRH conjugated PEG- coated Fe_3O_4 showed an additional peak at 1561 cm^{-1} matching to the N-H of the amine bond, alongside the amplification of peaks intensities at 1650 cm^{-1} comparable to the C=O of the amide bond. The spectrum of pure LHRH was also recorded. The bands seen at 1535 and 1662 cm^{-1} are signature peaks of LHRH.

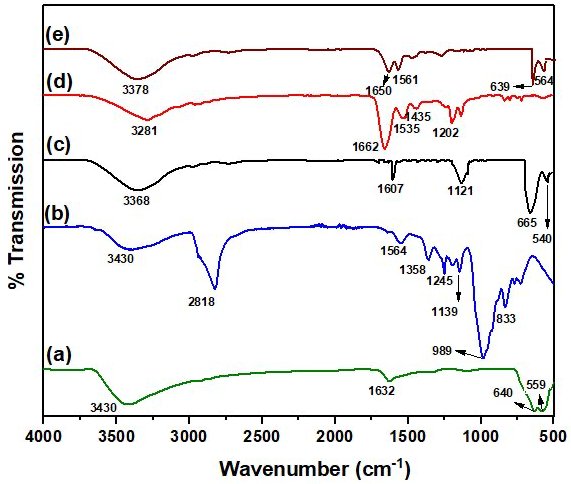

Fig 4.8: FTIR spectra of (a) bare Fe_3O_4, (b) PEG and (c) PEG-coated Fe_3O_4 (d) LHRH and (e) LHRH conjugated PEG-coated Fe_3O_4 nanoparticles. Measurement was performed in the spectral range of 4000 – 500 cm^{-1}

Table 4.3. Band interpretations of ATR-FTIR spectra of Fe_3O_4, PEG, and PEG-coated Fe_3O_4 and LHRH tagged PEG-coated Fe_3O_4 nanoparticles

Sample	IR bands (cm^{-1})	Description
Fe_3O_4	559	Stretching vibration of Fe–O
	640	Stretching vibration of Fe–O
	1632	-OH stretching
	3430	-OH stretching
PEG	833	C-H bending
	989	C-O-C stretching vibration of PEG
	1139	C-O stretching
	1242	C-H twisting
	1358	C-H bending
	1564	$–CH_3$
	2818	m_s (–CH)
	3430	-OH stretching
PEG-coated Fe_3O_4	540	Stretching vibration of Fe–O
	665	Stretching vibration of Fe–O
	1121	C-O-C stretching vibration of PEG
	1607	-OH stretching
	3368	-OH stretching
LHRH	3281	-OH stretching
	1662	C=O amide bond
	1535	N-H amine bond
	1435	C-H bending
	1202	C-N amine bond

LHRH tagged PEG-coated Fe_3O_4	3378	-OH stretching
	1650	C=O amide bond
	1561	N-H amine bond
	639	Stretching vibration of Fe-O
	564	Stretching vibration of Fe-O

4.1 Drug loading

In the study, we utilized doxorubicin (DOX), a hydrophilic anti-cancer agent, as the representative reference drug. Using UV–vis spectroscopy, we confirmed the loading of doxorubicin in LHRH-conjugated PEG-coated Fe_3O_4. Fig. 4.9 illustrates the absorption spectra of free doxorubicin and doxorubicin-loaded LHRH-conjugated PEG coated Fe_3O_4 nanoparticles in aqueous solutions. The characteristic peak of doxorubicin at 475 nm in the absorption spectrum of LHRH-conjugated PEG coated Fe_3O_4 and at 486 nm in the free doxorubicin solution (168) confirms the presence of doxorubicin. The shift to the shorter wavelength (475 nm) in the absorption maximum further validates the loading of doxorubicin in the LHRH-conjugated PEG-coated Fe_3O_4 nanoparticles.

4.2 Drug loading efficiency

The drug loading results from the conjugation of the $–NH_2$ and –OH groups in doxorubicin (DOX) with the active –OH groups present on the surface of PEG (202). Drug loading efficiency was determined using Eq. (3.1) The drug loading efficiency of DOX is observed to be 66 %.

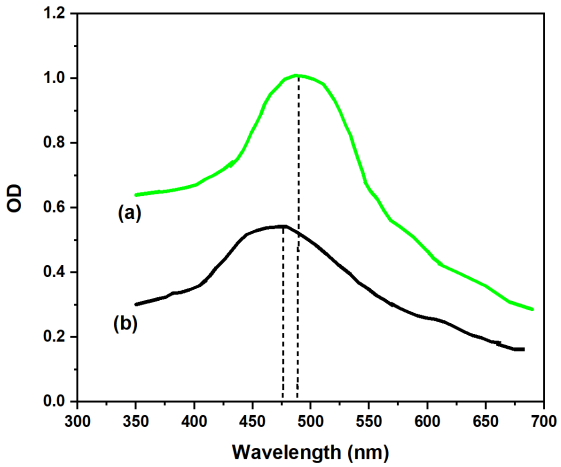

Fig 4.9: UV–visible absorption spectrum of aqueous solution of (a) free doxorubicin (geen color) and (b) DOX loaded LHRH tagged PEG-coated Fe_3O_4 nanoparticles (black color). The spectrum was recorded at 25 °C with HPLC grade water as reference

The drug loading efficiency of DOX to LHRH conjugated PEG-coated Fe_3O_4 nanoparticles observed at 66% indicates that 66% of the total weight of the nanoparticles is composed of the drug DOX. This high efficiency is significant because it means a substantial amount of the drug is successfully loaded onto the nanoparticles, which is crucial for effective targeted drug delivery.

Objective 3: To study the hyperthermic effect of conjugated MNPs on growth and cytokine release of cancer cells:

4.3 Magnetic hyperthermia of PEG-coated Fe_3O_4 nanoparticles

To evaluate the suitability of synthesized PEG-coated Fe_3O_4 nanoparticles for magnetic hyperthermia therapy of cancer, temperature (T) - time (t) profiles of PEG-coated Fe_3O_4 nanoparticles are recorded as a function of applied AC magnetic field frequency (162–935.6 kHz), field strength (5 mT, 10 mT and 12 mT) and nanoparticle concentration (1–100 mg/mL). These temperature (T) versus time (t) plots are shown in Fig. 4.10. To study how frequency affects the heating profile of nanoparticles, the magnetic field, and concentration were kept constant at 10 mT and 100 mg/mL, respectively, while the frequency was varied between 162–935.6 kHz. In this study, the highest temperature rise of 89.16 °C was observed at a frequency of 935.6 kHz when nanoparticles were exposed to a magnetic field (10 mT) for 20 minutes. At 580.8 kHz, this temperature rise was 68.15 °C. Since this temperature rise is adequate for

hyperthermia applications, we choose a relatively lower frequency (580.8 kHz) of a supplied magnetic field as the optimum field frequency instead of 935.6 kHz for biologically safer applications of these magnetic nanoparticles in magnetic hyperthermia.

To further investigate how magnetic field strength affects heating capacity of PEG coated Fe_3O_4 nanoparticles, the field frequency was held steady at 580.8 kHz, and field strength was varied between 5–12 mT. In this study, the highest temperature rise of 85.06 °C was recorded at 12 mT field. However, at 10 mT field also, adequate temperature rise (68.15 °C) was observed. Hence, for further studies, 10 mT field strength is considered the optimized field strength.

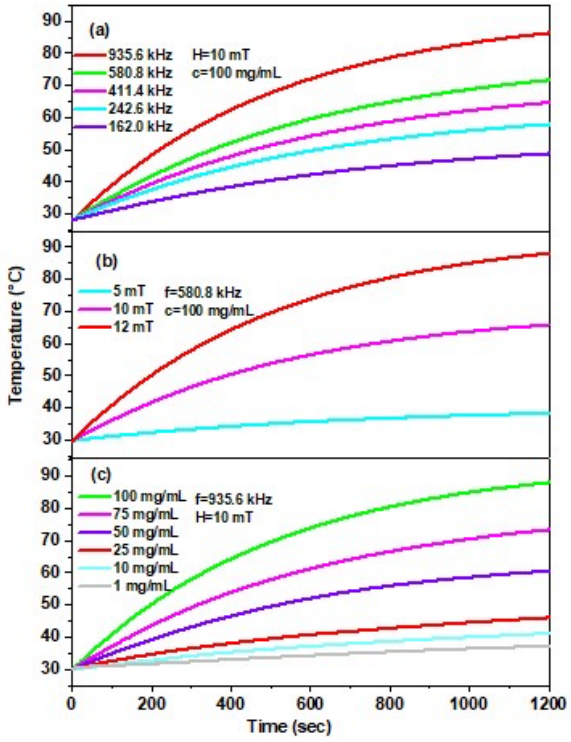

Fig 4.10: Temperature – time profiles of as-synthesized PEG-coated Fe_3O_4 nanoparticles measured as a function of **(a)** magnetic field frequency **(b)** magnetic field strength and **(c)** nanoparticle concentration

Subsequent to the optimization of magnetic field frequency and field strength, the role of nanoparticle concentration was evaluated by measuring temperature–time profiles of a series of PEG coated Fe_3O_4 nanoparticles having concentration in the range of 1–100 mg/mL. In this study, magnetic field frequency and field strength were held constant at 935.6 kHz and 10 mT, respectively. The maximum rise in temperature of PEG-coated Fe_3O_4 nanoparticles escalates

with increased concentration. The highest temperature rise (86.16 °C) was observed for a nanoparticle concentration of 100 mg/mL. However, an adequate (>45 °C) temperature rise (59.05 °C) was observed for a lower nanoparticle concentration of 50 mg/mL. Further, in the context of magnetic hyperthermia treatment, it has been observed that exceeding a temperature threshold of 42 °C can trigger cell apoptosis in cancer cells (12). This can be achieved at lower nanoparticle concentration of 25 mg/mL. At this temperature, the highest temperature rise is 44.02 °C Furthermore, when comparing the specific loss power (SLP) values, both concentrations of 25 mg/mL and 50 mg/mL exhibit nearly similar SLP values of 4.43 W/g and 4.66 W/g, respectively. Hence, 25 mg/mL of nanoparticle concentration is chosen as the optimal concentration for further studies. Therefore, we consider 25 mg/mL as the optimized nanoparticle concentration of PEG-coated Fe_3O_4 nanoparticles for magnetic hyperthermia therapy under an applied magnetic field frequency of 935.6 kHz and 10 mT of field strength. When these experiments were performed with previously optimized lower frequency (580.8 kHz), adequate heating could not be achieved in Fe_3O_4 nanoparticles with lower concentration of 25 mg/mL. Therefore, we consider 965.6 kHz as the optimum frequency in place of 580.8 kHz. To further grasp the influence of magnetic field frequency, field strength and nanoparticle concentration on the heating efficiency of PEG-coated Fe_3O_4 nanoparticles, the temperature–time profiles of Fig. 4.10 are fitted with the empirical box-Lucas model (181,182)

$$\Delta\theta(t) = \Delta\theta_s(1 - e^{-kt}) \tag{4.5}$$

Here, $\Delta\theta(t)$ denotes change in temperature [$= \theta(t) - \theta_0$], here θ_0 is initial temperature, $\theta(t)$ is the temperature at time t, and k represents a kinetic parameter. $\Delta\theta$ versus time plots fitted with Eq. (4.5) are revealed in Fig. 4.11. From the best fits, kinetic parameter, k and initial slope of temperature– time curve, $\Delta\theta s$, are determined, which are stated in Table 4.4.

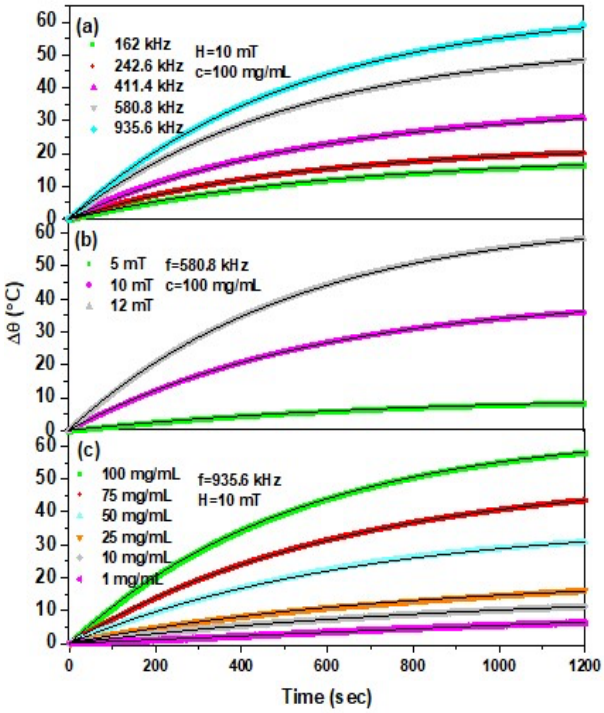

Fig 4.11: Δθ vs time plots of PEG-coated Fe_3O_4 nanoparticles measured as a function of **(a)** magnetic field frequency **(b)** magnetic field strength and **(c)** nanoparticle concentration, which are fitted with box-Lucas model (Eq. 4.5).

The heating efficiency of magnetic nanoparticles assisted hyperthermia applications is usually represented in the form of SLP, which is described as the amount of heat generated by the unit mass of the magnetic nanoparticles in the material (W/g) at a given strength and frequency of the induced magnetic field (183). SLP depends on the magnetic nanoparticle's properties, such as size, saturation magnetization (M_S), magnetic anisotropy and magnetic field parameters like strength and frequency (184). SLP values are calculated by using the following equation (181)

$$SLP = \frac{\rho}{x} c \Delta\theta_s k \qquad (4.6)$$

where ρ denotes the density of the medium (for water ρ = 1.0 g/mL), c is the specific heat of the medium (4.18 J/gK for water), Δθs denotes the initial slope of the temperature–time plot, k is kinetic parameter and x represents concentration of magnetic nanoparticles. SLP values of PEG- coated Fe_3O_4 nanoparticles measured with respect to the magnetic field frequency, field strength and nanoparticle concentrations are also reported in Table 4.4. SLP value of PEG-coated Fe_3O_4 nanoparticles increases with frequency and field strength and declines with

nanoparticle concentration (Fig. 4.12). The slope is 0.41 W/g mL per 100 kHz when monitored as a function of frequency.

Table 4.4. Fitting parameters ($\Delta\theta_s$ and k) of empirical box-Lucas model, specific loss power (SLP) and intrinsic loss power (ILP) measured as a function of magnetic field frequency, field strength, and nanoparticle concentration.

Frequency (kHz)	Magnetic field (mT)	Nanoparticle concentration (mg/mL)	$\Delta\theta_s$ (°C)	k x 10^{-5} (min^{-1})	SLP (W/g)	ILP (Wg^{-1}/ ($f H^2$))
162.0	10	100	19.4	160	1.04	0.10
242.6	10	100	22.2	195	1.99	0.13
411.4	10	100	34.5	181	2.30	0.08
580.8	10	100	54.1	179	2.87	0.07
935.6	10	100	65.0	187	4.54	0.07
580.8	5	100	10.5	136	0.60	0.06
580.8	10	100	54,1	179	2.87	0.07
580.8	12	100	65.0	189	5.13	0.09
935.6	10	1	6.1	91	24.13	0.04
935.6	10	10	15.5	107	6.92	0.12
935.6	10	25	20.0	133	4.43	0.07
935.6	10	50	37.0	151	4.66	0.07
935.6	10	75	51.3	158	4.51	0.07
935.6	10	100	65.0	187	4.54	0.07

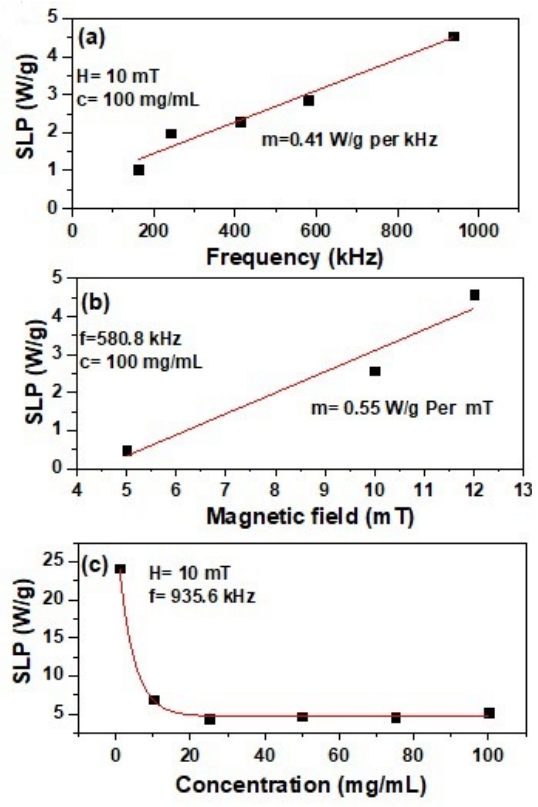

Fig 4.12: Effect of magnetic field frequency field strength, and nanoparticle concentration on the SLP of PEG-coated Fe_3O_4 nanoparticles

The heating capacity of nanoparticles is an important factor for magnetic hyperthermia. It is quantified in terms of intrinsic loss parameter (ILP)

$$ILP = \frac{SLP}{fH^2} \quad (4.6)$$

Here H is the external magnetic field exerted to the nanoparticles, and f is the frequency of excitation. In our study, we found that the values of ILP remained constant regardless of the frequency, magnetic field strength, and nanoparticle concentration. This specifies that the nanoparticle's heating capacity was not affected by these variables (185,186). Overall, ILP is useful for quantifying the heating capacity of nanoparticles irrespective of the field strength, field frequency or nanoparticle concentration.

4.4 Cell viability Assessment

Synthesized DOX-loaded LHRH tagged PEG-coated Fe_3O_4 was examined for their influence on growth of A549 cells and MCF-7 cells by the cell viability assay (MTT) in both scenarios: no magnetic field and with a magnetic field. Cell viability was measured for standalone thermotherapy, chemotherapy, and combinational thermo-chemotherapy.

Thermotherapy:

Cell viability test against A549 and MCF-7 cancer cells were performed for PEG-coated Fe_3O_4 nanoparticles and LHRH tagged PEG-coated Fe_3O_4 nanoparticles at different nanoparticle concentrations (5, 10, 20, and 25 mg/mL) in the presence magnetic field (10 mT) and absence of magnetic field. The results are presented in Figure 4.13 and Figure 4.14. The findings suggest that both types of nanoparticles have significantly higher toxicity in presence of magnetic field when compared to absence of field. Irrespective of the nanoparticle concentrations for PEG-coated Fe_3O_4, There was no notable reduction in cell viability in A549 and MCF-7 cells when experiments were carried out without their exposure to magnetic field.

This confirms good biocompatibility of PEG-coated Fe_3O_4 nanoparticles. Notably, at 25 mg/mL nanoparticle concentration, the most significant reduction in cell viability was detected upon being exposed to an alternating magnetic field, resulting in 47 % cell viability reduction for A549 and 45 % for MCF-7 cells.

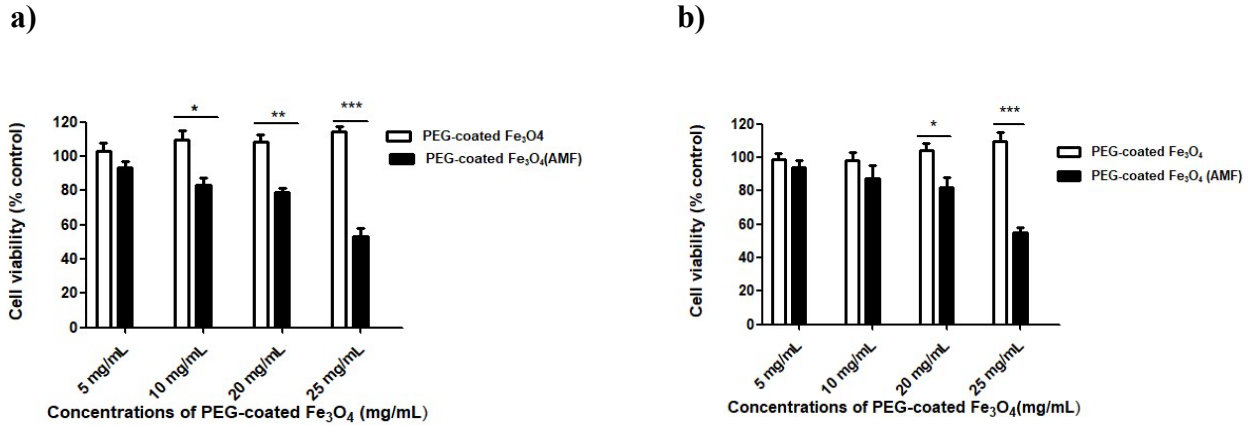

Fig 4.13 a) Cell viability of A549 cells in the absence and presence of magnetic field after treatment with different concentrations of PEG-coated Fe_3O_4. **b)** Cell viability of MCF-7 cells in the absence and presence of magnetic field after treatment with different concentrations of PEG-coated Fe_3O_4.. Unpaired t-tests were used for comparisons, *P<0.05, **P<0.01, ***P<0.001

Similar trend is observed for LHRH tagged PEG-coated Fe_3O_4. With out the application of magnetic field, nanoparticles do not indicate any significant loss of cell viability for both the cell lines. With the applied magnetic field, LHRH tagged PEG-coated Fe_3O_4 show concentration dependant toxicity. With increase in nanoparticle concentration, cell viability decreases in both the cell lines. Highest toxicity was observed at 25 mg/mL nanoparticle concentration. The reduction in cell viability is 47 % for A549 cell and it is 45 % for MCF-7 cells, which is comparable to the results observed in Fig. 4.12.

a) **b)**

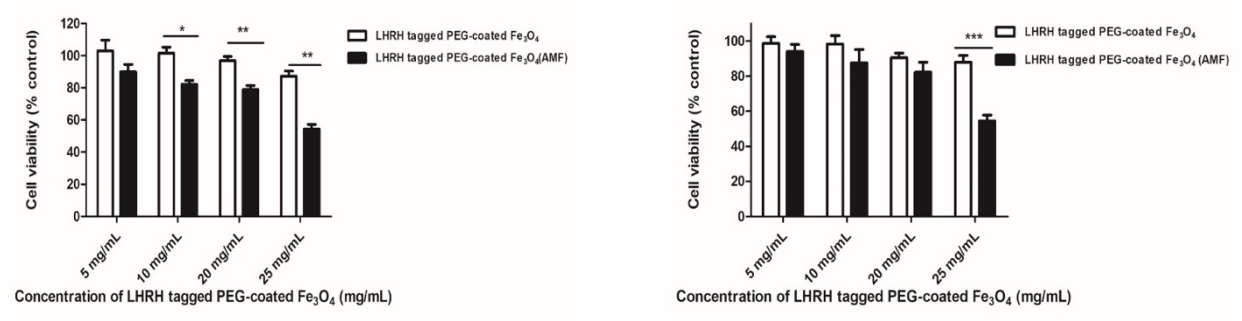

Fig 4.14 a) Cell viability of A549 cells in the absence and presence of magnetic field after treatment with different concentrations of LHRH tagged PEG-coated Fe_3O_4. b) Cell viability of MCF-7cells after treatment with different concentrations of PEG-coated Fe_3O_4. Unpaired t-tests were used for comparisons, *P<0.05, **P<0.01, ***P<0.001

Chemotherapy:

To study chemotherapeutic effect of doxorubicin, cell viability experiments were carried out on A549 and MCF-7 cell lines with free DOX, DOX-loaded PEG-coated Fe_3O_4 nanoparticles, and LHRH tagged DOX-loaded PEG-coated Fe_3O_4 nanoparticles. In this study, samples were not exposed to magnetic field. Concentration of PEG-coated Fe_3O_4 nanoparticles and LHRH tagged PEG-coated Fe_3O_4 nanoparticles was 25 mg/mL. DOX concentration was varied from 1.25, 2.5, 5, and 10 µg/mL. % reduction in cell viability of A549 and MCF-7 when tested against free DOX, DOX-loaded PEG-coated Fe_3O_4 nanoparticles, and LHRH tagged DOX-loaded PEG-coated Fe_3O_4 nanoparticles is presented in Fig. 4.15. As the concentration of doxorubicin increases there is corresponding increase in its effectiveness in reducing cell viability against A549 cells, with the maximum observed reduction being 72 % at doxorubicin concentration of 10 µg/mL (Fig. 4.15a). Furthermore, the efficacy of targeted chemotherapy using doxorubicin-loaded LHRH tagged PEG-coated Fe_3O_4 nanoparticles was compared to non-targeted chemotherapy with free doxorubicin and doxorubicin-loaded PEG-coated Fe_3O_4 nanoparticles. At DOX concentrations of 2.5 and 5 µg/mL, targeted chemotherapy demonstrated significant reductions in A549 cell viability (45 % and 58 %, respectively) compared to the non-targeted chemotherapy (24 % & 44 % for free DOX and 22 % & 40 % for DOX-loaded PEG-coated Fe_3O_4 nanoparticles). Non-targeted chemotherapy with free doxorubicin or doxorubicin-loaded PEG-coated Fe_3O_4 nanoparticles resulted in lower reductions in cell viability at the same DOX concentration.

To assess the effect of targeted and non-targeted DOX on MCF-7 cell lines, DOX concentration is varied between 1, 2, 4, and 8 µg/mL for free DOX, DOX-loaded PEG-coated Fe_3O_4 nanoparticles, and LHRH tagged DOX-loaded PEG-coated Fe_3O_4 nanoparticles. % Cell viability for these three tested samples on MCF-7 cells is displayed in Fig 4.15b. Increasing the concentration of doxorubicin resulted in a corresponding increase in its ability to reduce cell viability in MCF-7 cell lines as well. The findings revealed that targeted chemotherapy (DOX loaded LHRH tagged PEG-coated Fe_3O_4) exhibited a significant drop in cell viability (28 %, 45 %, & 58 % at concentrations of 1, 2, and 4 µg/mL, respectively) as compared to non-targeted chemotherapy (18 %, 28 % & 40 % for free DOX and 13 %, 27 % & 52 % at range of concentrations such as 1, 2, and 4 µg/mL, respectively intended for DOX-loaded PEG-coated Fe_3O_4 nanoparticles).

a) **b)**

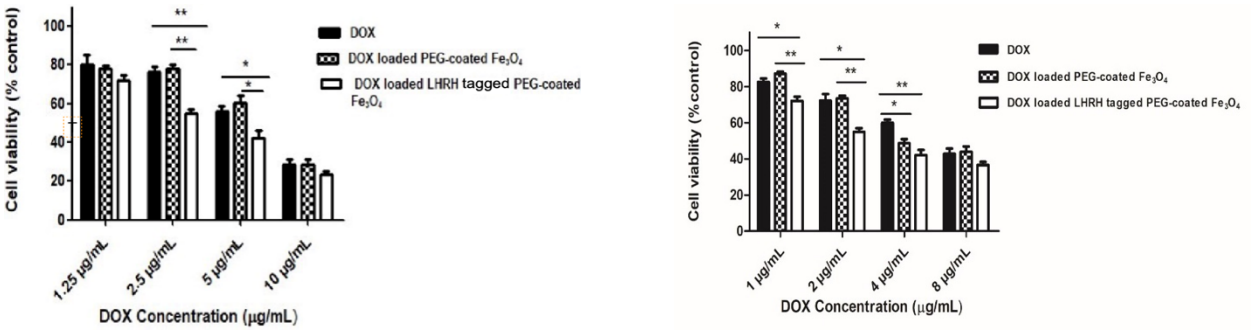

Fig 4.15 a) Cell viability of A549 cells in the absence of magnetic field after treatment with: free DOX, DOX loaded PEG-coated Fe_3O_4 and DOX loaded LHRH tagged PEG-coated Fe_3O_4., b) Cell viability of MCF-7 cells in the absence of magnetic field after treatment with: free DOX, DOX loaded PEG-coated Fe_3O_4 and DOX loaded LHRH tagged PEG-coated Fe_3O_4., Unpaired t-tests were used for comparisons, *P<0.05, **P<0.01, ***P<0.001

Thermo-chemotherapy:

To understand the effect of combinational therapy, thermal therapy is combined with the conventional chemotherapy. For this purpose, cell viability experiments on A549 and MCF-7 cell lines were executed against free DOX, DOX-loaded PEG-coated Fe_3O_4 nanoparticles, and LHRH tagged DOX-loaded PEG-coated Fe_3O_4 nanoparticles subjected to a magnetic field (10 mT). Nanoparticle concentration was fixed at 25 mg/mL and DOX concentrations were varied as descibed in standalone chemotherapy. The highest concentration of the chemotherapeutic

drug DOX (10 µg/mL) resulted in 88 % reduction in cell viability in combinational therapy. For the same conencetartion of DOX, standalone chemotherapy resulted in reduction of cell viablity of A549 to 62 %. Even for lower concentrations of DOX (1.25, 2.5, and 5 µg/mL), the combination thrapy resulted in greater reduction in % cell viability (47 %, 65 %, 72 %, respectively) as compared to corresponding chemotherapy (13 %, 23 %, 42 %, respectively) As shown in Fig. 4.16a, when targeted chemotherapy is combined with an alternating magnetic field, it leads to a statistically significant ($p<0.05$) reduction in A549 cell viability, as indicated in Fig. 4.14 a.

The highest concentration of the chemotherapeutic drug DOX (10 µg/mL) resulted in 91 % reduction in cell viability in combinational therapy. For the same conencetartion of DOX, standalone chemotherapy resulted in reduction of cell viablity of MCF-7 is 57%. Even for lower DOX concentrations (1, 2, and 8 µg/mL), the combination thrapy resulted in greater reduction in % cell viability (58 %, 74 %, 81 %, respectively) as compared to corresponding chemotherapy (18%, 28%, 40%, respectively) as shown in Fig. 4.16b. These results highlight the potential of thermo-chemotherapy, which combines targeted chemotherapy with an magnetic hyperthermia.

a)

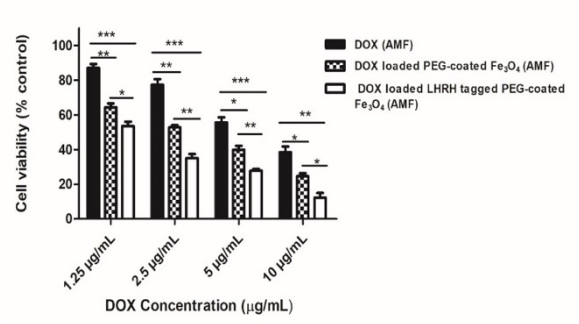

b)

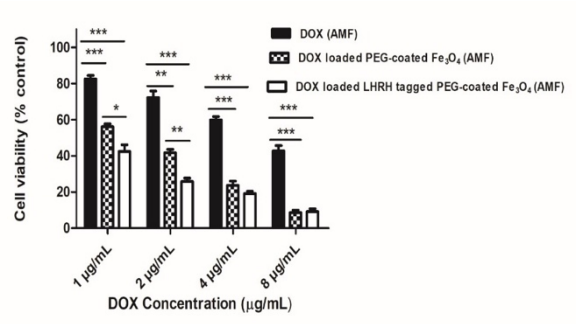

Fig 4.16 a) Cell viability of A549 cells in the presence of magnetic field after treatment with: free DOX, DOX loaded PEG-coated Fe_3O_4 and DOX loaded LHRH tagged PEG-coated Fe_3O_4., b) Cell viability of MCF-7 cells in the absence of magnetic field after treatment with: free DOX, DOX loaded PEG-coated Fe_3O_4 and DOX loaded LHRH tagged PEG-coated Fe_3O_4., Unpaired t-tests were used for comparisons, *P<0.05, **P<0.01, ***P<0.00**1**

4.5 Morphological study

To study the effects of magnetic nanoparticle conjugates on the morphology of A549 and MCF-7 cells, we used an inverted microscope to analyse the cell morphology. The resulting optical images are presented in Fig. 4.17 and 4.18, providing a visual representation of the cellular changes induced by the conjugates.

In the *in-vitro* analysis section, we exposed A549 and MCF-7 cells to different nanoparticle conjugates and analysed their impact. The A549 cells were treated with LHRH tagged PEG-coated Fe_3O_4 nanoparticles with a concentration of 25 mg/mL and DOX loaded LHRH tagged PEG-coated Fe_3O_4 nanoparticles with concentrations of doxorubicin set at 1.25, 2.5, 5, and 10 µg/mL. under an alternating magnetic field (10 mT). The corresponding MTT assay results showed 47 %, 46 %, 65 %, 72 %, and 88 % cell inhibition.

Similarly, MCF-7 cells were treated with LHRH tagged PEG-coated Fe_3O_4 nanoparticles at a concentration of 25 mg/mL and DOX loaded LHRH tagged PEG-coated Fe_3O_4 nanoparticles with doxorubicin concentrations of 1, 2, 4, and 8 µg/mL under AMF, resulting in 58 %, 74 %, 81 %, and 91 % cell inhibition in the MTT assay. We selected the samples with the most significant cell viability reduction for morphological analysis and put them in 96-well plates at a cell density of 1×10^4 per well. After incubating the plates in a 5 % CO2 incubator for 24 hours, we analysed the cells using an inverted microscope.

In Figure 4.17a, untreated A549 cells maintained their typical epithelial trigonal shape and close contact with each other under an AMF. However, in Figure 4.17b, after exposure to LHRH tagged PEG-coated Fe_3O_4 with AMF, some A549 cells lost their original shape and experienced cell shrinkage. Subsequent increases in the concentration of DOX-loaded LHRH tagged PEG-coated Fe_3O_4 led to more suspended (dead) cells under AMF and a rounded appearance. Moreover, there was a reduction in the cell population as the concentration of DOX-loaded LHRH tagged PEG-coated Fe_3O_4 increased. Cells treated with lower concentrations (1.25, 2.5, & 5 µg/mL) displayed more cell shrinkage and a decrease in cell numbers (refer to Fig. 4.17c, 4.17d, & 4.17e). In contrast, treated cells with a higher concentration (10 µg/mL) showed more irregular or round-shaped cells, or cells having shrinkage and a lower cell layer density (Fig. 4.17f).

Similarly, the untreated MCF-7 control cells exhibited a polygonal shape having typical epithelial morphology with densely packed cell layers in the presence of an AMF (Fig. 4.18a). However, after exposure to LHRH tagged PEG-coated Fe_3O_4 nanoparticles with AMF (Fig. 4.18b), the MCF-7 cells lost their original shape, showing distortion and shrinkage. As the

concentration of DOX-loaded LHRH tagged PEG-coated Fe_3O_4 nanoparticles increased, the cell population was reduced significantly. The treatment of cells with lower concentrations (1, 2, and 4 µg/mL) displayed more shrinkage and a decrease in cell numbers (Fig. 4.18c, 4.18d, and 4.18e). In contrast, cells treated with a higher concentration (8 µg/mL) showed more round-shaped cells, indicating dead cells in suspension. This change in cell shape suggested a greater effect, as measured by the MTT assay (Fig. 4.18f).

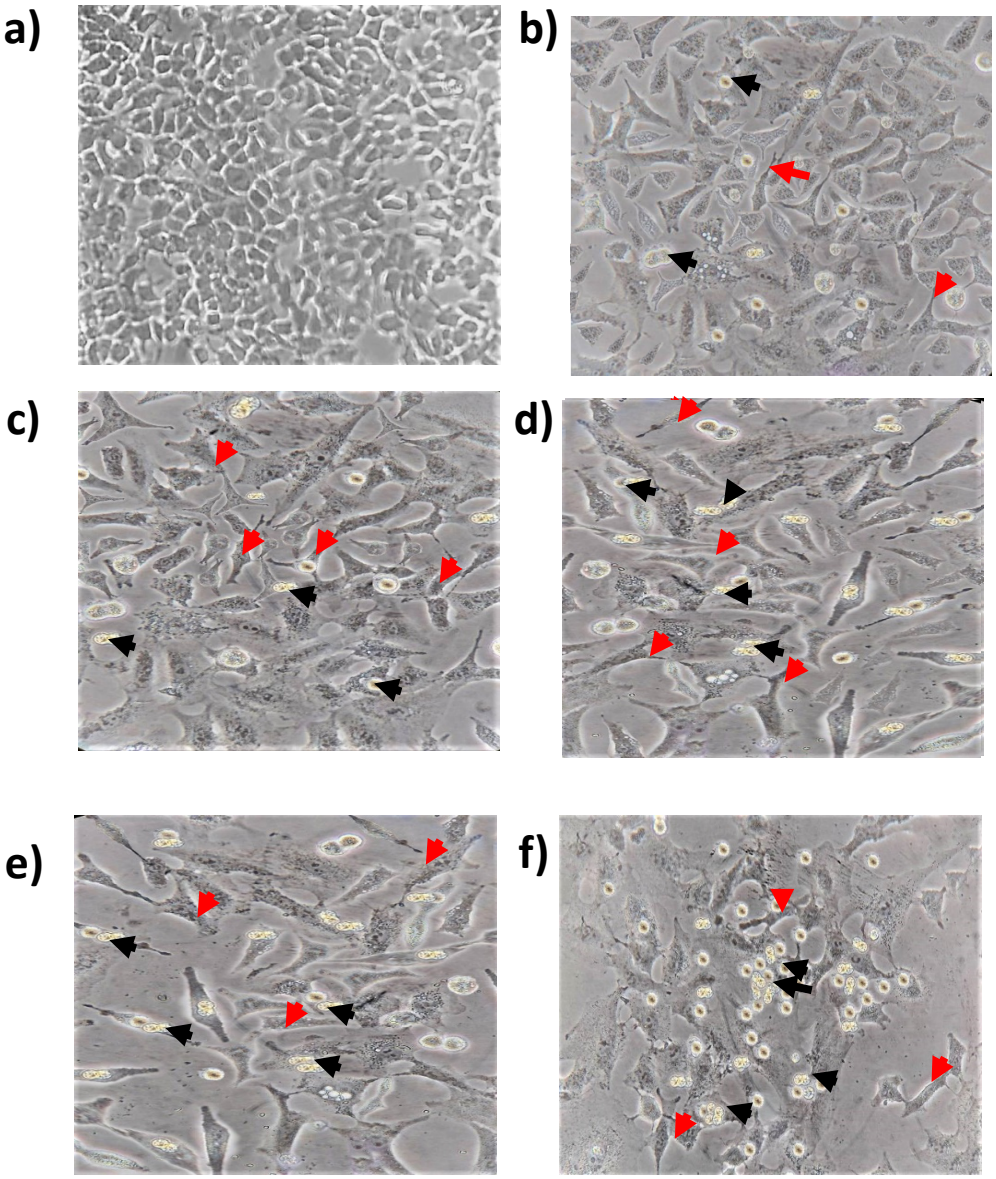

Fig 4.17: Cellular morphology of A549 cells under alternating magnetic field(AMF) **a)** untreated A549 cells, **b)** LHRH tagged PEG-coated Fe_3O_4 (25 µg/mL) treated A549 cells, **c)** DOX loaded LHRH tagged PEG-coated Fe_3O_4 (DOX concentration: 1.25 µg/mL) treated A549 cells, **d)** DOX loaded LHRH tagged PEG-coated Fe_3O_4 (DOX concentration: 2.5 µg/mL) treated A549 cells ,**e)** DOX loaded LHRH tagged PEG-coated Fe_3O_4 (DOX concentration: 5 µg/mL) treated A549 cells and **f)** DOX loaded LHRH tagged PEG-coated Fe_3O_4 (DOX concentration: 10 µg/mL) treated a549 cells were viewed using inverted microscope. Red arrow (➔) shows cell shrinkage while black arrow (➔) pointed at the suspension of dead cells. Magnification: x40;

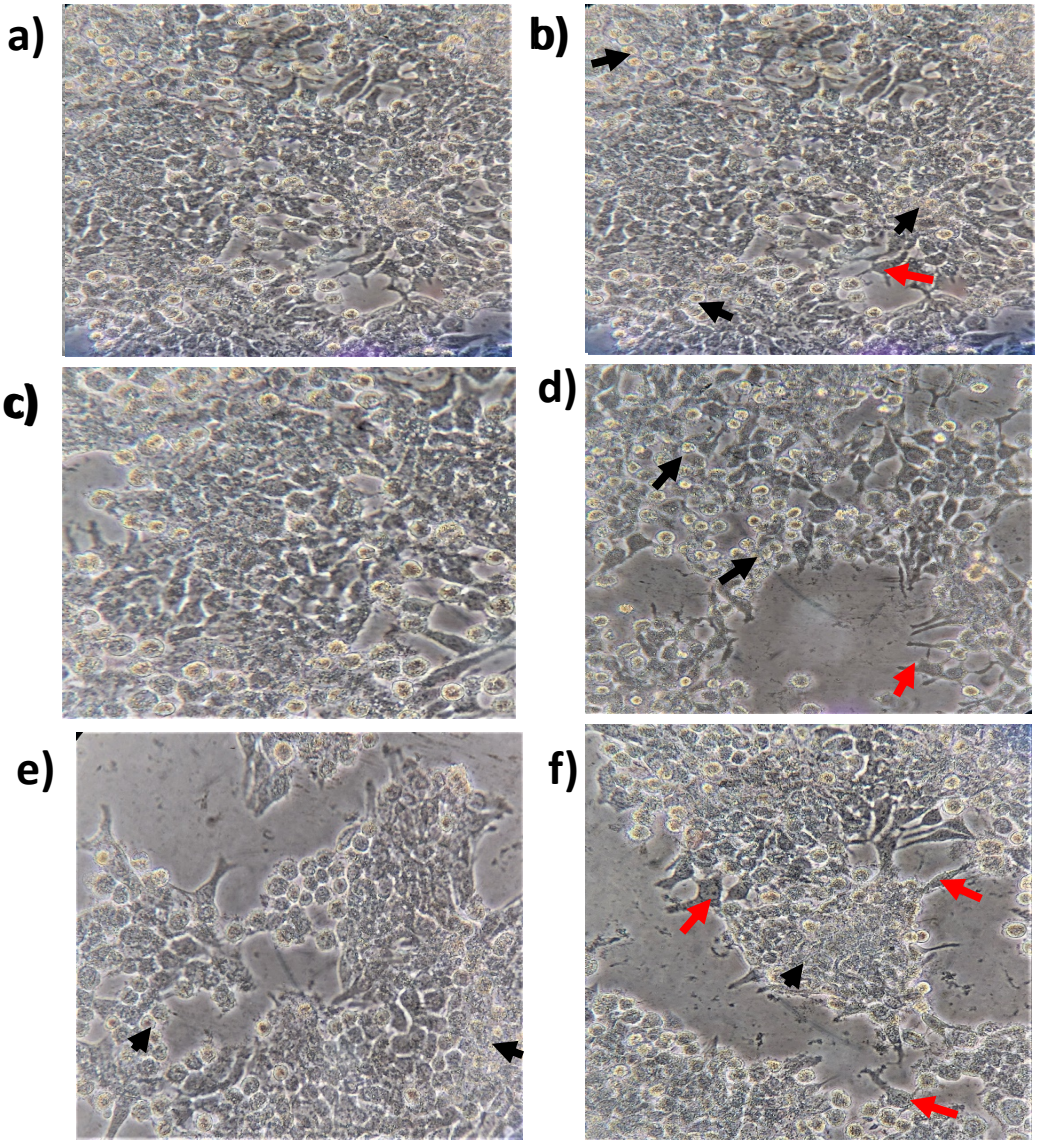

Fig 4.18: Cellular morphology of MCF-7 cells under alternating magnetic field(AMF) **a)** untreated MCF-7 cells, **b)** LHRH tagged PEG-coated Fe_3O_4 (25 µg/mL) treated MCF-7 cells, **c)** DOX loaded LHRH tagged PEG-coated Fe_3O_4 (DOX concentration: 1µg/mL) treated MCF-7 cells, **d)** DOX loaded LHRH tagged PEG-coated Fe_3O_4 (DOX concentration: 2µg/mL) treated MCF-7 cells ,**e)** DOX loaded LHRH tagged PEG-coated Fe_3O_4 (DOX concentration: 4µg/mL) treated MCF-7 cells and **f)** DOX loaded LHRH tagged PEG-coated Fe_3O_4 (DOX concentration: 8µg/mL) treated MCF-7 cells were viewed using inverted microscope. Red arrow (➔) shows cell shrinkage while black arrow (➔) pointed at the suspension of dead cells. Magnification: x40;

4.6 Cytokines Estimation

To analyse the contribution of IFN-γ in promoting cytotoxic effects in A549 and MCF-7 cells, we conducted a sandwich ELISA assay to measure the secretion of IFN-gamma. Present research intended to observe the outcome of different treatments on IFN-γ cytokine release in A549 and MCF-7 cancer cell lines. The treatments included free DOX, DOX-loaded PEG-coated Fe_3O_4 nanoparticles, and LHRH tagged DOX-loaded PEG-coated Fe_3O_4 nanoparticles, in the presence of magnetic field (10 mT) and absence of magnetic field.

To assess the cytokine release, we analysed the supernatants from the treated cancer cell lines using a sandwich ELISA test, measuring IFN-γ levels up to 24 hours. Our findings showed changes in the production of IFN-γ cytokine from A549 (Fig. 4.19) and MCF-7 (Fig. 4.20) when exposed to free DOX, DOX-loaded PEG-coated Fe_3O_4 nanoparticles, and LHRH tagged DOX-loaded PEG-coated Fe_3O_4 nanoparticles in the presence and absence of magnetic field. During our study, we observed that LHRH tagged DOX-loaded PEG-coated Fe_3O_4 nanoparticles exhibited an increased production of IFN-γ, both under conditions with and without a magnetic field, compared to non-targeted nanoconjugates. These findings demonstrate that treatment with targeted drug-loaded magnetic nanoparticles somehow potentiate the antitumor effect of IFN-γ towards both cancer cell lines.

The heightened cytokine response observed in this study could be pivotal in contributing to the cytotoxicity of the cancer cells. By analysing these changes, we gained valuable insights into the probable impact of targeted delivery of drugs and the influence of the magnetic field on IFN-γ cytokine release in A549 and MCF-7 cancer cell lines.

a) b)

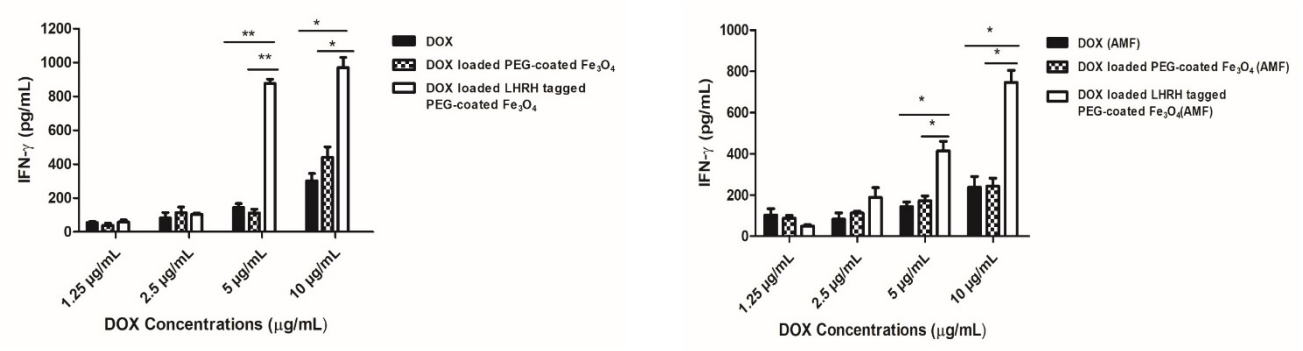

Fig 4.19: Secretion levels of IFN-γ in response to free DOX, DOX loaded PEG -coated Fe_3O_4 and DOX loaded LHRH tagged PEG-coated Fe_3O_4 against A549 cells a) in the absence of magnetic field and **b)** in the presence of magnetic field. Unpaired t-tests were used for comparisons, *P<0.05, **P<0.01, ***P<0.001

a) b)

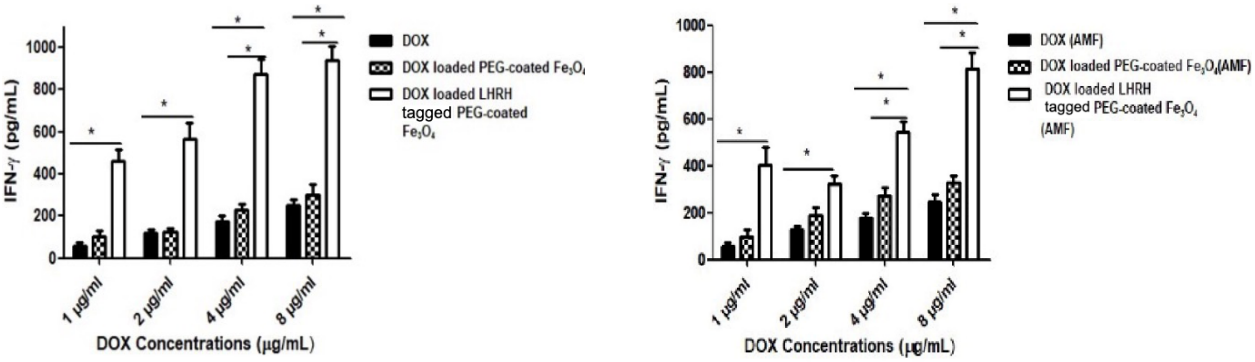

Fig 4.20: Secretion levels of IFN-γ in response to free DOX, DOX loaded PEG -coated Fe_3O_4 and DOX loaded LHRH tagged PEG-coated Fe_3O_4 against MCF-7 cells a) in the absence of magnetic field and b) in the presence of magnetic field. Unpaired t-tests were used for comparisons, *P<0.05, **P<0.01, ***P<0.001

Chapter 5:

Discussion:

Traditional cancer treatments, such as chemotherapy, radiation, and surgery, often damage both cancerous and healthy tissues, making it difficult to target cancer cells effectively while sparing normal cells. One of the critical challenges in cancer therapy is to selectively destroy tumour cells without harming surrounding healthy tissues. Nanotechnology has emerged as a promising solution, offering innovative approaches for cancer treatment. Extensive research has focused on developing nanoparticles with therapeutic potential, particularly magnetic nanoparticles (MNPs), which have exhibited great prospects in both cancer detection and treatment (77).

Magnetic hyperthermia (MHT) is one such application, where heat is generated through magnetic energy losses to selectively kill cancer cells. MNPs can convert electromagnetic energy into heat, raising the temperature of tumour cells to an apoptotic threshold, which leads to their destruction (78,187). By maintaining tumour region temperatures between 40 °C 44 °C, known as mild hyperthermia, researchers have found that the efficacy of chemotherapeutic drugs can be significantly enhanced. However, the precise delivery of both heat and anticancer drugs to tumour sites without impacting healthy tissues remains a significant challenge (79,188,189). Studies have shown the potential of combining chemotherapy with hyperthermia using nanoparticle-based delivery systems, particularly magnetic iron oxide nanoparticles (IONPs) (190). These nanoparticles can be loaded with anticancer drugs and, after localizing within the tumour, it can be remotely heated using an external alternating magnetic field. To increase the specificity of magnetic hyperthermia, researchers are exploring active targeting methods (191). By attaching ligands to the surface of MNPs, these particles can selectively bind to cancer cell receptors, enhancing the accumulation of nanoparticles in tumours and improving treatment effectiveness.

In this study, the LHRH agonist Triptorelin was selected as the ligand for nanoparticle conjugation. LHRH receptors are overexpressed in various cancers, with approximately 50% of estrogen receptor-positive breast tumour exhibiting upregulation of these receptors (192). This presents a significant opportunity for targeted therapy using LHRH analogs like Triptorelin. However, there is limited documentation on the expression of LHRH in human lung adenocarcinoma cells, which are widely studied in non-small cell lung cancer (NSCLC) (6).

The present research focuses on the synthesis of a magnetic drug delivery system designed to induce cytotoxic effects on LHRH-positive cancer cells, with or without the use of an alternating magnetic field (AMF). Additionally, the secretion levels of interferon-gamma (IFN-γ) were measured in cancer cell lines. This dual approach of targeted drug delivery and magnetic hyperthermia may boost cancer treatment results by enhancing specificity and minimizing damage to healthy tissues.

Objective 1: Preparation and characterization of functionalized magnetic nanoparticles (MNPs):

In our study, we used the coprecipitation method to synthesize magnetite nanoparticles with their magnetic traits affected by factors like temperature, pH, and concentration. The coprecipitation method is known for its efficiency, simplicity, high yields, purity, low cost, and production of a large amount of nanoparticles (193,194,195). While magnetite is naturally chemically inert, its functionality can be significantly improved through surface modification using various materials such as poly-ethylene glycol (PEG). These modifications not only broaden its potential applications but also prevent nanoparticle aggregation, which is crucial for maintaining stability. Coating magnetite nanoparticles with biocompatible materials has become a significant area of focus, ensuring safe interaction with biological environments (196). The analysis of as-synthesized nanoparticles involves different characterization techniques such as X-ray diffraction, FTIR, transmission electron microscopy, dynamic light scattering and vibrating sample magnetometer.

X-ray diffraction technique served to evaluate the crystal structure, lattice parameter and crystallite size of Fe_3O_4 nanoparticles. The results revealed that the XRD spectrum of as-synthesized Fe_3O_4 nanoparticles showed distinct peaks corresponding to the inverse spinel cubic structure (169,170,197). No impurity peaks have been observed in the XRD pattern of Fe_3O_4 nanoparticles confirmed the formation of single phase with good crystallinity. It is worth noting that the crystallite size (D) plays a crucial part in the X-ray diffraction. All diffraction profiles exhibit a broad profile distribution as a result of scattering of X-rays from small nanocrystals. The average crystallite size of Fe_3O_4 nanoparticles measured from the peak broadening of the highest intense peak (311) is 9.1 nm. This value is consistent with an earlier report (198). This crystallite size of nanoparticles is below the superparamagnetic limit of Fe_3O_4, suggesting that as-synthesized nanoparticles are single domain and hence

superparamagnetic in nature. This finding is consistent with the results of a previous study, providing further validation of the results obtained from X-ray diffraction study (169). These results suggest that as-synthesized Fe_3O_4 nanoparticles possess excellent crystallinity with small crystallite size, which makes them appropriate for various biomedical purposes.

The HR-TEM image is a powerful tool for analyzing the lattice structure of materials, as it provides a highly detailed and magnified view of the sample. This allowed for an in-depth analysis of the lattice structure of the Fe_3O_4 nanoparticle being examined. Upon careful examination of the high-resolution TEM image (HR-TEM) presented in Fig 4.2(b), it was possible to determine inter planner spacing was approximately 0.49 nm. This measurement is consistent with the d-spacing of the (111) plane of Fe_3O_4, providing strong evidence that the sample under investigation has a crystal structure that matches with Fe_3O_4. Further analysis was conducted using a selected area diffraction pattern, which provided additional evidence of the highly crystalline nature of the Fe_3O_4 nanoparticle. The diffraction rings [(220), (311), (400), (422), (511), and (440)] in the electron diffraction pattern can be indexed as magnetite, (Fig 4.2(c)). collectively, these findings strongly indicate that the nanoparticle being analyzed has a crystal structure that is consistent with magnetite (Fe_3O_4).

The size distribution histograms of hydrodynamic particle sizes of Fe_3O_4 and PEG-coated Fe_3O_4 nanoparticles are shown in Fig 4.4. The hydrodynamic size of Fe_3O_4 and PEG-coated Fe_3O_4 nanoparticles is 87 nm and 118 nm, respectively. Additionally, the polydispersity index of Fe_3O_4 and PEG-coated Fe_3O_4 nanoparticles is 0.31 and 0.25, respectively. The polydispersity index measures the size variation of particles in a sample. A lower value indicates that the particles are more uniformly sized, while a higher value indicates that the particles have a wider range of sizes. The polydispersity index of PEG-coated Fe_3O_4 nanoparticles is lower as compared to the bare nanoparticles. This suggests that PEG functionalization reduces the aggregation of nanoparticles, resulting in more uniform size distribution. These insights are crucial to grasp the properties and potential applications of Fe_3O_4 and PEG-coated Fe_3O_4 nanoparticles.

FTIR spectroscopy was employed as analytical tool of choice to ascertain the presence of PEG-coating on Fe_3O_4 nanoparticles (199). Fig 4.5 showcases the FTIR spectra of three distinct samples: bare Fe_3O_4 nanoparticles, PEG-coated Fe_3O_4 nanoparticles, and PEG-600. The intricate vibrational patterns noticed in Fig 4.5 have been meticulously outlined in Table 4.1 to facilitate comprehensive analysis. The distinct absorption bands observed at 559 and 640 cm^{-1}

in the FTIR spectra match the Fe-O stretching vibrations of bare Fe_3O_4 nanoparticles (168), notably, these observations align closely with established literature (169). Upon PEG-coating of the Fe_3O_4 nanoparticles, a shift in vibrational bands is observed. Specifically, the vibrational band observed at 559 cm^{-1} undergoes a red shift to 540 cm^{-1}, while the band at 640 cm^{-1} experiences a blue shift, moving to 665 cm^{-1}. These shifts in vibrational frequencies serve as indicative markers of the chemical alterations induced by PEG-coating on the surface of Fe_3O_4 nanoparticles.

Furthermore, the FTIR spectra of PEG-600 reveal a prominent absorption band at 989 cm^{-1}, attributable to the C-O-C stretching vibrations of PEG molecule. Interestingly, upon PEG-coating of Fe_3O_4 nanoparticles, this band exhibits a significant red shift, relocating to 1121 cm^{-1}. This observed shift closely mirrors previous studies (198,200), corroborating the consistent behaviour of PEG under varying experimental conditions. Collectively, the shifts in the vibrational frequencies corresponding to Fe-O stretching and C-O-C stretching vibrations in PEG-coated Fe_3O_4 nanoparticles provide compelling evidence of the chemi-adsorption of PEG onto the surface of Fe_3O_4 nanoparticles. These findings not only confirm the successful PEG-coating but also shed light on the underlying molecular interactions governing the surface modification process.

The saturation magnetization (M_S) values of Fe_3O_4 nanoparticles, both before and after PEG coating are 53.36 emu/g and 46.89 emu/g, respectively. The decrease in M_S of PEG-coated Fe_3O_4 nanoparticles can be attributed to the nonmagnetic contribution of PEG to the total mass of coated nanoparticles. This indicates that the PEG coating on Fe_3O_4 nanoparticles could lead to a decrease in magnetic properties. The findings of the study are consistent with previous reports (168,201), which suggest that the drop in saturation magnetization of PEG-coated Fe_3O_4 nanoparticles is cause of the presence of a nonmagnetic PEG layer on the surface of Fe_3O_4 nanoparticles.

Our study aligns well with previous research on the magnetic properties of Fe_3O_4 nanoparticles coated with PEG. For instance, one study found that coating Fe_3O_4 nanoparticles with PEG decreased the saturation magnetization from 77.0 to 49.6 emu/g due to surface modifications (202). Another study observed a decrease in saturation magnetization from 77.16 emu/g to 37.15 emu/g as the PEG content increased from 0 % to 50 %, with zero coercivity indicating no residual magnetism after the external magnetic field was withdrawn (203). Additionally, a separate study revealed that the saturation magnetization of Fe_3O_4 nanoparticles decreased as

the PEG layer thickness increased[R]. Despite this, nanoparticles maintained zero remnant magnetization and coercivity, preserving their superparamagnetic behaviour and high saturation magnetization (204). Similarly, another study reported that the saturation magnetization of Fe_3O_4 nanoparticles were reduced from 62 to 51 emu/g as the PEG weight increased from 1 to 3 g. The magnetization curves exhibited an S-shaped profile under the applied magnetic field, characteristic of superparamagnetic behaviour with zero coercivity (205). Our research highlights significant changes in the magnetic properties of nanoparticles upon surface functionalization with PEG. Specifically, the coercivity of bare nanoparticles decreased from 32.42 Oe to 3.56 Oe, and the remanence dropped from 1.78 emu/g to 0.159 emu/g, indicating reduced clustering of the magnetic nanoparticles. Similarly, another study observed a reduction in coercivity from 2.3 Oe to 1.25 Oe and a decrease in remanence from 0.81 emu/g to 0.54 emu/g, further confirming the impact of PEG functionalization on reducing nanoparticle clustering (206). Overall, our findings are consistent with previous studies, providing valuable insights into the magnetic characteristics of Fe_3O_4 nanoparticles and their potential applications in nanotechnology.

Objective 2: Conjugation of functionalized MNPs with Luteinizing Hormone-Releasing Hormone and anticancer drug Doxorubicin:

In our study, nanostructures were functionalized with Triptorelin to target LHRH receptors on cancer cells, that enables precise delivery of anti-cancer drugs like doxorubicin to cancer cells. The interaction of the LHRH and PEG-coated Fe_3O_4 nanoparticles takes place via carbodiimide reduction reaction, which involves activation of carboxyl groups on the nanoparticles by carbodiimide (commonly EDC, or 1-ethyl-3-(3-dimethylaminopropyl) carbodiimide). This activation converts the carboxyl groups into an active ester intermediate, which then undergoes reaction with the amine groups on the LHRH, forming a stable amide bond and effectively conjugating the LHRH peptide to the PEG-coated Fe_3O_4 nanoparticles (171,207). In our study we utilized doxorubicin (DOX) as anticancer drug. It is a type of anthracycline known for its ability to combat tumour growth in variety of cancer. In general, DOX works by integrating itself between the DNA base pairs, effectively halting the synthesis of DNA and RNA and impeding the replication and transcription processes (208). To investigate the conjugation of LHRH to nanostructure, ATR-FTIR technique is used. For DOX loading on LHRH-tagged nanostructures, UV-visible spectroscopy is used (209).

The ATR-FTIR analysis is a sophisticated analytical technique used to study the chemical bonds in a sample. In this study, the ATR-FTIR analysis revealed that the C=O peak at 1607 cm^{-1}, which matches the carboxylic acid of the PEG-coated Fe_3O_4, has shifted to 1650 cm^{-1}. This shift indicates the formation of the amide bond in the case of LHRH conjugated PEG-coated Fe_3O_4. This is a significant finding because the formation of the amide bond is crucial for the successful conjugation of LHRH to the PEG-coated Fe_3O_4. Furthermore, the sharp peak at 1561 cm^{-1} is attributed to the NH bond of the amide group. This peak is visible in the conjugate (as shown in Fig 4.8), indicating that the amide group is indeed present in the conjugate. This finding is important because it confirms that the LHRH has been successfully conjugated to the PEG-coated Fe_3O_4 through the formation of the amide bond (210,211). Overall, the ATR-FTIR analysis provides valuable insights into the chemistry of the LHRH conjugated PEG-coated Fe_3O_4, which is crucial for understanding its properties and potential applications in nanotechnology.

To investigate the adsorption of DOX on PEG-coated Fe_3O_4, UV-vis spectroscopy was employed. Fe_3O_4 coated with surfactants like PEG exhibits a favourable adsorption capacity. This enhanced capacity can be attributed to the formation of a porous PEG shell, providing additional sites for drug interaction. Furthermore, the length of the polymeric chains covering the particles may also influence their drug loading capacity, with longer PEG chains potentially enabling higher loading capacity on the particle surface. The successful loading of DOX is determined by the physical properties of both the drug and the PEG coated Fe_3O_4 nanoparticles. DOX, being a hydrophobic drug with chemical groups capable of forming electrostatic interactions and hydrogen bonding, can interact with the surface active OH groups in PEG (172). The conjugation of the $–NH_2$ and –OH groups in DOX with the surface active –OH groups in PEG is responsible for the drug loading.

In our study, we achieved doxorubicin drug loading efficiency of 66 % for PEG-600 coated magnetic iron oxide nanoparticles. This is higher compared to the outcomes of Kovrigina et al. (2022) (212), who documented efficiency of 59 % and it is also marginally better than 63.9 % reported by Yallapu et al. (2011) (213). Another study (172) demonstrated that increasing the polyvinyl alcohol (PVA) content enhanced drug loading, with 35 µg, 41 µg, 47 µg, and 58 µg of DOX per mg of carrier being loaded within 26 hours using 0.5 %, 1 %, 2 %, and 5 % PVA, respectively. One of the studies (201) showed folic acid-modified nanoparticles with PEG and (Oleic acid) OA/(Oleylamine) OL coatings had a loading efficiency of 52.5 %. In a separate

study, researchers demonstrated the drug loading efficiency of DOX (Doxorubicin) on PEG-coated Fe_3O_4 nanoparticles. The findings revealed that the Fe_3O_4 nanoparticles achieved a DOX loading percentage of 38.8% (214). In another study, a comparison was made between the loading efficiencies of DOX on PEG 6000-coated Fe_3O_4 nanoparticles over different periods. It was observed that after 48 hours, the loading efficiency was significantly higher, achieving 40.94%, compared to a 24-hour period, which had a loading efficiency of 24.5%. This difference highlights the importance of incubation time in achieving optimal drug loading. The extended exposure period allows more DOX molecules to interact and bind with the nanoparticles, thus increasing the loading efficiency (215). Our drug delivery system not only has higher drug loading efficiency but also benefits from being smaller and lighter, which improves its overall effectiveness. The shortened chain length of PEG- 600 helps them break down quickly into smaller compounds, making it easier for the body to process and clear them.

Objective 3: To study the hyperthermic effect of conjugated MNPs on growth and cytokine release of cancer cells:

We conducted a thorough investigation to determine the optimum frequency and strength of the alternating magnetic field (AMF) required to achieve maximum hyperthermia performance before starting the *in vitro* experiments. The study investigated the magnetic heating effect of nanoparticle conjugates with the nanoTherics magneTherm hyperthermia setup (216). This involved exposing 100 mg/mL nanoparticle conjugates suspensions to a range of frequencies and field strengths. After testing various combinations, the results were carefully evaluated to identify the most effective combination. Ultimately, a frequency of 580.8 kHz, a field strength of 10 mT, and a nanoparticle concentration of 25 mg/mL were selected as the optimal parameters for further experiments. As a result, we utilized this specific magnetic field-frequency combination for all subsequent *in vitro* experiments. The existing research aimed to examine the effect of targeted chemotherapy and magnetic hyperthermia on A549 and MCF-7 cancer cell lines. An MTT assay was used to assess the treatment. After treating the cells with conjugates, the collected supernatant from the cancer cells (A549 & MCF-7) was analysed for IFN-γ cytokine secretion using a sandwich ELISA.

The magnetic hyperthermia efficiency of PEG-coated Fe_3O_4 nanoparticles was assessed across various magnetic field frequencies (162–935.6 kHz), field strengths (5–12 mT), and nanoparticle concentrations (1–100 mg/mL). The temperature increase in an aqueous dispersion of these nanoparticles was monitored over a 20-minute period. The best

hyperthermia performance was observed at a frequency of 935.6 kHz, a field strength of 10 mT, and a concentration of 25 mg/mL. At 580.0 kHz, a temperature rise of 68.15 °C was observed. Since this temperature rise is adequate for hyperthermia applications, we choose a relatively lower frequency (580.0 kHz) of an applied magnetic field for biologically safer applications of these nanoparticles in magnetic hyperthermia.

The kinetic parameter 'k' of Box-Lucas model (Table 4.4) remains constant regardless of the applied field frequency, but it increases with both field strength and nanoparticle concentration. Additionally, the initial slope ($\Delta\theta_s$) of the temperature-time profiles of PEG-coated Fe_3O_4 nanoparticles increases with higher magnetic field frequency, field strength, and nanoparticle concentration. These observed trends in $\Delta\theta_s$ and k align well with previous studies (189, 181, 182).

In our study, the specific loss power (SLP) values of PEG-coated Fe_3O_4 nanoparticles were analysed in relation to magnetic field frequency, field strength, and nanoparticle concentrations, and the results are presented in Table 4.4. It was observed that the SLP value of PEG-coated Fe_3O_4 nanoparticles exhibits a rise with frequency and field strength, while showing a decrease with nanoparticle concentration (Fig 4.12). When examined as a function of frequency, the slope was determined to be 0.41 W/g mL per 100 kHz. It has been established in the literature that interparticle interactions significantly influence the SLP values of nanoparticle suspensions. An increase in nanoparticle concentration leads to heightened dipolar interactions between the nanoparticles, impeding Brownian motion and subsequently resulting in diminished SLP values (212,217-219).

To evaluate the reduction in cell viability of synthesized magnetic drug delivery system, MTT assay was performed on A549 and MCF-7 cell lines. In our study, we observed that both targeted and non-targeted magnetic drug delivery systems exhibited maximum reduction in cell viability when exposed to a magnetic field as in contrast to the same groups when no magnetic field is present, for both A549 and MCF-7 cell lines. The biocompatibility of LHRH-tagged PEG-coated Fe_3O_4 nanoparticles was evident in the MTT assay, as concentrations of 5 mg/mL, 10 mg/mL, 20 mg/mL, and 25 mg/mL did not result in any significant cell viability reduction (0 %, 2 % ,4 %, 11 % for A549 and 1 %, 3 % ,6 %, 13 % for MCF-7 cells, respectively) when there is no magnetic field. However, at concentrations of 20 mg/mL and 25 mg/mL, a significant reduction in cell viability (21 % & 47 % in case of A549 cells and 18 % & 45 % in case of MCF-7 cells, respectively) was observed during exposure to the magnetic field. These

findings underscore the effectiveness of the magnetic field in enhancing the cytotoxicity of the targeted drug delivery system. Our choice of 25 mg/mL concentration was also based on the fact that it can deliver a temperature rise of 44 °C when subject to an alternating magnetic field for 20 min. Earlier studies have reported that a temperature of 44 °C is lethal to cancer cells, leading to apoptosis (142, 220-222). These studies reported that hyperthermia at 44 °C induces apoptosis in cancer cells through several mechanisms. Apoptosis can be initiated by numerous factors such as UV radiation, chemotherapy, and heat. During this process, the cell undergoes morphological changes: it shrinks, its chromatin condenses, and the nucleus fragments (221). Cancer cells exhibit heightened sensitivity to heat due to their elevated metabolic rates and compromised heat shock response systems. The abnormal vasculature within tumours results in inefficient heat dissipation, causing localized hyperthermia. Additionally, the acidic microenvironment of tumours exacerbates heat-induced cellular damage. Hyperthermia also elevates the levels of reactive oxygen species, leading to oxidative stress that damages cancer cells. Furthermore, hyperthermia enhances the efficacy of chemotherapeutic agents by increasing cellular membrane permeability and inhibiting DNA repair mechanisms. Collectively, these factors contribute to the selective cytotoxicity of hyperthermia in cancer cells while minimizing damage to normal tissues (222).

Our study demonstrates that targeted magnetic hyperthermia significantly amplifies the reduction in cell viability induced by doxorubicin, showing 88 % and 91 % reductions in A549 and MCF-7 cells, respectively. This effect is notably stronger compared to nanoparticle-mediated hyperthermia, which resulted in reductions of 47 % for A549 and 45 % for MCF-7, and standalone chemotherapy, which caused 62 % and 57 % reductions for the same cell lines. These results align with those reported by Taratula et al. (2013) (157), who used an LHRH-targeted magnetic drug delivery system to treat the ovarian cancer, achieving a 95 % reduction in cell viability through the combined effects of chemotherapy and magnetic hyperthermia. In their study, chemotherapy alone produced a 27 % reduction, while nanoparticle-mediated mild hyperthermia led to a 72 % reduction. Similarly, Varshosaz et al. (2016) (160) found that drug-loaded poly (methyl vinyl ether maleic acid)/chitosan copolymer, functionalized with LHRH-targeted magnetite nanoparticles, was effective in treating breast cancer under a magnetic field (0.420 T) at 37 °C for 48 hours. Their study showed that, at concentrations of 0.2 and 0.4 μM of DOX, cell survival percentages were lower in both targeted and non-targeted nanoparticle groups when exposed to a magnetic field compared to the absence of the field. At a higher

concentration of 1.6 μM, no significant difference was seen between groups with and without the magnetic field, likely due to the high drug concentration causing substantial cytotoxicity.

Our findings demonstrate that even with a comparatively lower magnetic field strength and shorter duration, magnetic hyperthermia can produce significant therapeutic effects, surpassing those reported in earlier studies (99,100). This highlights the potential of our approach in achieving effective cancer treatment with optimized conditions.

Our study indicates that LHRH-tagged PEG-coated Fe_3O_4nanoparticles used in magnetic hyperthermia can elevate cell temperatures to 44 °C, triggering apoptosis. Specifically, A549 and MCF-7 cells treated with these nanoparticles exhibited cellular shrinkage, unlike the control cells which are exposed only to the magnetic field.

Morphological analysis revealed that, under magnetic hyperthermia, higher DOX concentrations (ranging from 1.25 to 10 μg/mL for A549 cells and 1 to 8 μg/mL for MCF-7 cells) led to more irregular or round-shaped dead cells in suspension and lower cell density in both cell lines. Large cellular debris observed in the micrographs suggests that apoptotic cell death has occurred. This observation aligns well with the MTT assay results (Fig 4.16), which showed that at higher DOX concentration, approximately 88 % and 91 % cell viability reduction in A549 and MCF-7 cells, respectively. These findings indicate that the cells no longer adhered to the surface and appeared in suspension.

Our study is in good accordance with Maity et al. (2010) (100), who showed that optical microscope images of MCF-7 breast cancer cells reveal distinct differences when treated with an AC magnetic field alone versus magnetic hyperthermia using magnetite nanoparticles. The cells subjected to magnetic hyperthermia lost their ability to adhere to the surface and failed to proliferate. In contrast, cells exposed only to the magnetic field remained attached. This observation, further supported by MTT assay results, clearly indicates that the reduction in cell viability is attributable to the magnetic hyperthermia treatment. In a separate study (99), researchers showed that hyperthermia treatment using Fe_3O_4 nanoparticles coated with pluronic reduced the viability of HeLa cells. The treatment was conducted at field strengths of 16 kA/m and 20 kA/m for 15, 30, and 60 minutes. Remarkably, after 30 and 60 minutes of hyperthermia, the HeLa cells displayed noticeable shrinkage.

Interferon-gamma (IFN-γ) plays a pivotal role as a soluble effector molecule in orchestrating anti-tumour immune responses. It exerts its influence by directly inducing cytotoxic or

cytostatic effects on tumour cells, thereby inhibiting their growth and survival (223). Additionally, IFN-γ contributes to promoting tumour cell senescence, further limiting tumour progression and enhancing the body's ability to suppress cancer development (224).The measurement of IFN-γ secretion has revealed its capacity to hinder the growth of various non-hematopoietic cell types, including different tumour types (225,226). This noteworthy characteristic has prompted its consideration as a potential antitumor agent. In our research, we found that LHRH-tagged DOX-loaded PEG-coated Fe_3O_4 nanoparticles led to a marked increase in IFN-γ production, surpassing the levels observed with non-tagged nanoconjugates. This enhancement was seen both when a magnetic field is applied and when it is not. The outcomes reveal that IFN-γ is essential for enhancing the overall effectiveness of anticancer treatments in both cell lines, potentially boosting the therapeutic response.

Several studies have demonstrated IFNγ's ability to suppress the growth of various tumour cell lines, among them related to breast cancer. Study also showed that IFN-γ can augment the growth inhibitory effect of tamoxifen in breast metastatic carcinomas (227,228). These findings underscore the potential synergistic benefits of combining IFN-γ with tamoxifen as a promising therapeutic approach to combat metastatic breast cancer. This study highlights the significance of IFN-γ in the domain of cancer research and its potential applications in targeted treatments for breast cancer. Moreover, IFN-γ's therapeutic promise extends beyond breast cancer. Another study (229) has highlighted its potential in treating metastatic castration-resistant prostate cancer (mCRPC). IFN-γ not only helps target the tumour for immunotherapy but also sensitizes the cancer cells to chemotherapy. This dual effect suggests that IFN-γ could be a critical component in improving treatment outcomes for mCRPC, an especially challenging form of prostate cancer. Through these findings, IFN-γ emerges as a powerful agent in the field of cancer research, offering new possibilities for targeted therapies that could improve the effectiveness of both traditional treatments and emerging immunotherapies.

Chapter 6:

6.1 Summary:

The PEG-coated Fe_3O_4 nanoparticles were successfully synthesized using the chemical coprecipitation method and were found to exhibit superparamagnetic properties, making them ideal candidates for magnetic hyperthermia applications. Furthermore, the FTIR analysis revealed intriguing details about the functionalization of the nanoparticles. Specifically, it showed a shift in the C=O peak from 1607 cm^{-1} to 1650 cm^{-1}, indicating the formation of amide bonds during the conjugation of LHRH to PEG-coated Fe_3O_4. Moreover, the occurrence of a sharp peak at 1561 cm^{-1} in the FTIR spectrum further validated the successful conjugation of LHRH, confirming the presence of −NH bonds. These observations reveal important details about the chemical modifications of the nanoparticles and their potential for targeted drug delivery and other biomedical applications.

The UV-Vis absorption spectrum of the LHRH-conjugated PEG-coated Fe_3O_4 nanoparticles displayed a characteristic peak for doxorubicin (DOX) at 475 nm, accompanied by a blue shift, indicating the successful loading of DOX. The calculated drug loading efficiency of DOX onto these nanoparticles was determined to be 66 %, showcasing the potential of this nanoparticle system for drug delivery applications, particularly for targeted cancer therapies.

To evaluate their potential, the nanoparticle's performance was investigated across a range of magnetic field frequencies, field strengths, and nanoparticle concentrations. The optimal conditions for achieving effective magnetic hyperthermia were identified as a magnetic field frequency of 580.8 kHz, a field strength of 10 mT, and a nanoparticle concentration of 25 mg/mL.

The heating efficiency of these nanoparticles was measured in the context of specific loss power. (SLP), a key parameter that quantifies their ability to generate heat in response to an external magnetic field. It has been noted that the SLP increased linearly with rising magnetic field strength and frequency, indicating that higher frequencies and stronger fields enhanced the output. The SLP value of nanoparticles decreased exponentially as the concentration of nanoparticles. This exponential decline in efficiency is attributed to the increased dipolar interactions between closely packed nanoparticles, which hinder their ability to generate heat independently through Brownian rotation.

PEG-coated Fe_3O_4 nanoparticles demonstrated the capacity to reach the target therapeutic temperature of 44 °C for magnetic hyperthermia within biologically safe limits of field frequency and strength, even when much lower nanoparticle concentrations were used. This ability to achieve the required temperature for effective cancer treatment while minimizing nanoparticle dosage is significant, as it reduces the potential side-effects and enhances biocompatibility.

These findings suggest that the PEG-coated Fe_3O_4 nanoparticles synthesized in this study are suitable for use in cancer hyperthermia therapy, offering both efficient heat generation within safe therapeutic limits, making them promising tools for targeted cancer treatment. In magnetic hyperthermia research, precise experimental conditions were established to achieve optimal results. These conditions included a magnetic field frequency of 580.8 kHz, a field strength of 10 mT, and nanoparticle concentration of 25 mg/mL. To evaluate the biocompatibility of the nanoparticles, MTT assays were conducted on A549 (lung cancer) and MCF-7 (breast cancer) cell lines. The results revealed that both PEG-coated Fe_3O_4 and LHRH tagged PEG-coated Fe_3O_4 nanoparticles did not significantly affect the viability of the cancer cells in the absence of magnetic field exposure. This finding indicates that the nanoparticles themselves, without any external field, are non-toxic and safe for use in biological systems. However, when nanoparticles were used in conjugation with the doxorubicin in the presence of magnetic field, a significant enhancement in therapeutic efficacy was observed. In A549 cells, this combination therapy reduced cell viability by 88 %, which was higher compared to the 62 % reduction seen with DOX chemotherapy alone. A similar pattern emerged in the MCF-7 cell line, where the dual treatment reduced cell viability by 91 %, while DOX on its own achieved a 57 % reduction. These results suggest that by combining magnetic nanoparticles with chemotherapy greatly amplifies the cytotoxic impact on cancer cells.

Further analysis of the cells under a microscope provided insights into the cellular changes induced by increasing DOX concentrations under alternating magnetic field. In both A549 and MCF-7 cell lines, higher concentrations of DOX resulted in a greater number of dead cells, which appeared irregular and rounded. Additionally, the overall cell density decreased, reflecting the extent of cell death. These morphological observations were consistent with the MTT assay data, reinforcing the effectiveness of the combination therapy. To explore the immune response elicited by the treatment, ELISA analysis was performed. This test revealed that LHRH tagged Fe_3O_4, DOX loaded LHRH tagged PEG-coated Fe_3O_4 and PEG-coated Fe_3O_4 nanoparticles significantly boosted the production of interferon-gamma (IFN-γ), a

critical cytokine involved in the immune response against tumours. This increase in IFN-γ was observed regardless of whether the magnetic field was present, and it was much higher in comparison to the response elicited by non-targeted nanoconjugates. The elevated IFN-γ levels were noted in both A549 and MCF-7 cells, suggesting that the targeted nanoparticles not only enhance the direct cytotoxic effect of chemotherapy but also stimulate an immune-mediated antitumor response.

In summary, these findings demonstrate that the integration of targeted magnetic nanoparticles with conventional chemotherapy can substantially improve the therapeutic outcomes in cancer treatment. The combination therapy not only enhances the direct killing of cancer cells but also promotes a robust immune response, particularly through the elevation of IFN-γ. This dual mechanism highlights the potential of using such a strategy to achieve more effective and comprehensive cancer treatment.

6.2 Scope for future work

Magnetic hyperthermia holds significant promise for cancer therapy, but the development of suitable magnetic nanostructures remains a critical challenge for its broader clinical application. Future research should focus on optimizing magnetic hyperthermia therapy by fine-tuning parameters such as magnetic field strength, frequency, and nanoparticle concentration. It is essential to avoid the elevated field strengths and prolonged exposure durations that have been used in previous studies, as these can lead to undesirable side effects.

Additionally, there is a need to investigate other cancer-specific biological markers that can further enhance the targeting capability of magnetic nanoparticles (MNPs). By improving their overall effectiveness and specificity, we can minimize toxicity to healthy tissues. Future studies should also explore investigating the attachment of cancer drugs to LHRH tagged MNPs. This approach could enable targeted detection and destruction of various cancer types, thereby enhancing the precision and efficacy of cancer treatments.

To ensure efficient metabolism and clearance, nanoparticles should be designed using biodegradable and biocompatible materials. Optimizing their size and surface charge is critical to avoid rapid clearance by the reticuloendothelial system (RES) while ensuring renal clearance. Radiolabelling or fluorescence tagging of nanoparticles can be employed to track biodistribution and clearance over extended periods in vivo. Proper surface functionalization

is crucial to prevent nanoparticle aggregation in biological fluids. Additionally, toxicity studies should include histological examinations of key organs (liver, kidneys, heart, and lungs) and inflammatory marker analysis.

In summary, while magnetic hyperthermia shows great potential, its clinical success will depend on the continued development and optimization of magnetic nanostructures, as well as the exploration of new targeting strategies and drug conjugation techniques.

By integrating imaging tools like magnetic resonance imaging (MRI) and fluorescence imaging, we can create truly intelligent theranostics. Future research will likely focus on developing these systems to enable not only noninvasive tracking of drug behaviour in the body but also real-time monitoring of treatment effectiveness. We believe that biomedical nanotechnology especially hyperthermia-based treatments and drug delivery using magnetic nanomaterials will help shift the pharmaceutical industry from a "one-size-fits-all" approach to more personalized medicine.

Future clinical trials in targeted drug delivery need to be conducted to unlock their immense potential for revolutionizing medical treatments. This approach could maximize therapeutic outcomes while minimizing side effects. Conducting such extensive clinical trials could evaluate the safety, efficacy, and long-term effects of targeted drug delivery systems. The valuable data obtained from these trials could support regulatory approvals and clinical adoption. In future studies, it's essential to compare biodegradable and nonbiodegradable carriers to assess their metabolic fates and long-term toxicity profiles. These evaluations will be critical for identifying the most suitable platform for human applications, ensuring both safety and efficacy in clinical settings.

References

(1) Wong, R. S. (2011). Apoptosis in cancer: from pathogenesis to treatment. *Journal of experimental & clinical cancer research*, *30*(1), 1-14.

(2) Warburg, O. (1925). The metabolism of carcinoma cells. *The Journal of Cancer Research*, *9*(1), 148-163.

(3) Bray, F., Laversanne, M., Sung, H., Ferlay, J., Siegel, R. L., Soerjomataram, I., Jemal, A. (2024). Global cancer statistics 2022: GLOBOCAN estimates of incidence and mortality worldwide for 36 cancers in 185 countries. *CA: a cancer journal for clinicians*, *74*(3), 229-263.

(4) International Agency for Research on Cancer. (2024). Global cancer burden growing, amidst mounting need for services. *Saudi Med J*, *45*(3), 326-327.

(5) Ali, A., Goffin, J. R., Arnold, A., & Ellis, P. M. (2013). Survival of patients with non-small-cell lung cancer after a diagnosis of brain metastases. *Current Oncology*, *20*(4), 300-306.

(6) Gridelli, C., Rossi, A., Carbone, D. P., Guarize, J., Karachaliou, N., Mok, T., ... & Rosell, R. (2015). Non-small-cell lung cancer. *Nature reviews Disease primers*, *1*(1), 1-16.

(7) Ong, Y. S., Banobre Lopez, M., Lima, S. A. C., Reis, S. (2020). A multifunctional nanomedicine platform for co-delivering methotrexate and mild hyperthermia towards breast cancer therapy. *Materials Science and Engineering: C*, *116*, 111255.

(8) Juthani, R., Punatar, S., & Mittra, I. (2024). New light on chemotherapy toxicity and its prevention. *BJC Reports*, *2*(1), 41.

(9) Alnaim, L. (2007). Therapeutic drug monitoring of cancer chemotherapy. *Journal of Oncology Pharmacy Practice*, *13*(4), 207-221.

(10) Ramalingam, P., Prabakaran, D. S., Sivalingam, K., Nallal, V. U. M., Razia, M., Patel, M., Krishnamoorthy, D. (2022). Recent advances in nanomaterials-based drug delivery system for cancer treatment. *Emerging Nanomaterials for Advanced Technologies*, 83-116.

(11) Chang, D., Lim, M., Goos, J. A., Qiao, R., Ng, Y. Y., Mansfeld, F. M., Kavallaris, M. (2018). Biologically targeted magnetic hyperthermia: Potential and limitations. *Frontiers in pharmacology*, *9*, 831.

(12) Behrouzkia, Z., Joveini, Z., Keshavarzi, B., Eyvazzadeh, N., Aghdam, R. Z. (2016). Hyperthermia: how can it be used?. *Oman medical journal*, *31*(2), 89.

(13) Baronzio, G., Parmar, G., Ballerini, M., Szasz, A., Baronzio, M., Cassutti, V. (2014). A brief overview of hyperthermia in cancer treatment. *J Integr Oncol*, *3*(115), 2.

(14) Dürr, S., Janko, C., Lyer, S., Tripal, P., Schwarz, M., Zaloga, J., Alexiou, C. (2013). Magnetic nanoparticles for cancer therapy. *Nanotechnology Reviews*, *2*(4), 395-409.

(15) Fatima, H., Charinpanitkul, T., Kim, K. S. (2021). Fundamentals to apply magnetic nanoparticles for hyperthermia therapy. *Nanomaterials*, *11*(5), 1203.

(16) Gavas, S., Quazi, S., Karpiński, T. M. (2021). Nanoparticles for cancer therapy: current progress and challenges. *Nanoscale research letters*, *16*(1), 173.

(17) Jose, J., Kumar, R., Harilal, S., Mathew, G. E., Parambi, D. G. T., Prabhu, A., Mathew, B. (2020). Magnetic nanoparticles for hyperthermia in cancer treatment: an emerging tool. *Environmental Science and Pollution Research*, *27*, 19214-19225.

(18) Guibert, C., Dupuis, V., Peyre, V., Fresnais, J. (2015). Hyperthermia of magnetic nanoparticles: experimental study of the role of aggregation. *The Journal of Physical Chemistry C*, *119*(50), 28148-28154.

(19) Yoo, D., Jeong, H., Noh, S. H., Lee, J. H., & Cheon, J. (2013). Magnetically triggered dual functional nanoparticles for resistance-free apoptotic hyperthermia. *Angewandte Chemie International Edition*, *52*(49), 13047-13051.

(20) Tran, P. H. L., Tran, T. T. D., Vo, T. V., & Lee, B. J. (2012). Promising iron oxide-based magnetic nanoparticles in biomedical engineering. *Archives of Pharmacal Research*, *35*, 2045-2061.

(21) Liu, X., Zhang, Y., Wang, Y., Zhu, W., Li, G., Ma, X., Liang, X. J. (2020). Comprehensive understanding of magnetic hyperthermia for improving antitumor therapeutic efficacy. *Theranostics*, *10*(8), 3793.

(22) Niculescu, A. G., Grumezescu, A. M. (2022). Novel tumor-targeting nanoparticles for cancer treatment—A review. *International Journal of Molecular Sciences*, *23*(9), 5253.

(23) Wu, J. (2021). The enhanced permeability and retention (EPR) effect: the significance of the concept and methods to enhance its application. *Journal of personalized medicine*, *11*(8), 771.

(24) Chen, Z., Kankala, R. K., Long, L., Xie, S., Chen, A., & Zou, L. (2023). Current understanding of passive and active targeting nanomedicines to enhance tumor accumulation. *Coordination Chemistry Reviews*, *481*, 215051.

(25) Jani, R. K., & Krupa, G. (2019). Active targeting of nanoparticles: An innovative technology for drug delivery in cancer therapeutics. *Journal of Drug Delivery and Therapeutics*, *9*(1-s), 408-415.

(26) Giustini, A. J., Petryk, A. A., Cassim, S. M., Tate, J. A., Baker, I. A. N., & Hoopes, P. J. (2010). Magnetic nanoparticle hyperthermia in cancer treatment. *Nano Life*, *1*(01n02), 17-32.

(27) Yoo, J., Park, C., Yi, G., Lee, D., & Koo, H. (2019). Active targeting strategies using biological ligands for nanoparticle drug delivery systems. *Cancers*, *11*(5), 640.

(28) Srivastava, N., Chudasama, B., Baranwal, M. (2022). Advancement in magnetic hyperthermia-based targeted therapy for cancer treatment. *Biointerphases*, *18*(6).

(29) Venturelli, M., Guaitoli, G., Omarini, C., Moscetti, L. (2018). Spotlight on triptorelin in the treatment of premenopausal women with early-stage breast cancer. *Breast Cancer: Targets and Therapy*, 39-49.

(30) Nagy, A., & Schally, A. V. (2005). Targeting of cytotoxic luteinizing hormone-releasing hormone analogs to breast, ovarian, endometrial, and prostate cancers. *Biology of reproduction*, *73*(5), 851-859.

(31) Li, X., Taratula, O., Taratula, O., Schumann, C., & Minko, T. (2017). LHRH-targeted drug delivery systems for cancer therapy. *Mini reviews in medicinal chemistry*, *17*(3), 258-267.

(32) Huerta-Reyes, M., Maya-Núñez, G., Pérez-Solis, M. A., López-Muñoz, E., Guillén, N., Olivo-Marin, J. C., Aguilar-Rojas, A. (2019). Treatment of breast cancer with gonadotropin-releasing hormone analogs. *Frontiers in Oncology*, *9*, 943.

(33) Feitelson, M. A., Arzumanyan, A., Kulathinal, R. J., Blain, S. W., Holcombe, R. F., Mahajna, J., Nowsheen, S. (2015). Sustained proliferation in cancer: Mechanisms and novel therapeutic targets. In *Seminars in cancer biology*,35, 25-54.

(34) Hanahan, D.,Weinberg, R. A. (2011). Hallmarks of cancer: the next generation. *cell*, *144*(5), 646-674.

(35) Siegel, R., Ma, J., Zou, Z., Jemal, A. (2014). Cancer statistics, 2014. *CA: a cancer journal for clinicians*, *64*(1).

(36) Zappa, C., Mousa, S. A. (2016). Non-small cell lung cancer: current treatment and future advances. *Translational lung cancer research*, *5*(3), 288.

(37) Sher, T., Dy, G. K., & Adjei, A. A. (2008, March). Small cell lung cancer. In *Mayo Clinic Proceedings*,83,355-367.

(38) Kenfield, S. A., Wei, E. K., Stampfer, M. J., Rosner, B. A., Colditz, G. A. (2008). Comparison of aspects of smoking among the four histological types of lung cancer. *Tobacco control*, *17*(3), 198-204.

(39) Noguchi, M., Morikawa, A., Kawasaki, M., Matsuno, Y., Yamada, T., Hirohashi, S., Shimosato, Y. (1995). Small adenocarcinoma of the lung. Histologic characteristics and prognosis. *Cancer*, *75*(12), 2844-2852.

(40) Singh, A., Kant, R., Saluja, T. S., Tripathi, T., Srivastava, K., Naithani, M., Singh, S. K. (2020). Differential diagnosis of non-small cell lung carcinoma by circulating microRNA. *Journal of cancer research and therapeutics*, *16*(1), 127-131.

(41) Chakraborty, S., Ganti, A. K., Marr, A., & Batra, S. K. (2010). Lung cancer in women: role of estrogens. *Expert review of respiratory medicine*, *4*(4), 509-518.

(42) He, M., Yu, W., Chang, C., Miyamoto, H., Liu, X., Jiang, K., & Yeh, S. (2020). Estrogen receptor α promotes lung cancer cell invasion via increase of and cross-talk with infiltrated macrophages through the CCL2/CCR2/MMP9 and CXCL12/CXCR4 signaling pathways. *Molecular Oncology*, *14*(8), 1779-1799.

(43) Omoto, Y., Kobayashi, Y., Nishida, K., Tsuchiya, E., Eguchi, H., Nakagawa, K., Hayashi, S. I. (2001). Expression, function, and clinical implications of the estrogen receptor β in human lung cancers. *Biochemical and biophysical research communications*, *285*(2), 340-347.

(44) Chen, P., Li, B., & Ou-Yang, L. (2022). Role of estrogen receptors in health and disease. *Frontiers in endocrinology*, *13*, 839005.

(45) Burguin, A., Diorio, C., & Durocher, F. (2021). Breast cancer treatments: updates and new challenges. *Journal of personalized medicine*, *11*(8), 808.

(46) Belury, M. A., Cole, R. M., Andridge, R., Keiter, A., Raman, S. V., Lustberg, M. B., Kiecolt-Glaser, J. K. (2021). Erythrocyte Long-Chain ω-3 Fatty Acids Are Positively Associated with Lean Mass and Grip Strength in Women with Recent Diagnoses of Breast Cancer. The Journal of nutrition, 151(8), 2125-2133.

(47) Gao, J. J., Swain, S. M. (2018). Luminal a breast cancer and molecular assays: a review. *The oncologist*, *23*(5), 556-565.

(48) Yersal, O., Barutca, S. (2014). Biological subtypes of breast cancer: Prognostic and therapeutic implications. *World journal of clinical oncology*, *5*(3), 412.

(49) Ades, F., Zardavas, D., Bozovic-Spasojevic, I., Pugliano, L., Fumagalli, D., De Azambuja, E., Piccart, M. (2014). Luminal B breast cancer: molecular characterization, clinical management, and future perspectives. *Journal of clinical oncology*, *32*(25), 2794-2803.

(50) Sørlie, T., Perou, C. M., Tibshirani, R., Aas, T., Geisler, S., Johnsen, H., Børresen-Dale, A. L. (2001). Gene expression patterns of breast carcinomas distinguish tumor subclasses with clinical implications. *Proceedings of the National Academy of Sciences*, *98*(19), 10869-10874.

(51) Tran, B., & Bedard, P. L. (2011). Luminal-B breast cancer and novel therapeutic targets. *Breast Cancer Research*, *13*(6), 221.

(52) Bhat, Y., Thrishna, M. R., & Banerjee, S. (2023). Molecular targets and therapeutic strategies for triple-negative breast cancer. *Molecular Biology Reports*, *50*(12), 10535-10577.

(53) Pellegrino, B., Hlavata, Z., Migali, C., De Silva, P., Aiello, M., Willard-Gallo, K., Solinas, C. (2021). Luminal breast cancer: Risk of recurrence and tumor-associated immune suppression. *Molecular Diagnosis & Therapy*, *25*(4), 409-424.

(54) Patani, N., Martin, L. A., & Dowsett, M. (2013). Biomarkers for the clinical management of breast cancer: international perspective. *International journal of cancer*, *133*(1), 1-13.

(55) Dowsett, M., Houghton, J., Iden, C., Salter, J., Farndon, J., A'hern, R., Baum, M. (2006). Benefit from adjuvant tamoxifen therapy in primary breast cancer patients according oestrogen receptor, progesterone receptor, EGF receptor and HER2 status. *Annals of Oncology*, *17*(5), 818-826.

(56) Cho, N. (2021). Imaging features of breast cancer molecular subtypes: state of the art. *Journal of pathology and translational medicine*, *55*(1), 16.

(57) Knight, S. R., Shaw, C. A., Pius, R., Drake, T. M., Norman, L., Ademuyiwa, A. O., Fermani, C. G. (2021). Global variation in postoperative mortality and complications after cancer surgery: a multicentre, prospective cohort study in 82 countries. *The Lancet*, *397*(10272), 387-397.

(58) Keshri, S., & Biswas, S. (2022). Synthesis, physical properties, and biomedical applications of magnetic nanoparticles: a review. *Progress in Biomaterials*, *11*(4), 347-372.

(59) Mondal, J., Panigrahi, A. K., & Khuda-Bukhsh, A. R. (2014). Conventional chemotherapy: problems and scope for combined therapies with certain herbal products and dietary supplements. *Austin J Mol Cell Biol*, *1*(1), 1-10.

(60) Gyanani, V., Haley, J. C., & Goswami, R. (2021). Challenges of current anticancer treatment approaches with focus on liposomal drug delivery systems. *Pharmaceuticals*, *14*(9), 835.

(61) Minchinton, A. I., & Tannock, I. F. (2006). Drug penetration in solid tumours. *Nature Reviews Cancer*, *6*(8), 583-592.

(62) Ioele, G., Chieffallo, M., Occhiuzzi, M. A., De Luca, M., Garofalo, A., Ragno, G., Grande, F. (2022). Anticancer drugs: recent strategies to improve stability profile, pharmacokinetic and pharmacodynamic properties. *Molecules*, *27*(17), 5436.

(63) Mollaei, M., Hassan, Z. M., Khorshidi, F., & Langroudi, L. (2021). Chemotherapeutic drugs: Cell death-and resistance-related signaling pathways. Are they really as smart as the tumor cells? *Translational Oncology*, *14*(5), 101056.

(64) Cheng, Y., Weng, S., Yu, L., Zhu, N., Yang, M., Yuan, Y. (2019). The role of hyperthermia in the multidisciplinary treatment of malignant tumors. *Integrative cancer therapies*, *18*.

(65) Hofer, K. G. (2002). Hyperthermia and cancer. *Eur Cells Mater*, *3*(12), 915-7.

(66) Fatehi, D., Zee, J., Notenboom, A., Rhoon, G. C. (2007). Comparison of intratumor and intraluminal temperatures during locoregional deep hyperthermia of pelvic tumors. *Strahlentherapie und Onkologie*, *183*(9), 479-486.

(67) Sharma, P. K., Malviya, R. (2016). Hyperthermia: role and risk factor for cancer treatment. *Achievements in the life sciences*, *10*(2), 161-167.

(68) Sethi, M., Chakarvarti, S. K. (2015). Hyperthermia techniques for cancer treatment: A review. *Int. J. PharmTech Res*, *8*(6), 292-299.

(69) Falk, M. H., Issels, R. D. (2001). Hyperthermia in oncology. *International Journal of Hyperthermia*, *17*(1), 1-18.

(70) Landon, C. D., Benjamin, S. E., Ashcraft, K. A., Dewhirst, M. W. (2013). A role for the copper transporter Ctr1 in the synergistic interaction between hyperthermia and cisplatin treatment. *International Journal of Hyperthermia*, *29*(6), 528-538.

(71) Choi, E. K., Park, S. R., Lee, J. H., Chung, H. S., Ahn, H. E., Rhee, Y. H., Park, H. J. (2003). Induction of apoptosis by carboplatin and hyperthermia alone or combined in WERI human retinoblastoma cells. *International journal of hyperthermia*, *19*(4), 431-443.

(72) Zhang, J. F., Yan, X. M., Lan, B., Lei, Y. R., Li, X. H., Gao, S., Guo, F. (2016). Molecular mechanisms of synergistic induction of apoptosis by the combination therapy with hyperthermia and cisplatin in prostate cancer cells. *Biochemical and biophysical research communications*, *479*(2), 159-165.

(73) Chae, S. Y., Kim, Y. S., Park, M. J., Yang, J., Park, H., Namgung, M. S., Lim, H. K. (2014). High-intensity focused ultrasound-induced, localized mild hyperthermia to enhance anti-cancer efficacy of systemic doxorubicin: an experimental study. *Ultrasound in Medicine & Biology*, *40*(7), 1554-1563.

(74) Tang, Y., McGoron, A. J. (2013). Increasing the rate of heating: a potential therapeutic approach for achieving synergistic tumour killing in combined hyperthermia and chemotherapy. *International Journal of Hyperthermia*, *29*(2), 145-155.

(75) Veltsista, P. D., Oberacker, E., Ademaj, A., Corradini, S., Eckert, F., Flörcken, A., Ghadjar, P. (2023). Hyperthermia in the treatment of high-risk soft tissue sarcomas: a systematic review. *International Journal of Hyperthermia*, *40*(1), 2236337.

(76) Klimanov, M. Y., Syvak, L. A., Orel, V. E., Lavryk, G. V., Tarasenko, T. Y., Orel, V. B., Nesterenko, A. O. (2018). Efficacy of combined regional inductive moderate hyperthermia and chemotherapy in patients with multiple liver metastases from breast cancer. *Technology in cancer research & treatment*, *17*, 1533033818806003.

(77) Liu, J. F., Jang, B., Issadore, D., Tsourkas, A. (2019). Use of magnetic fields and nanoparticles to trigger drug release and improve tumor targeting. *Wiley Interdisciplinary Reviews: Nanomedicine and Nanobiotechnology*, *11*(6), e1571.

(78) Cole, A. J., Yang, V. C., David, A. E. (2011). Cancer theranostics: the rise of targeted magnetic nanoparticles. *Trends in biotechnology*, *29*(7), 323-332.

(79) Gilchrist, R. K., Medal, R., Shorey, W. D., Hanselman, R. C., Parrott, J. C., Taylor, C. B. (1957). Selective inductive heating of lymph nodes. *Annals of surgery*, *146*(4), 596-606.

(80) Yadollahpour, A., Hosseini, S. A., Yadollahpour, A. (2016). Magnetic nanoparticle-based hyperthermia: A review of the physiochemical properties and synthesis methods. *Int J Pharm Res Allied Sci*, *5*(2), 242-246.

(81) Gavilán, H., Avugadda, S. K., Fernández-Cabada, T., Soni, N., Cassani, M., Mai, B. T., Pellegrino, T. (2021). Magnetic nanoparticles and clusters for magnetic hyperthermia: optimizing their heat performance and developing combinatorial therapies to tackle cancer. *Chemical Society Reviews*, *50*(20), 11614-11667.

(82) Rajan, A., & Sahu, N. K. (2020). Review on magnetic nanoparticle-mediated hyperthermia for cancer therapy. *Journal of Nanoparticle Research*, *22*, 1-25.

(83) Obaidat, I. M., Narayanaswamy, V., Alaabed, S., Sambasivam, S., Muralee Gopi, C. V. (2019). Principles of magnetic hyperthermia: a focus on using multifunctional hybrid magnetic nanoparticles. *Magnetochemistry*, *5*(4), 67.

(84) Shaterabadi, Z., Nabiyouni, G., Soleymani, M. (2018). Physics responsible for heating efficiency and self-controlled temperature rise of magnetic nanoparticles in magnetic hyperthermia therapy. *Progress in biophysics and molecular biology*, *133*, 9-19.

(85) Gupta, R., Kaur, T., Chauhan, A., Kumar, R., Kuanr, B. K., Sharma, D. (2022). Tailoring nanoparticles design for enhanced heating efficiency and improved magneto-chemo therapy for glioblastoma. *Biomaterials Advances*, *139*, 213021.

(86) Yu, X., Yang, R., Wu, C., Liu, B., Zhang, W. (2022). The heating efficiency of magnetic nanoparticles under an alternating magnetic field. *Scientific Reports*, *12*(1), 16055.

(87) Sharma, R., Chen, C. J. (2009). Newer nanoparticles in hyperthermia treatment and thermometry. *Journal of Nanoparticle Research*, *11*, 671-689.

(88) Kaur, P., Aliru, M. L., Chadha, A. S., Asea, A., Krishnan, S. (2016). Hyperthermia using nanoparticles–promises and pitfalls. *International Journal of Hyperthermia*, *32*(1), 76-88.

(89) Martinkova, P., Brtnicky, M., Kynicky, J., Pohanka, M. (2018). Iron oxide nanoparticles: innovative tool in cancer diagnosis and therapy. *Advanced healthcare materials*, *7*(5), 1700932.

(90) Besenhard, M. O., LaGrow, A. P., Hodzic, A., Kriechbaum, M., Panariello, L., Bais, G., Gavriilidis, A. (2020). Co-precipitation synthesis of stable iron oxide nanoparticles with NaOH: New insights and continuous production via flow chemistry. *Chemical Engineering Journal*, *399*, 125740.

(91) Park, J. Y., Daksha, P., Lee, G. H., Woo, S., Chang, Y. (2008). Highly water-dispersible PEG surface modified ultra small superparamagnetic iron oxide nanoparticles useful for target-specific biomedical applications. *Nanotechnology*, *19*(36), 365603.

(92) Zhu, N., Ji, H., Yu, P., Niu, J., Farooq, M. U., Akram, M. W., Niu, X. (2018). Surface modification of magnetic iron oxide nanoparticles. *Nanomaterials*, *8*(10), 810.

(93) Quinto, C. A., Mohindra, P., Tong, S., Bao, G. (2015). Multifunctional superparamagnetic iron oxide nanoparticles for combined chemotherapy and hyperthermia cancer treatment. *Nanoscale*, *7*(29), 12728-12736.

(94) Prijic, S., & Sersa, G. (2011). Magnetic nanoparticles as targeted delivery systems in oncology. *Radiology and oncology*, *45*(1), 1-16.

(95) Belyanina, I., Kolovskaya, O., Zamay, S., Gargaun, A., Zamay, T., Kichkailo, A. (2017). Targeted magnetic nanotheranostics of cancer. *Molecules*, *22*(6), 975.

(96) Sudame, A., Kandasamy, G.,Maity, D. (2019). Single and dual surfactants coated hydrophilic superparamagnetic iron oxide nanoparticles for magnetic fluid hyperthermia applications. *Journal of nanoscience and nanotechnology*, *19*(7), 3991-3999.

(97) Vassallo, M., Martella, D., Barrera, G., Celegato, F., Coïsson, M., Ferrero, R., Manzin, A. (2023). Improvement of hyperthermia properties of iron oxide nanoparticles by surface coating. *ACS omega*, *8*(2), 2143-2154.

(98) Rajan, A., Sharma, M., & Sahu, N. K. (2020). Assessing magnetic and inductive thermal properties of various surfactants functionalised Fe_3O_4 nanoparticles for hyperthermia. *Scientific reports*, *10*(1), 15045.

(99) Tomitaka, A., Yamada, T., & Takemura, Y. (2012). Magnetic nanoparticle hyperthermia using Pluronic-coated Fe_3O_4 nanoparticles: an in vitro study. *Journal of Nanomaterials*, *2012*, 1-5.

(100) Maity, D., Chandrasekharan, P., Yang, C. T., Chuang, K. H., Shuter, B., Xue, J. M., Feng, S. S. (2010). Facile synthesis of water-stable magnetite nanoparticles for clinical MRI and magnetic hyperthermia applications. *Nanomedicine*, *5*(10), 1571-1584.

(101) Demirci, H., Slimani, N., Pawar, M., Kumon, R. E., Vaishnava, P.,Besirli, C. G. (2019). Magnetic hyperthermia in Y79 retinoblastoma and ARPE-19 retinal epithelial cells: tumor selective apoptotic activity of iron oxide nanoparticle. *Translational Vision Science & Technology*, *8*(5), 18-18.

(102) Peer D, Karp JM, Hong S, Farokhzad OC, Margalit R, Langer R: Nanocarriers as an emerging platform for cancer therapy. *Nature nanotechnology* 2007, 2(12):751.

(103) Li Z, Ye E, Lakshminarayanan R, Loh XJ: Recent advances of using hybrid nanocarriers in remotely controlled therapeutic delivery. *Small* 2016, 12(35):4782-4806.

(104) Lee, J. H., Jang, J. T., Choi, J. S., Moon, S. H., Noh, S. H., Kim, J. W., Cheon, J. (2011). Exchange-coupled magnetic nanoparticles for efficient heat induction. *Nature nanotechnology*, *6*(7), 418-422.

(105) Sun, L., Liu, H., Ye, Y., Lei, Y., Islam, R., Tan, S.,Cai, L. (2023). Smart nanoparticles for cancer therapy. *Signal transduction and targeted therapy*, *8*(1), 418.

(106) Chehelgerdi, M., Chehelgerdi, M., Allela, O. Q. B., Pecho, R. D. C., Jayasankar, N., Rao, D. P.,Akhavan-Sigari, R. (2023). Progressing nanotechnology to improve targeted cancer treatment: overcoming hurdles in its clinical implementation. *Molecular cancer*, *22*(1), 169.

(107) Shen, X., Pan, D., Gong, Q., Gu, Z., Luo, K. (2024). Enhancing drug penetration in solid tumors via nanomedicine: Evaluation models, strategies and perspectives. *Bioactive Materials*, *32*, 445-472.

(108) Lorscheider, M., Gaudin, A., Nakhlé, J., Veiman, K. L., Richard, J., Chassaing, C. (2021). Challenges and opportunities in the delivery of cancer therapeutics: Update on recent progress. *Therapeutic Delivery*, *12*(1), 55-76.

(109) Nasongkla, N., Bey, E., Ren, J., Ai, H., Khemtong, C., Guthi, J. S., Gao, J. (2006). Multifunctional polymeric micelles as cancer-targeted, MRI-ultrasensitive drug delivery systems. *Nano letters*, *6*(11), 2427-2430.

(110) Zhou, J., Li, J., Ding, X., Liu, J., Luo, Z., Liu, Y., Cai, K. (2015). Multifunctional Fe2O3@ PPy-PEG nanocomposite for combination cancer therapy with MR imaging. *Nanotechnology*, *26*(42), 425101.

(111) Choukrani, G., Maharjan, B., Park, C. H., Kim, C. S., Sasikala, A. R. K. (2020). Biocompatible superparamagnetic sub-micron vaterite particles for thermo-chemotherapy: From controlled design to in vitro anticancer synergism. *Materials Science and Engineering: C*, *106*, 110226.

(112) Albarqi, H. A., Wong, L. H., Schumann, C., Sabei, F. Y., Korzun, T., Li, X.,Taratula, O. (2019). Biocompatible nanoclusters with high heating efficiency for systemically delivered magnetic hyperthermia. *ACS nano*, *13*(6), 6383-6395.

(113) Li, M., Bu, W., Ren, J., Li, J., Deng, L., Gao, M., Wang, P. (2018). Enhanced synergism of thermo-chemotherapy for liver cancer with magnetothermally responsive nanocarriers. *Theranostics*, *8*(3), 693.

(114) Wust, P., Gneveckow, U., Wust, P., Gneveckow, U., Johannsen, M., Böhmer, D.,Jordan, A. (2006). Magnetic nanoparticles for interstitial thermotherapy–feasibility, tolerance and achieved temperatures. *International Journal of Hyperthermia*, *22*(8), 673-685.

(115) Gupta, R., Chauhan, A., Kaur, T., Kuanr, B. K., Sharma, D. (2022). Transmigration of magnetite nanoparticles across the blood–brain barrier in a rodent model: influence of external and alternating magnetic fields. *Nanoscale*, *14*(47), 17589-17606.

(116) Wani, K. D., Kadu, B. S., Mansara, P., Gupta, P., Deore, A. V., Chikate, R. C., Kaul-Ghanekar, R. (2014). Synthesis, characterization and in vitro study of biocompatible cinnamaldehyde functionalized magnetite nanoparticles (CPGF Nps) for hyperthermia and drug delivery applications in breast cancer. *PloS one*, *9*(9), e107315.

(117) Nigam, S.,Bahadur, D. (2017). Dendrimer-conjugated iron oxide nanoparticles as stimuli-responsive drug carriers for thermally-activated chemotherapy of cancer. *Colloids and Surfaces B: Biointerfaces*, *155*, 182-192.

(118) Sato, I., Umemura, M., Mitsudo, K., Kioi, M., Nakashima, H., Iwai, T., Ishikawa, Y. (2014). Hyperthermia generated with ferucarbotran (Resovist®) in an alternating magnetic field enhances cisplatin-induced apoptosis of cultured human oral cancer cells. *The journal of physiological sciences*, *64*, 177-183.

(119) Kumar, S., Daverey, A., Sahu, N. K., Bahadur, D. (2013). In vitro evaluation of PEGylated mesoporous $MgFe_2O_4$ magnetic nanoassemblies (MMNs) for chemo-thermal therapy. *Journal of Materials Chemistry B*, *1*(30), 3652-3660.

(120) Loomis, K., McNeeley, K., & Bellamkonda, R. V. (2011). Nanoparticles with targeting, triggered release, and imaging functionality for cancer applications. *Soft Matter*, *7*(3), 839-856.

(121) Wu, M., Huang, S. (2017). Magnetic nanoparticles in cancer diagnosis, drug delivery and treatment. *Molecular and clinical oncology*, *7*(5), 738-746.

(122) Attia, M. F., Anton, N., Wallyn, J., Omran, Z., Vandamme, T. F. (2019). An overview of active and passive targeting strategies to improve the nanocarriers efficiency to tumour sites. *Journal of Pharmacy and Pharmacology*, *71*(8), 1185-1198.

(123) Malik, A., Tahir Butt, T., Zahid, S., Zahid, F., Waquar, S., Rasool, M., .Qazi, A. M. (2017). Use of magnetic nanoparticles as targeted therapy: theranostic approach to treat and diagnose cancer. *Journal of Nanotechnology*, 2017,8.

(124) Byrne, J. D., Betancourt, T., Brannon-Peppas, L. (2008). Active targeting schemes for nanoparticle systems in cancer therapeutics. *Advanced drug delivery reviews*, *60*(15), 1615-1626.

(125) Bazak, R., Houri, M., El Achy, S., Kamel, S., Refaat, T. (2015). Cancer active targeting by nanoparticles: a comprehensive review of literature. *Journal of cancer research and clinical oncology*, *141*, 769-784.

(126) Ganipineni, L. P., Ucakar, B., Joudiou, N., Riva, R., Jérôme, C., Gallez, B., Préat, V. (2019). Paclitaxel-loaded multifunctional nanoparticles for the targeted treatment of glioblastoma. *Journal of drug targeting*, *27*(5-6), 614-623.

(127) Gomes, J. A. P., Amankwah, R., Powell-Richards, A., Dua, H. S. (2004). Sodium hyaluronate (hyaluronic acid) promotes migration of human corneal epithelial cells in vitro. *British journal of ophthalmology*, *88*(6), 821-825.

(128) Liu, D., Hong, Y., Li, Y., Hu, C., Yip, T. C., Yu, W. K., Yang, M. (2020). Targeted destruction of cancer stem cells using multifunctional magnetic nanoparticles that enable combined hyperthermia and chemotherapy. *Theranostics*, *10*(3), 1181.

(129) Zhao, W., Li, Y., Zhang, X. (2017). Stemness-related markers in cancer. *Cancer translational medicine*, *3*(3), 87.

(130) Yang, S. J., Tseng, S. Y., Wang, C. H., Young, T. H., Chen, K. C., & Shieh, M. J. (2020). Magnetic nanomedicine for CD133-expressing cancer therapy using locoregional hyperthermia combined with chemotherapy. *Nanomedicine*, *15*(26), 2543-2561.

(131) Liu, D., Li, X., Chen, C., Li, C., Zhou, C., Zhang, W., Chen, L. (2018). Target-specific delivery of oxaliplatin to HER2-positive gastric cancer cells in vivo using oxaliplatin-au- Fe_3O_4 -herceptin nanoparticles. *Oncology Letters*, *15*(5), 8079-8087.

(132) Gawęda, W., Osial, M., Żuk, M., Pękała, M., Bilewicz, A., Krysinski, P. (2020). Lanthanide-doped SPIONs bioconjugation with trastuzumab for potential multimodal anticancer activity and magnetic hyperthermia. *Nanomaterials*, *10*(2), 288.

(133) Jaidev, L. R., Chellappan, D. R., Bhavsar, D. V., Ranganathan, R., Sivanantham, B., Subramanian, A., Sethuraman, S. (2017). Multi-functional nanoparticles as theranostic agents for the treatment & imaging of pancreatic cancer. *Acta Biomaterialia*, *49*, 422-433.

(134) Minaei, S. E., Khoei, S., Khoee, S., Vafashoar, F., Mahabadi, V. P. (2019). In vitro anti-cancer efficacy of multi-functionalized magnetite nanoparticles combining alternating magnetic hyperthermia in glioblastoma cancer cells. *Materials Science and Engineering: C*, *101*, 575-587.

(135) Ha, P. T., Le, T. T. H., Bui, T. Q., Pham, H. N., Ho, A. S., Nguyen, L. T. (2019). Doxorubicin release by magnetic inductive heating and in vivo hyperthermia-chemotherapy combined cancer treatment of multifunctional magnetic nanoparticles. *New Journal of Chemistry*, *43*(14), 5404-5413.

(136) Balasubramanian, S., Girija, A. R., Nagaoka, Y., Iwai, S., Suzuki, M., Kizhikkilot, V., Nair, S. D. (2014). Curcumin and 5-fluorouracil-loaded, folate-and transferrin-decorated polymeric magnetic nanoformulation: a synergistic cancer therapeutic approach, accelerated by magnetic hyperthermia. *International journal of nanomedicine*,9, 437-459.

(137) Wu, H., Liu, L., Ma, M., & Zhang, Y. (2023). Modulation of blood-brain tumor barrier for delivery of magnetic hyperthermia to brain cancer. *Journal of Controlled Release*, *355*, 248-258.

(138) Carmeliet, P. (2005). VEGF as a key mediator of angiogenesis in cancer. *Oncology*, *69*, 4-10.

(139) Pan, J., Xu, Y., Wu, Q., Hu, P., Shi, J. (2021). Mild magnetic hyperthermia-activated innate immunity for liver cancer therapy. *Journal of the American Chemical Society*, *143*(21), 8116-8128.

(140) Park, Y., Demessie, A. A., Luo, A., Taratula, O. R., Moses, A. S., Do, P., Taratula, O. (2022). Targeted nanoparticles with high heating efficiency for the treatment of endometriosis with systemically delivered magnetic hyperthermia. *Small*, *18*(24), 2107808.

(141) LHRH-agonists in Early Breast Cancer Overview group. (2007). Use of luteinising hormone-releasing hormone agonists as adjuvant treatment in premenopausal patients with hormone-receptor-positive breast cancer: a meta-analysis of individual patient data from randomised adjuvant trials. The Lancet, 369(9574), 1711-1723.

(142) Gründker, C., Günthert, A. R., Millar, R. P., & Emons, G. (2002). Expression of gonadotropin-releasing hormone II (GnRH-II) receptor in human endometrial and ovarian cancer cells and effects of GnRH-II on tumor cell proliferation. The Journal of Clinical Endocrinology & Metabolism, 87(3), 1427-1430.

(143) Limonta, Patrizia, Marina Montagnani Marelli, Stefania Mai, Marcella Motta, Luciano Martini, Roberta M. Moretti. "GnRH receptors in cancer: from cell biology to novel targeted therapeutic strategies." *Endocrine reviews*,33(5),784-811.

(144) Ulm, M., Ramesh, A. V., McNamara, K. M., Ponnusamy, S., Sasano, H., & Narayanan, R. (2019). Therapeutic advances in hormone-dependent cancers: focus on prostate, breast and ovarian cancers. *Endocrine connections*, *8*(2), R10-R26.

(145) Szende, B., Srkalovic, G., Timar, J., Mulchahey, J. J., Neill, J. D., Lapis, K., Schally, A. V. (1991). Localization of receptors for luteinizing hormone-releasing hormone in pancreatic and mammary cancer cells. *Proceedings of the National Academy of Sciences*, *88*(10), 4153-4156.

(146) Koushik, K., Bandi, N., Sundaram, S., Kompella, U. B. (2004). Evidence for LHRH-receptor expression in human airway epithelial (Calu-3) cells and its role in the transport of an LHRH agonist. *Pharmaceutical research*, *21*, 1034-1046.

(147) Gründker, C., Emons, G. (2003). Role of gonadotropin-releasing hormone (GnRH) in ovarian cancer. *Reproductive Biology and Endocrinology*, *1*, 1-7.

(148) Moretti, R. M., Montagnani Marelli, M., Van Groeninghen, J. C., Limonta, P. (2002). Locally expressed LHRH receptors mediate the oncostatic and antimetastatic activity of LHRH agonists on melanoma cells. *The Journal of Clinical Endocrinology & Metabolism*, *87*(8), 3791-3797.

(149) Wu, H. M., Chang, H. M., Leung, P. C. (2021). Gonadotropin-releasing hormone analogs: Mechanisms of action and clinical applications in female reproduction. *Frontiers in neuroendocrinology*, *60*, 100876.

(150) Danesh-Doust, M., Irajirad, R., Nezamdoust, F. V., Khademi, S., Montazerabadi, A. (2023). Triptorelin peptide conjugated alginate coated gold nanoparticles as a new contrast media for targeted computed tomography imaging of cancer cells. *Cell Journal (Yakhteh)*, *25*(2), 126.

(151) Frampton, J. E. (2017). Triptorelin: a review of its use as an adjuvant anticancer therapy in early breast cancer. *Drugs*, *77*, 2037-2048.

(152) Marini, L., Iacopino, F., Schinzari, G., Robustelli della Cuna, F. S., Mantovani, G., Sica, G. (1994). Direct antiproliferative effect of triptorelin on human breast cancer cells. *Anticancer research*, *14*(5A), 1881-1885.

(153) Garcia-Giralt, E., Beuzeboc, P., Dieras, V., Dorval, T., Jouve, M., Livartowski, A., Pouillart, P. (1996). Phase II trial of decapeptyl (D-TRP-6), a potent luteinizing hormone-releasing hormone analogue in untreated advanced breast cancer. *American journal of clinical oncology*, *19*(5), 455-458.

(154) Kumari, R., Muneshwar, K. N., Pathade, A. G., Yelne, S. (2023). Unveiling the Effects of Triptorelin on Endocrine Profiles: Insights From Healthy, Polycystic Ovary Syndrome, and Hypothalamic Amenorrhea Women. *Cureus*, *15*(9).

(155) Ferraro, E., Trapani, D., Marrucci, E., Curigliano, G. (2019). Evaluating triptorelin as a treatment option for breast cancer. *Expert Opinion on Pharmacotherapy*, *20*(15), 1809-1818.

(156) Celio, L., Martinetti, A., Ferrari, L., Buzzoni, R., Mariani, L., Miceli, R., Bajetta, E. (1999). Premenopausal breast cancer patients treated with a gonadotropin-releasing hormone analog alone or in combination with an aromatase inhibitor: a comparative endocrine study. *Anticancer research*, *19*, 2261-2268.

(157) Taratula, O., Dani, R. K., Schumann, C., Xu, H., Wang, A., Song, H., Taratula, O. (2013). Multifunctional nanomedicine platform for concurrent delivery of chemotherapeutic drugs and mild hyperthermia to ovarian cancer cells. *International journal of pharmaceutics*, *458*(1), 169-180.

(158) Shitole, A. A., Sharma, N., Giram, P., Khandwekar, A., Baruah, M., Garnaik, B., Koratkar, S. (2020). LHRH-conjugated, PEGylated, poly-lactide-co-glycolide nanocapsules for targeted delivery of combinational chemotherapeutic drugs Docetaxel and Quercetin for prostate cancer. *Materials Science and Engineering: C*, *114*, 111035.

(159) Taratula, O., Garbuzenko, O. B., Chen, A. M., Minko, T. (2011). Innovative strategy for treatment of lung cancer: targeted nanotechnology-based inhalation co-delivery of anticancer drugs and siRNA. *Journal of drug targeting*, *19*(10), 900-914.

(160) Varshosaz, J., Hassanzadeh, F., Aliabadi, H. S., Khoraskani, F. R., Mirian, M., Behdadfar, B. (2016). Targeted delivery of doxorubicin to breast cancer cells by magnetic LHRH chitosan bioconjugated nanoparticles. *International journal of biological macromolecules*, *93*, 1192-1205.

(161) Nuzhina, J. V., Shtil, A. A., Prilepskii, A. Y., Vinogradov, V. V. (2019). Preclinical evaluation and clinical translation of magnetite-based nanomedicines. *Journal of Drug Delivery Science and Technology*, *54*, 101282.

(162) Johannsen, M., Gneveckow, U., Eckelt, L., Feussner, A., Waldöfner, N., Scholz, R., Jordan, A. (2005). Clinical hyperthermia of prostate cancer using magnetic nanoparticles: presentation of a new interstitial technique. *International journal of hyperthermia*, *21*(7), 637-647.

(163) Mahmoudi, K., Bouras, A., Bozec, D., Ivkov, R., Hadjipanayis, C. (2018). Magnetic hyperthermia therapy for the treatment of glioblastoma: a review of the therapy's history, efficacy and application in humans. *International Journal of Hyperthermia*, *34*(8), 1316-1328.

(164) Day, N. B., Wixson, W. C., Shields IV, C. W. (2021). Magnetic systems for cancer immunotherapy. *Acta Pharmaceutica Sinica B*, *11*(8), 2172-2196.

(165) Zhao Y, Zhao X, Cheng Y, Guo X, Yuan W: Iron Oxide Nanoparticles-Based Vaccine Delivery for Cancer Treatment. *Molecular pharmaceutics* 2018, 15(5):1791-1799.

(166) Mejías, R., Pérez-Yagüe, S., Gutiérrez, L., Cabrera, L. I., Spada, R., Acedo, P., Barber, D. F. (2011). Dimercaptosuccinic acid-coated magnetite nanoparticles for magnetically guided in vivo delivery of interferon gamma for cancer immunotherapy. *Biomaterials*, *32*(11), 2938-2952.

(167) Xu, J., Yu, Y., Zhang, Y., Dai, H., Yang, Q., Wang, B., Wang, C. (2024). Oral administration of garlic-derived nanoparticles improves cancer immunotherapy by inducing intestinal IFNγ-producing γδ T cells. *Nature Nanotechnology*, 1-10.

(168) Andhariya, N., Chudasama, B., Mehta, R. V., Upadhyay, R. V. (2011). Biodegradable thermoresponsive polymeric magnetic nanoparticles: a new drug delivery platform for doxorubicin. *Journal of Nanoparticle research*, *13*, 1677-1688.

(169) Chudasama, B., Vala, A. K., Andhariya, N., Upadhyay, R. V., Mehta, R. V. (2009). Enhanced antibacterial activity of bifunctional Fe 3 O 4-Ag core-shell nanostructures. *Nano Research*, *2*, 955-965.

(170) Srivastava, N., Baranwal, M., Chudasama, B. (2023). Evaluation of Magnetic Hyperthermia Efficiency of PEG-Coated Fe_3O_4 Nanoparticles. *Nano*, *18*(12), 2350094.

(171) Leuschner, C., Kumar, C. S., Hansel, W., Soboyejo, W., Zhou, J., Hormes, J. (2006). LHRH-conjugated magnetic iron oxide nanoparticles for detection of breast cancer metastases. *Breast cancer research and treatment*, *99*, 163-176.

(172) S., Ramanujan, R. V. (2010). Doxorubicin loaded PVA coated iron oxide nanoparticles for targeted drug delivery. *Materials Science and Engineering: C*, *30*(3), 484-490.

(173) Louis, K. S., Siegel, A. C. (2011). Cell viability analysis using trypan blue: manual and automated methods. *Mammalian cell viability: methods and protocols*, 7-12.

(174) Ghasemi, M., Turnbull, T., Sebastian, S., Kempson, I. (2021). The MTT assay: utility, limitations, pitfalls, and interpretation in bulk and single-cell analysis. *International journal of molecular sciences*, *22*(23), 12827.

(175) Kamiloglu, S., Sari, G., Ozdal, T., Capanoglu, E. (2020). Guidelines for cell viability assays. *Food Frontiers*, *1*(3), 332-349.

(176) Van Meerloo, J., Kaspers, G. J., Cloos, J. (2011). Cell sensitivity assays: the MTT assay. *Cancer cell culture: methods and protocols*, 237-245.

(177) Sharma, V., Lohia, N., Handa, V., Baranwal, M. (2017). Amomum subulatum seed extract exhibit antioxidant, cytotoxic and immune-suppressive effect. *Indian J Biochem Biophys*, *54*, 135.

(178) Maziveyi, M., Dong, S., Baranwal, S., Mehrnezhad, A., Rathinam, R., Huckaba, T. M., Alahari, S. K. (2019). Exosomes from nischarin-expressing cells reduce breast cancer cell motility and tumor growth. *Cancer research*, *79*(9), 2152-2166.

(179) Corstjens, P. L., Zuiderwijk, M., Tanke, H. J., van der Ploeg van, J. J., Ottenhoff, T. H., Geluk, A. (2008). A user-friendly, highly sensitive assay to detect the IFN-γ secretion by T cells. *Clinical biochemistry*, *41*(6), 440-444.

(180) Agallou M., Athanasiou E., Koutsoni O., Dotsika E. and Karagouni E. (2014). Experimental validation of multi-epitope peptides including promising MHC Class I- and II-restricted epitopes of four known Leishmania infantum proteins. *Front Immunol*, 5, 268.

(181) Kouzoudis, D., Samourgkanidis, G., Kolokithas-Ntoukas, A., Zoppellaro, G., Spiliotopoulos, K. (2021). Magnetic hyperthermia in the 400–1,100 kHz frequency range using MIONs of condensed colloidal nanocrystal clusters. *Frontiers in Materials*, *8*, 638019.

(182) Kumar, R., Chauhan, A., Jha, S. K., Kuanr, B. K. (2018). Localized cancer treatment by radio-frequency hyperthermia using magnetic nanoparticles immobilized on graphene oxide: from novel synthesis to in vitro studies. *Journal of Materials Chemistry B*, *6*(33), 5385-5399.

(183) Soetaert, F., Kandala, S. K., Bakuzis, A., Ivkov, R. (2017). Experimental estimation and analysis of variance of the measured loss power of magnetic nanoparticles. *Scientific reports*, *7*(1), 6661.

(184) Dennis, C. L., Ivkov, R. (2013). Physics of heat generation using magnetic nanoparticles for hyperthermia. *International Journal of Hyperthermia*, *29*(8), 715-729.

(185) Iglesias, G. R., Jabalera, Y., Peigneux, A., Checa Fernández, B. L., Delgado, Á. V., Jimenez-Lopez, C. (2019). Enhancement of magnetic hyperthermia by mixing synthetic inorganic and biomimetic magnetic nanoparticles. *Pharmaceutics*, *11*(6), 273.

(186) Xu, H., Pan, Y. (2019). Experimental evaluation on the heating efficiency of magnetoferritin nanoparticles in an alternating magnetic field. *Nanomaterials*, *9*(10), 1457.

(187) Zhang, Y. F., & Lu, M. (2024). Advances in magnetic induction hyperthermia. *Frontiers in Bioengineering and Biotechnology*, *12*, 1432189.

(188) Kok, H. P., Cressman, E. N., Ceelen, W., Brace, C. L., Ivkov, R., Grüll, H., ... & Crezee, J. (2020). Heating technology for malignant tumors: A review. *International Journal of Hyperthermia*, *37*(1), 711-741.

(189) Guibert C, Dupuis V, Peyre V, Fresnais J: Hyperthermia of magnetic nanoparticles: experimental study of the role of aggregation. *The Journal of Physical Chemistry C* 2015,119(50):28148-28154.

(190) Kulshrestha, P., Gogoi, M., Bahadur, D., & Banerjee, R. (2012). In vitro application of paclitaxel loaded magnetoliposomes for combined chemotherapy and hyperthermia. *Colloids and Surfaces B: Biointerfaces*, *96*, 1-7.

(191) Branda, F., Costantini, A., Luciani, G., Silvestri, B. (2012). Smart nanoparticles for cancer therapy. In *AICIng 2012 VIII Convegno Nazionale dell'Associazione di Chimica per Ingegneria*.

(192) Lumachi, F., Brunello, A., Maruzzo, M., Basso, U., & Mm Basso, S. (2013). Treatment of estrogen receptor-positive breast cancer. *Current medicinal chemistry*, *20*(5), 596-604.

(193) Gutierrez, F. V., Lima, I. S., De Falco, A., Ereias, B. M., Baffa, O., de Abreu Lima, C. D., Araujo, J. F. D. F. (2024). The effect of temperature on the synthesis of magnetite nanoparticles by the coprecipitation method. *Heliyon*, *10*(4).

(194) Vayssieres, L., Chanéac, C., Tronc, E., & Jolivet, J. P. (1998). Size tailoring of magnetite particles formed by aqueous precipitation: an example of thermodynamic stability of nanometric oxide particles. *Journal of colloid and interface science*, *205*(2), 205-212.

(195) Rashad, M. M., Khalifa, A., Rayan, D. A., & Fayed, M. G. (2018). Superparamagnetic Cu 2+ substituted Mn–MgFe 2 O 4 powders prepared through co-precipitation strategy:

structural, microstructure and magnetic properties. *Journal of Materials Science: Materials in Electronics*, *29*, 3391-3400.

(196) Eivazzadeh-Keihan, R., Bahreinizad, H., Amiri, Z., Aliabadi, H. A. M., Salimi-Bani, M., Nakisa, A., & Madanchi, H. (2021). Functionalized magnetic nanoparticles for the separation and purification of proteins and peptides. *TrAC Trends in Analytical Chemistry*, *141*, 116291.

(197) Castellanos-Rubio, I., Arriortua, O., Iglesias-Rojas, D., Barón, A., Rodrigo, I., Marcano, L., Insausti, M. (2021). A milestone in the chemical synthesis of Fe_3O_4 nanoparticles: Unreported bulklike properties lead to a remarkable magnetic hyperthermia. *Chemistry of Materials*, *33*(22), 8693-8704.

(198) Kurniawan, C., Eko, A. S., Ayu, Y. S., Sihite, P. T. A., Ginting, M., Simamora, P., & Sebayang, P. (2017). Synthesis and characterization of magnetic elastomer based PEG-coated Fe_3O_4 from natural iron sand. In *IOP Conference Series: Materials Science and Engineering* (Vol. 202, No. 1, p. 012051). IOP Publishing.

(199) Kaushal, N., Sharma, A. L., & Saha, A. (2022). Visible LED-based photo-redox properties of sulfur and nitrogen-doped carbon dots designed by solid-state synthesis. *Materials Advances*, *3*(1), 355-361.

(200) Zhao, D. L., Teng, P., Xu, Y., Xia, Q. S., & Tang, J. T. (2010). Magnetic and inductive heating properties of Fe_3O_4/polyethylene glycol composite nanoparticles with core–shell structure. *Journal of alloys and compounds*, *502*(2), 392-395.

(201) Andhariya, N., Upadhyay, R., Mehta, R., & Chudasama, B. (2013). Folic acid conjugated magnetic drug delivery system for controlled release of doxorubicin. *Journal of nanoparticle research*, *15*, 1-12.

(202) Suharyadi, E., Alfansuri, T., Handriani, L. S., Wibowo, N. A., & Sabarman, H. (2021). Detection of Fe_3O_4 /PEG nanoparticles using one and two spin-valve GMR sensing elements in wheatstone bridge circuit. *Journal of Materials Science: Materials in Electronics*, *32*(19), 23958-23967.

(203) Antarnusa, G., & Suharyadi, E. (2020). A synthesis of polyethylene glycol (PEG)-coated magnetite Fe_3O_4 nanop articles and their characteristics for enhancement of biosensor. *Materials Research Express*, *7*(5), 056103.

(204) Antarnusa, G., Jayanti, P. D., Denny, Y. R., & Suherman, A. (2022). Utilization of co-precipitation method on synthesis of Fe_3O_4/PEG with different concentrations of PEG for biosensor applications. *Materialia*, *25*, 101525.

(205) Anbarasu, M., Anandan, M., Chinnasamy, E., Gopinath, V., & Balamurugan, K. (2015). Synthesis and characterization of polyethylene glycol (PEG) coated Fe_3O_4 nanoparticles by chemical co-precipitation method for biomedical applications. *Spectrochimica Acta Part A: Molecular and Biomolecular Spectroscopy*, *135*, 536-539.

(206) Karimzadeh, I., Aghazadeh, M., Doroudi, T., Ganjali, M. R., & Kolivand, P. H. (2017). Superparamagnetic iron oxide (Fe_3O_4) nanoparticles coated with PEG/PEI for biomedical applications: A facile and scalable preparation route based on the cathodic electrochemical deposition method. *Advances in Physical Chemistry*, *2017*(1), 9437487.

(207) Zhou, J., Leuschner, C., Kumar, C., Hormes, J. F., & Soboyejo, W. O. (2006). Sub-cellular accumulation of magnetic nanoparticles in breast tumors and metastases. *Biomaterials*, *27*(9), 2001-2008.

(208) Sritharan, S., & Sivalingam, N. (2021). A comprehensive review on time-tested anticancer drug doxorubicin. *Life sciences*, *278*, 119527.

(209) Tiernan, H., Byrne, B., & Kazarian, S. G. (2020). ATR-FTIR spectroscopy and spectroscopic imaging for the analysis of biopharmaceuticals. *Spectrochimica Acta Part A: Molecular and Biomolecular Spectroscopy*, *241*, 118636.

(210) Hu, J., Obayemi, J. D., Malatesta, K., Košmrlj, A., & Soboyejo, W. O. (2018). Enhanced cellular uptake of LHRH-conjugated PEG-coated magnetite nanoparticles for specific targeting of triple negative breast cancer cells. *Materials Science and Engineering: C*, *88*, 32-45.

(211) Obayemi, J. D., Dozie-Nwachukwu, S., Danyuo, Y., Odusanya, O. S., Anuku, N., Malatesta, K., & Soboyejo, W. O. (2015). Biosynthesis and the conjugation of magnetite nanoparticles with luteinizing hormone releasing hormone (LHRH). *Materials Science and Engineering: C*, *46*, 482-496.

(212) Kovrigina, E., Chubarov, A., & Dmitrienko, E. (2022). High drug capacity doxorubicin-loaded iron oxide nanocomposites for cancer therapy. *Magnetochemistry*, *8*(5), 54.

(213) M. M., Foy, S. P., Jain, T. K., & Labhasetwar, V. (2010). PEG-functionalized magnetic nanoparticles for drug delivery and magnetic resonance imaging applications. *Pharmaceutical research*, *27*, 2283-2295.

(214) Mannu, R., Karthikeyan, V., Velu, N., Arumugam, C., Roy, V. A., Gopalan, A. I., Kannan, V. (2021). Polyethylene glycol coated magnetic nanoparticles: Hybrid nanofluid formulation, properties and drug delivery prospects. *Nanomaterials*, *11*(2), 440.

(215) Popescu, R. C., Savu, D. I., Olarescu, A. D., Gherasim, O., Banita, S., Straticiuc, M., Andronescu, E. (2020). *In vitro* magnetic targeted delivery of doxorubicin using iron oxide nanoparticles leads to enhanced cell death in glioblastoma. *UPB Sci. Bull. Ser. B*, *82*, 73-84.

(216) Gupta, R., & Sharma, D. (2021). (Carboxymethyl-stevioside)-coated magnetic dots for enhanced magnetic hyperthermia and improved glioblastoma treatment. *Colloids and Surfaces B: Biointerfaces*, *205*, 111870.

(217) Iqbal, Y., Bae, H., Rhee, I., & Hong, S. (2016). Intensive analysis of core–shell silica-coated iron-oxide nanoparticles for magnetic hyperthermia. *Journal of Nanoscience and Nanotechnology*, *16*(11), 11862-11867.

(218) Narayanaswamy, V., Sambasivam, S., Saj, A., Alaabed, S., Issa, B., Al-Omari, I. A., & Obaidat, I. M. (2021). Role of magnetite nanoparticles size and concentration on hyperthermia under various field frequencies and strengths. *Molecules*, *26*(4), 796.

(219) Wells, J., Ortega, D., Steinhoff, U., Dutz, S., Garaio, E., Sandre, O., Natividad, E., RADIOMAG consortium. (2021). Challenges and recommendations for magnetic hyperthermia characterization measurements. *International Journal of Hyperthermia*, *38*(1), 447-460.

(220) Hannon, G., Tansi, F. L., Hilger, I., Prina-Mello, A. (2021). The effects of localized heat on the hallmarks of cancer. *Advanced Therapeutics*, *4*(7), 2000267.

(221) Saliev, T., Feril Jr, L. B., Begimbetova, D., Baiskhanova, D., Klodzinskyi, A., Bobrova, X., & Tachibana, K. (2017). Hyperthermia enhances bortezomib-induced apoptosis in human white blood cancer cells. *Journal of Thermal Biology*, *67*, 9-14.

(222) Yi, G. Y., Kim, M. J., Kim, H. I., Park, J., & Baek, S. H. (2022). Hyperthermia treatment as a promising anti-cancer strategy: Therapeutic targets, perspective mechanisms and synergistic combinations in experimental approaches. *Antioxidants*, *11*(4), 625.

(223) Ivashkiv, L. B. (2018). IFNγ: signalling, epigenetics and roles in immunity, metabolism, disease and cancer immunotherapy. *Nature Reviews Immunology*, *18*(9), 545-558.

(224) Thibaut, R., Bost, P., Milo, I., Cazaux, M., Lemaître, F., Garcia, Z., ... & Bousso, P. (2020). Bystander IFN-γ activity promotes widespread and sustained cytokine signaling altering the tumor microenvironment. *Nature cancer*, *1*(3), 302-314.

(225) García-Tuñón, I., Ricote, M., Ruiz A, A., Fraile, B., Paniagua, R., & Royuela, M. (2007). Influence of IFN-gamma and its receptors in human breast cancer. *BMC cancer*, *7*(1), 1-11.

(226) H., Flury, N., Liu, R., Scheidegger, S., & Eppenberger, U. (1996). Tumour necrosis factor and interferon are selectively cytostatic *in vitro* for hormone-dependent and hormone-independent human breast cancer cells. *European Journal of Cancer*, *32*(13), 2312-2318.

(227) Macheledt, J. E., Buzdar, A. U., Hortobagyi, G. N., Frye, D. K., Gutterman, J. U., & Holmes, F. A. (1991). Phase II evaluation of interferon added to tamoxifen in the treatment of metastatic breast cancer. *Breast cancer research and treatment*, *18*, 165-170.

(228) Seymour, L., & Bezwoda, W. R. (1993). Interferon plus tamoxifen treatment for advanced breast cancer: in vivo biologic effects of two growth modulators. *British journal of cancer*, *68*(2), 352-356.

(229) Korentzelos, D., Wells, A., & Clark, A. M. (2022). Interferon-γ increases sensitivity to chemotherapy and provides immunotherapy targets in models of metastatic castration-resistant prostate cancer. *Scientific reports*, *12*(1), 6657.

NANO: Brief Reports and Reviews
Vol. 18, No. 12 (2023) 2350094 (11 pages)

DOI: 10.1142/S1793292023500947

Evaluation of Magnetic Hyperthermia Efficiency of PEG-Coated Fe_3O_4 Nanoparticles

Neha Srivastava*, Manoj Baranwal* and Bhupendra Chudasama†,‡,§

*Department of Biotechnology
Thapar Institute of Engineering and Technology
Patiala 147004, India

†School of Physics and Materials Science
Thapar Institute of Engineering and Technology
Patiala 147004, India

‡TIET-VT Center of Excellence in Emerging Materials
Thapar Institute of Engineering and Technology
Patiala 147004, India

§bnchudasama@gmail.com

Received 18 May 2023
Accepted 15 September 2023
Published 8 November 2023

Magnetic nanoparticle hyperthermia has drawn considerable interest in cancer therapy. In this study, we report the synthesis of PEG-coated Fe_3O_4 nanoparticles and evaluate their suitability for magnetic hyperthermia applications. Fe_3O_4 nanoparticles were synthesized by the chemical coprecipitation method, which are coated with polyethylene glycol (PEG). PEG-coated Fe_3O_4 nanoparticles were characterized by X-ray powder diffraction (XRD), Fourier transform infrared spectroscopy (FTIR), vibrating sample magnetometer (VSM), dynamic light scattering (DLS) and transmission electron microscopy (TEM). Synthesized nanoparticles possess inverse-spinel structural with a crystallite size of 9.1 nm. From the M-H hysteresis loops, it was confirmed that the synthesized Fe_3O_4 nanoparticles were superparamagnetic. The physical size of bare Fe_3O_4 nanoparticles, as determined from the HR-TEM, is 9.5 ± 0.12 nm, and the corresponding hydrodynamic size of PEG-coated Fe_3O_4 nanoparticles is 118 ± 0.25 nm. Magnetic hyperthermia efficiency of PEG-coated Fe_3O_4 nanoparticles was determined as a function of magnetic field frequency (162–935.6 kHz), field strength (5–12 mT) and nanoparticle concentration (1–100 mg/mL). Temperature rise in an aqueous dispersion of PEG-coated Fe_3O_4 nanoparticles was measured for 20 min. The specific loss power (SLP) was calculated by the corrected slope method. SLP values of PEG-coated Fe_3O_4 nanoparticles increase with magnetic field frequency and field strength and decrease with nanoparticle concentration. The optimum hyperthermia performance of PEG-coated Fe_3O_4 nanoparticles was observed for 935.6 kHz frequency, 10 mT field strength and 25 mg/mL concentration. Under these conditions, the measured SLP of PEG-coated Fe_3O_4 nanoparticles was 4.43 W/g. These results show that the synthesized PEG-coated Fe_3O_4 nanoparticles could be a potential candidate for magnetic hyperthermia treatment of cancer.

Keywords: Hyperthermia; cancer; magnetic nanoparticles; specific loss power; coprecipitation.

§Corresponding author.

1. Introduction

Hyperthermia is one of the oldest therapies for the treatment of cancer. In this therapy, tumor temperature is raised between 41°C and 45°C leading to cell apoptosis due to lower heat tolerance of cancer cells.[1,2] Although this treatment modality is very simple, it has several challenges like failure to supply heat to the affected sites without killing the healthy cells and difficulty in attaining homogenous heat distribution throughout the tumor.[3] These limitations can be overcome by targeted magnetic hyperthermia.[4] In magnetic hyperthermia, the cancerous tissues can be selectively killed by localizing magnetic nanoparticles inside the cancer cells and exposing them to an alternating magnetic field with appropriate frequency and strength. When magnetic nanoparticles are exposed to an alternating magnetic field, they relax via Brownian and Neel rotation, converting magnetic energy into heat.[5] Thus, nanoparticle relaxation in an AC magnetic field will result in localized heating of cancer cells. If the cell temperature goes beyond 42°C, cancer cells induce cell apoptosis due to their lower heat tolerance.[6] The use of nanoparticles in magnetic hyperthermia must fulfil two requirements: (i) Nanoparticles should possess requisite heating capacity and (ii) nanoparticles should have high dispersion stability with good biocompitibility.[7]

Among various magnetic nanoparticles, iron oxide nanoparticles (IONPs) are extensively studied as heat mediators in magnetic hyperthermia because of their ease of synthesis, self-heating in the presence of an alternating magnetic field, tunable magnetic characteristics and good biocompatibility.[8,9] Magnetic nanoparticles because of their large surface-to-volume ratio also leads to their agglomeration, which compromises colloidal stability.[10] Therefore, to maintain good colloidal dispersion, nanoparticles need to be coated with suitable biocompatible surfactant. Surface modification of IONPs can be achieved with polymers such as dextran, chitosan, alginate, polyethylene glycol (PEG), polyvinyl alcohol (PVA), polydopamine (PDA), polysaccharides, polyethylenimine, polyvinylpyrrolidone (PVP), polyacid polyetherimide, polyamidoamine (PAMAM), oleic acid (OA), etc. Among these, PEG is widely used due to its good biocompatibility in magnetic hyperthermia applications.[11]

In phospholipid– PEG-coated Fe_3O_4 nanoparticles and oleic acid (OA)-coated Fe_3O_4 nanoparticles a temperature rise up to 42°C at low-nanoparticle concentration was reported.[12] In another study, superparamagnetic IONPs coated with phospholipid–PEG were loaded with doxorubicin.[13] These nanoparticles generate adequate heat to increase the local temperature up to 43°C, which was sufficient to kill HeLa cells. Belyanina *et al.*[14] reported that for magnetic hyperthermia, IONPs should be superparamagnetic and form a stable dispersion in physiological media. In the past, Sudame *et al.*[15] and Vassallo *et al.*[16] showed that enhanced colloidal stability of magnetic nanoparticles leads to rise in the hyperthermic response of nanoparticles. In one of the studies, researchers reported that magnetic hyperthermia-mediated heating efficacy varied with different surface coatings such as glutamic acid, citric acid, PEG, polyvinylpyrrolidone, ethylene diamine and cetyl-trimethyl ammonium bromide on Fe_3O_4 nanoparticles at fixed frequency (316 kHz) and field strength (450 Oe).[17] In another study, pluronic-coated Fe_3O_4 nanoparticles showed hyperthermic response against HeLa cancer cells by applying an AC magnetic field of 4.0–20 kA/m at 210 kHz frequency.[18]

In most of these studies, the hyperthermic response of nanoparticles was measured at certain magnetic field strength, field frequency, or nanoparticle concentration. Since the hyperthermic response of nanoparticles strongly depends on these parameters, they need to be optimized for optimal performance of magnetic nanoparticles in magnetic hyperthermia therapy. In this study, we have optimized magnetic field frequency (162–935.6 kHz), field strength (5–12 mT) and nanoparticle concentration (1–100 mg/mL) for the magnetic hyperthermia of PEG-coated Fe_3O_4 nanoparticles.

2. Materials and Methods

2.1. *Materials*

Ferric chloride ($FeCl_3 \cdot 6H_2O$) (97%), ferrous sulphate heptahydrate ($FeSO_4 \cdot 7H_2O$) (99%), PEG-600 and sodium hydroxide (NaOH) were purchased from Sigma-Aldrich. Hydrochloric acid (HCl) was purchased from Loba Chemicals Pvt. Ltd. All aqueous solutions were prepared in Milli-Q ultrapure water ($R = 18.2\,M\Omega$).

2.2. *Synthesis of Fe_3O_4 nanoparticles*

Fe_3O_4 nanoparticles were synthesized by chemical coprecipitation method.[19–21] The stoichiometric

solutions of iron (II) sulphate heptahydrate ($FeSO_4.7H_2O$) (5 mM) and iron (III) chloride hexahydrate ($FeCl_3 \cdot 6H_2O$) (10 mM) (75 mL each) were prepared in 3 neck round–bottom flask. The pH of the solution was adjusted to <1.5 with dilute HCl. To this, aqueous solution of sodium hydroxide (150 mL) (NaOH) (40 mM) was added under continuous mechanical stirring at 60°C. Adding sodium hydroxide (NaOH) converts metal salts (Fe^{2+}/Fe^{3+}) into their hydroxides. The pH of the solution was maintained at 11. After continuous stirring for 20 min at 60°C, metal hydroxides get converted into oxides and black precipitates of Fe_3O_4 were formed. Fe_3O_4 nanoparticles were extracted from the aqueous medium by magnetic decantation. Precipitates were washed multiple times with warm Milli-Q water to remove water-soluble impurities. After washing, the water-wet slurry of nanoparticles was divided equally in two parts. One part was subject to acetone wash followed by magnetic decantation and drying overnight at 50°C in hot air oven. Dried Fe_3O_4 nanoparticles were grinded with a mortal pestle into a fine powder and stored at room temperature for further studies.

2.3. *Surface modification of Fe_3O_4 nanoparticles with PEG*

The second part of water-wet slurry of as-synthesized Fe_3O_4 nanoparticles was coated with PEG. To prepare PEG-coated Fe_3O_4 nanoparticles, as-synthesized water-wet slurry of Fe_3O_4 nanoparticles was stirred and heated at 60°C followed by the addition of PEG solution. PEG to Fe_3O_4 weight ratio was optimized as 20:100. The solution was stirred for another 30 min. PEG-coated Fe_3O_4 nanoparticles were extracted from the medium by magnetic decantation. In order to remove any uncoated PEG and other water-soluble impurities, PEG-coated Fe_3O_4 nanoparticles were washed multiple times with warm distilled water and collected by magnetic decantation. PEG-coated Fe_3O_4 nanoparticles thus obtained were stored at room temperature for further analysis.

2.4. *Characterization of Fe_3O_4 and PEG-coated Fe_3O_4 nanoparticles*

X-ray diffraction pattern of as-synthesized Fe_3O_4 nanoparticles was recorded on PANalytical X'Pert Pro powder X-ray diffractometer operated at 45 kV and 40 mA by using monochromatic CuKα radiation ($\lambda = 1.54056$ nm). To investigate the morphology of as-synthesized Fe_3O_4 nanoparticles, high-resolution transmission electron microscope (HR-TEM) images were recorded on JEOL (model JEM 2100F) transmission electron microscope operated at 200 kV. Functionalization of Fe_3O_4 nanoparticles with PEG was confirmed by attenuated total reflectance Fourier transform infrared spectroscopy (ATR-FTIR). FTIR spectra of bare and PEG-coated Fe_3O_4 nanoparticles were recorded on Spectrum GX (Perkin Elmer) single beam spectrophotometer. Measurement was carried out in the 4000–500 cm^{-1} spectrum range using the KBr pellet method for Fe_3O_4 nanoparticles, while for PEG-coated Fe_3O_4 nanoparticles, the measurement was carried out in the spectral range of 4000–500 cm^{-1} with an ATR attachment. Hydrodynamic size and polydispersity index of bare and PEG-coated Fe_3O_4 nanoparticles were measured by photon correlation spectroscopy. Measurements were carried out on Brookhaven 90 plus particle size analyzer at 25°C. Magnetization measurements of bare and PEG-coated Fe_3O_4 nanoparticles were carried out on LakeShore 7404 vibrating sample magnetometer (VSM) at 25°C. M-H loops were recorded in the field range of −10 kOe to + 10 kOe.

2.5. *Magnetic hyperthermia measurement of PEG-coated Fe_3O_4 nanoparticles*

The heating capacity of PEG-coated Fe_3O_4 nanoparticles was determined by a magnetic hyperthermia study. For this purpose, temperature–time profiles of PEG-coated Fe_3O_4 nanoparticles were recorded on nanoTherics magneTherm hyperthermia setup. 1.0 mL aqueous solution of PEG-coated Fe_3O_4 nanoparticles was added to the test vial and heating profiles were recorded under variable magnetic field frequencies (162–935.6 kHz), magnetic field strength (5 mT, 10 mT and 12 mT) and nanoparticle concentrations (1–100 mg/mL). Three channel optical fiber thermometers were used to measure the temperature rise in the colloidal dispersion of PEG-coated Fe_3O_4 nanoparticles.

3. Results and Discussion

To study crystal structure of as-synthesized Fe_3O_4 nanoparticles, powder X-ray diffraction was

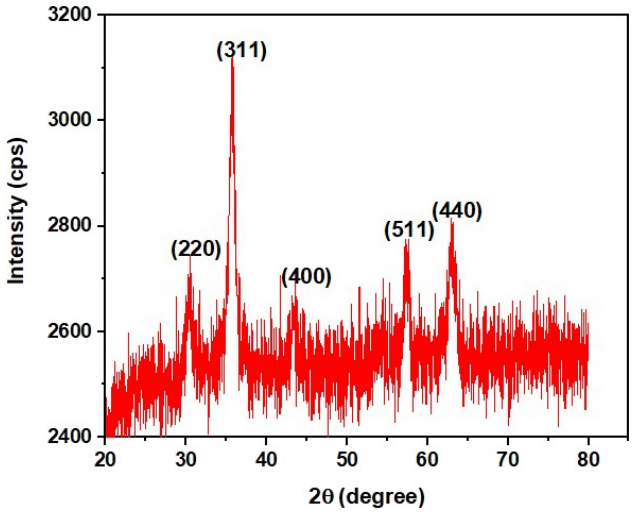

Fig. 1. X-ray powder diffraction (XRD) pattern of as-synthesized Fe_3O_4nanoparticles.

performed. X-ray diffractogram of Fe_3O_4 nanoparticles recorded in the 2θ range of 20°–80° is shown in Fig. 1. This X-ray diffractogram is indexed well with the FCC inverse spinel lattice and matches well with the JCPDS card No. 19-0629. The lattice parameter (a) of Fe_3O_4 nanoparticles determined from the highest intense peak (311) is 0.837 nm. This value of lattice parameter (a) is also in good agreement with earlier report[22] and matches well with that reported in JCPDS data base (card No. 19-0629). The average crystallite size (d) of Fe_3O_4 nanoparticles was calculated by using the classical Scherrer's equation

$$d = \frac{0.9\lambda}{\beta \cos\theta}, \tag{1}$$

where λ is the wavelength of X-rays, β is the full-width half maximum (FWHM) of the highest intense peak (311) and θ is the angle of diffraction of the highest intense peak. FWHM of the highest intense peak was determined by fitting it with the pseudo-voigt peak function. The average crystallite size obtained from Eq. (1) is 9.1 nm, which is below the superparamagnetic limit of Fe_3O_4.[21] Hence, we expect the synthesized nanoparticles to possess superparamagnetism.

To examine the morphology of Fe_3O_4 nanoparticles, high-resolution transmission electron microscopy (HR-TEM) was performed. Micrographs are presented in Fig. 2. Aggregated nanoparticles with near spherical morphology are visible in the micrograph. Inset (b) of Fig. 2 shows a lattice fringe image of Fe_3O_4 nanoparticles. Inter planner spacing is 0.49 nm, corresponding to (111) plane

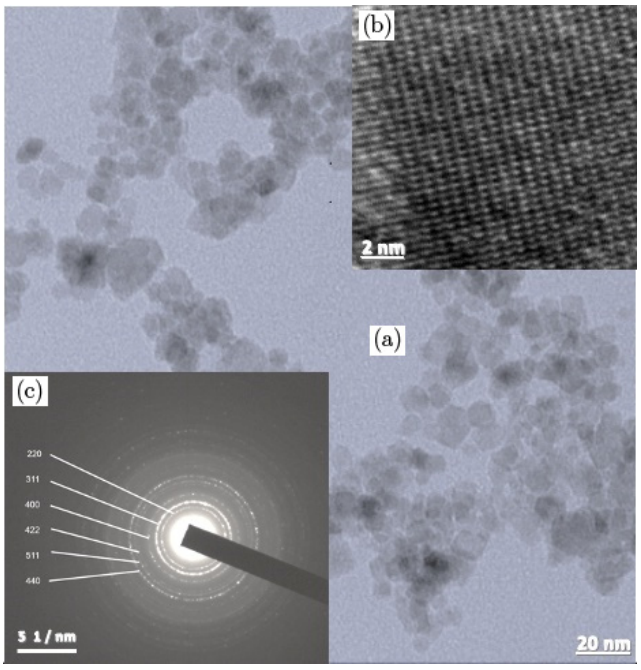

Fig. 2. (a) TEM image, (b) Lattice fringe image and (c) Selected area electron diffraction pattern of Fe_3O_4 nanoparticles.

of the inverse spinel lattice of Fe_3O_4 nanoparticles. Inset (c) of Fig. 2 represents the selected area electron diffraction (SAED) pattern of nanoparticles. Diffraction fringes in the SAED pattern in Fig. 2(c) are indexed well with the inverse spinel structure of Fe_3O_4 nanoparticles and corroborate well with the X-ray diffractogram reported in Fig. 1. Size distribution histogram of Fe_3O_4 nanoparticles obtained from the TEM micrograph is shown

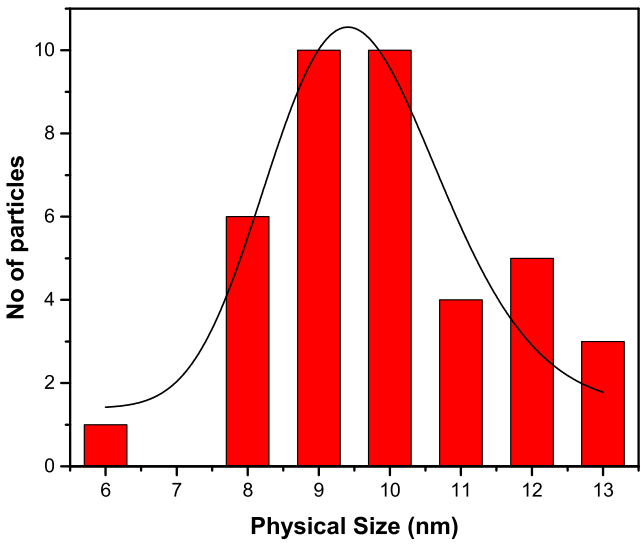

Fig. 3. Size distribution histogram of Fe_3O_4 nanoparticles.

in Fig. 3. This size distribution histogram was prepared by measuring the diameter of 37 nanoparticles with the help of Carl Zeiss AxioVision software. This size distribution histogram is fitted with the log-normal particle size distribution function. The average physical size of the nanoparticles thus obtained from the fit is 9.5 ± 0.12 nm, which is in good agreement with the crystallite size of the nanoparticles, indicating each nanoparticle is single grain.

Hydrodynamic particle size (D) and polydispersity (σ) of as-synthesized Fe_3O_4 and PEG-coated Fe_3O_4 nanoparticles were determined by photon correlation spectroscopy. Hydrodynamic particle size distribution histograms of Fe_3O_4 and PEG-coated Fe_3O_4 nanoparticles are shown in Fig. 4. Each histogram is fitted with log-normal particle size distribution function:

$$P(D) = \frac{1}{(D\sigma\sqrt{2\pi})} \exp\left[-\frac{\left(\ln\left(\frac{D}{D_0}\right)\right)^2}{2\sigma^2}\right]. \quad (2)$$

Here, σ is the polydispersity, D is the hydrodynamic particle size and $\ln D_0$ is the mean of $\ln D$. From the best fits, hydrodynamic particle size and polydispersity of Fe_3O_4 and PEG-coated Fe_3O_4 nanoparticles were determined. The hydrodynamic size of Fe_3O_4 and PEG-coated Fe_3O_4 nanoparticles are 87 nm and 118 nm, respectively. The polydispersity index of Fe_3O_4 and PEG-coated Fe_3O_4 nanoparticles are 0.31 and 0.25, respectively. This suggests that bare and PEG-coated Fe_3O_4 nanoparticles are polydispersed in size. Compared to bare nanoparticles, the polydispersity index of PEG-coated Fe_3O_4 nanoparticles is less, suggesting a reduction in aggregation of nanoparticles post PEG functionalization.

To confirm PEG-coating on Fe_3O_4 nanoparticles, FTIR spectroscopy was used. FTIR spectra of bare Fe_3O_4 nanoparticles, PEG-coated Fe_3O_4 nanoparticles, and PEG-600 are shown in Fig. 5. Various vibrational bands observed in Fig. 5 are summarized in Table 1. The presence of absorption bands at 559 cm^{-1} and 640 cm^{-1} is due to Fe–O stretching vibrations of bare Fe_3O_4.[20,21] In the case of PEG-coated Fe_3O_4, vibrational band at 559 cm^{-1} red shift to 540 cm^{-1} and 640 cm^{-1} band blue shifts to 665 cm^{-1}. Further, a strong absorption band at 1001 cm^{-1} was observed in the FTIR spectra of PEG 600. This band red shifts to 1121 cm^{-1} in the case of PEG-coated Fe_3O_4. This band is ascribed to the C–O–C stretching vibrations in PEG.[22,23] These shifts in the band positions of Fe–O stretching vibrations and C–O–C stretching vibrations in PEG-coated Fe_3O_4 nanoparticles suggest that PEG is chemi-adsorbed on the surface of Fe_3O_4 nanoparticles.

To understand magnetic properties of bare and PEG-coated Fe_3O_4 nanoparticles, magnetization (M) versus magnetic field (H) hysteresis loops were recorded at room temperature by VSM. These M-H loops are presented in Fig. 6. As evident from these hysteresis loops, both bare and PEG-coated Fe_3O_4

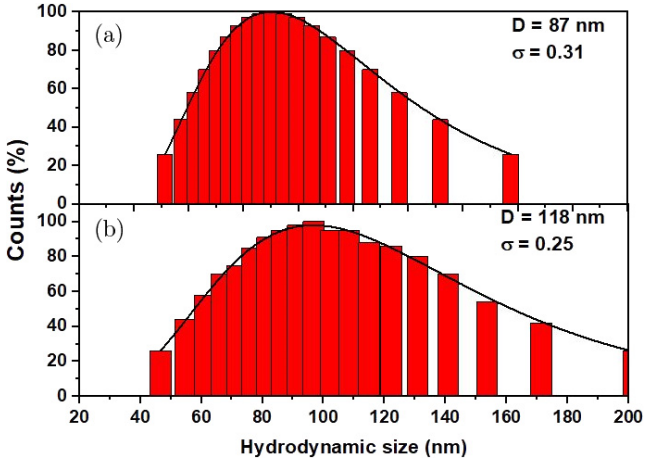

Fig. 4. Hydrodynamic particle size distribution histograms of (a) Fe_3O_4 and (b) PEG-coated Fe_3O_4 nanoparticles dispersed in water. Histograms are fitted with log-normal distribution function (Eq. (2)).

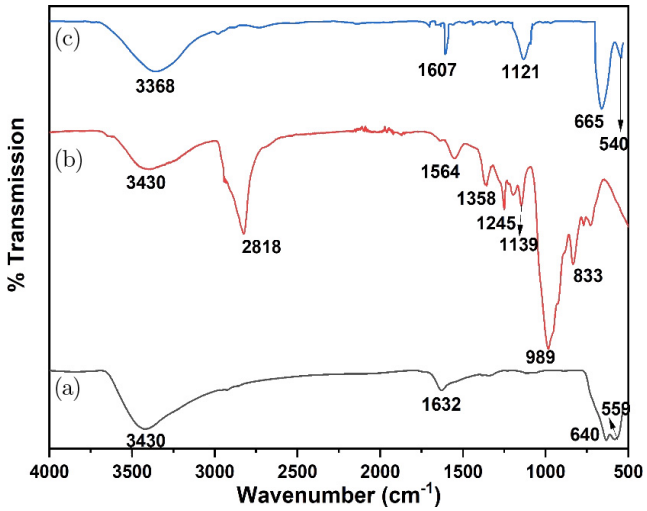

Fig. 5. FTIR spectra of (a) Fe_3O_4, (b) PEG and (c) PEG-coated Fe_3O_4 nanoparticles measured in the spectral range of 4000–500 cm^{-1}.

Table 1. Band interpretations of FTIR spectra (Fig. 5) of Fe_3O_4, PEG and PEG-coated Fe_3O_4 nanoparticles.

Sample	IR bands (cm^{-1})	Description
Fe_3O_4	559	Stretching vibration of Fe–O
	640	Stretching vibration of Fe–O
	3430	–OH stretching
PEG	1001	C–O–C stretching vibration of PEG
	1242	C–H twisting
	1358	C–H bending
	2818	m_s (–CH)
	3430	–OH stretching
PEG–Fe_3O_4	540	Stretching vibration of Fe–O
	665	Stretching vibration of Fe–O
	1121	C–O–C stretching vibration of PEG
	3368	–OH stretching

nanoparticles are superparamagnetic. A magnified view of M-H loops from −100 Oe to 100 Oe, for bare and PEG-coated Fe_3O_4 nanoparticles, shows that the coercivity of bare nanoparticles reduces from 32.42 Oe to 3.56 Oe and remanence drops from 1.78 emu/g to 0.159 emu/g, confirming the reduction in the clustering of magnetic nanoparticles post surface functionalization with PEG. This was also evident in the reduction in polydispersity index measured by photon correlation spectroscopy (Fig. 4). Saturation magnetization (M_S) of bare and PEG-coated Fe_3O_4 nanoparticles is 53.36 emu/g and 46.89 emu/g, respectively. Reduction in saturation magnetization of PEG-coated Fe_3O_4 nanoparticles can be attributed to nonmagnetic contribution of PEG to the total mass in coated nanoparticles. These results are in sync with previous reports.[20,24] Magnetization (M) versus the magnetic field (H) of bare and PEG-coated Fe_3O_4 nanoparticles recorded in the first quadrant (of Fig. 6) are also fitted with the modified Langevin function:

$$M = M_s \int_0^\infty f(D) L\left(\frac{\mu(H)}{k_B T}\right) dD + \chi H, \qquad (3)$$

where M_s corresponds to the saturation magnetization of nanoparticles and $L(\alpha)$ denotes Langevin function. The Langevin parameter, $\alpha = \mu(H)/k_B T$, where μ is the magnetic moment of individual spin clusters, H is the applied external magnetic field, k_B is the Boltzmann constant and T is the absolute temperature.

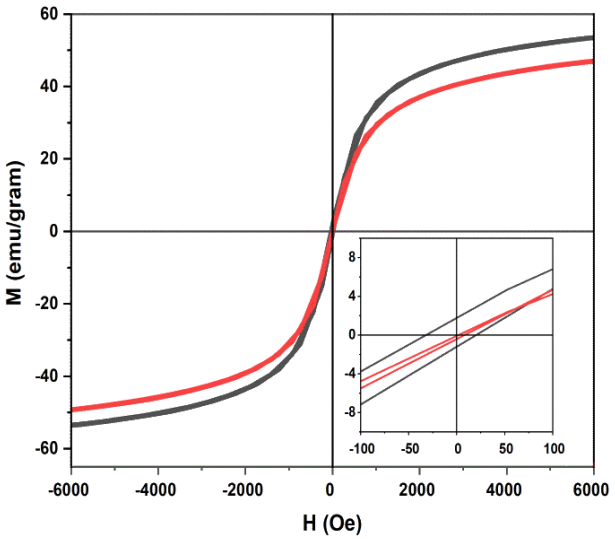

Fig. 6. Magnetization (M) versus applied magnetic field (H) plots of (—) bare Fe_3O_4 and (—) PEG-coated Fe_3O_4 nanoparticles. Inset shows the magnified view of M–H curves in the field range of −100 Oe–+100 Oe.

$$f(D)\mathrm{d}D = \frac{1}{(\sqrt{2\pi}D)} \exp\left[-\frac{\ln\left(\frac{D}{D_m}\right)}{2\sigma^2}\right] dD. \qquad (4)$$

Here, $f(D)\mathrm{d}D$ denotes the log-normal cluster size distribution function with mean cluster size D_m,

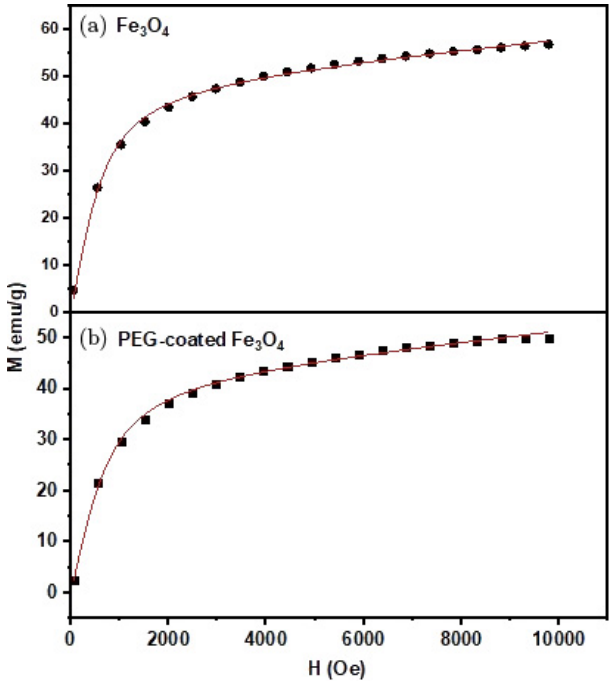

Fig. 7. Magnetization (M) versus applied magnetic field (H) plots of (a) Fe_3O_4 and (b) PEG-coated Fe_3O_4 nanoparticles fitted with modified Langevin function (Eq. (3)).

Table 2. Saturation magnetization (M_S), mean cluster size (D_m), polydispersity (σ), magnetic moment (μ) and susceptibility (χ) of Fe_3O_4 and PEG-coated Fe_3O_4 nanoparticles obtained by fitting M-H curve with modified Langevin function.

Sample	Saturation magnetization (emu/gm)	Polydispersity	Mean cluster size (nm)	Magnetic moment $\times \mu_B$	Susceptibility $\times 10^{-5}$
Fe_3O_4	56	0.18	6.2	16000	1.25
PEG-Fe_3O_4	46	0.12	7.8	15999	1.25

polydispersity σ. χ is the susceptibility of paramagnetic component of nanoparticles. The fitted graph is shown in Fig. 7. From the best fits, mean cluster size (D_m), saturation magnetization (M_s) and polydispersity (σ) are determined, which are reported in Table 2.

3.1. *Magnetic hyperthermia of PEG-coated Fe_3O_4 nanoparticles*

To evaluate the suitability of synthesized PEG-coated Fe_3O_4 nanoparticles for magnetic hyperthermia therapy of cancer, temperature (T) versus time (t) profiles of PEG-coated Fe_3O_4 nanoparticles are recorded as a function of applied AC magnetic field frequency (162–935.6 kHz), field strength (5 mT, 10 mT and 12 mT) and nanoparticle concentration (1–100 mg/mL). These temperature (T) versus time (t) plots are shown in Fig. 8. To study the effect of frequency on the heating profile of IONPs, the magnetic field, and concentration were kept constant at 10 mT and 100 mg/mL, respectively, while the frequency varied between 162–935.6 kHz. In this study, the highest temperature rise of 86.16°C was observed at a frequency of 935.6 kHz when nanoparticles were exposed to a magnetic field (10 mT) for 20 min. At 580.0 kHz, this temperature rise was 68.15°C. Since this temperature rise is adequate for hyperthermia applications, we choose a relatively lower frequency (580.0 kHz) of an applied magnetic field as the optimum field frequency instead of 935.6 kHz for biologically safer applications of these magnetic nanoparticles in magnetic hyperthermia.

To further investigate the effect of magnetic field strength on the heating capacity of PEG-coated Fe_3O_4 nanoparticles, the field frequency was kept constant at 580.8 kHz, and field strength was varied between 5–12 mT. In this study, the highest temperature rise of 85.06°C was attained at 12 mT field. However, at 10 mT field also, adequate temperature rise (68.15°C) was observed. Hence, for

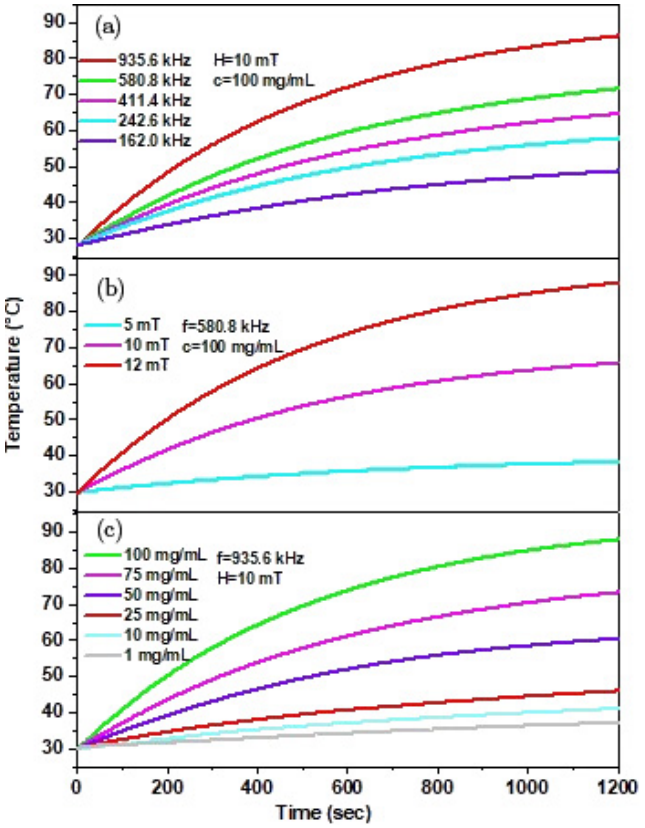

Fig. 8. Temperature–time profiles of as-synthesized PEG-coated Fe_3O_4 nanoparticles measured as a function of (a) Magnetic field frequency, (b) Magnetic field strength and (c) Nanoparticle concentration.

further studies, 10 mT field strength is considered the optimized field strength.

Subsequent to the optimization of magnetic field frequency and field strength, the role of nanoparticle concentration was evaluated by measuring temperature–time profiles of a series of PEG-coated Fe_3O_4 nanoparticles having concentration in the range of 1–100 mg/mL. In this study, magnetic field frequency and field strength were kept constant at 935.6 kHz and 10 mT, respectively. The maximum rise in temperature of PEG-coated Fe_3O_4 nanoparticles increases with increase in their concentration. The highest temperature rise (86.16°C)

was observed for a nanoparticle concentration of 100 mg/mL. However, an adequate (>45°C) temperature rise (59.05°C) was observed for a lower nanoparticle concentration of 50 mg/mL. Further, in the context of magnetic hyperthermia treatment, it has been observed that exceeding a temperature threshold of 42°C can trigger cell apoptosis in cancer cells.[6] To achieve this, a concentration of 25 mg/mL of magnetic nanoparticles has shown to produce an adequate temperature rise of 44.02°C. Furthermore, when comparing the specific loss power (SLP) values, both concentrations of 25 mg/mL and 50 mg/mL exhibit nearly similar SLP values of 4.43 W/g and 4.66 W/g, respectively. This similarity in SLP values contributes to the rationale for selecting 25 mg/mL as the optimal concentration for the treatment. Therefore, we consider 25 mg/mL as the optimized nanoparticle concentration of PEG-coated Fe_3O_4 nanoparticles for magnetic hyperthermia therapy under an applied magnetic field frequency of 935.6 kHz and 10 mT of field strength. When these experiments were performed with previously optimized lower frequency (580 kHz), adequate heating could not be achieved in Fe_3O_4 nanoparticles with lower concentration of 25 mg/mL. Therefore, we consider 965.6 kHz as the optimum frequency in place of 580 kHz.

To further understand the effect of magnetic field frequency, field strength and nanoparticle concentration on the heating efficiency of PEG-coated Fe_3O_4 nanoparticles, the temperature–time profiles of Fig. 8 are fitted with the empirical box-Lucas model.[25,26]

$$\Delta\theta(t) = \Delta\theta_s(1 - e^{-kt}). \tag{5}$$

Here, $\Delta\theta(t)$ denotes change in temperature [$= \theta(t) - \theta_0$], where θ_0 is initial temperature, $\theta(t)$ is the temperature at time t, and k represents a kinetic parameter. $\Delta\theta$ versus time plots fitted with Eq. (5) are shown in Fig. 9. From the best fits, kinetic parameter, k and initial slope of temperature–time curve, $\Delta\theta_s$, are determined, which are also reported in Table 3. As can be seen in Table 3, the kinetic parameter k is independent of applied field frequency, while it increases with field strength and nanoparticle concentration. Further, the initial slope ($\Delta\theta_s$) of the temperature–time profiles of PEG-coated Fe_3O_4 nanoparticles increases with increase in magnetic field frequency, field strength and nanoparticle concentration. These observed trends in $\Delta\theta_s$ and k are in good agreement with the previous studies.[23,25,26]

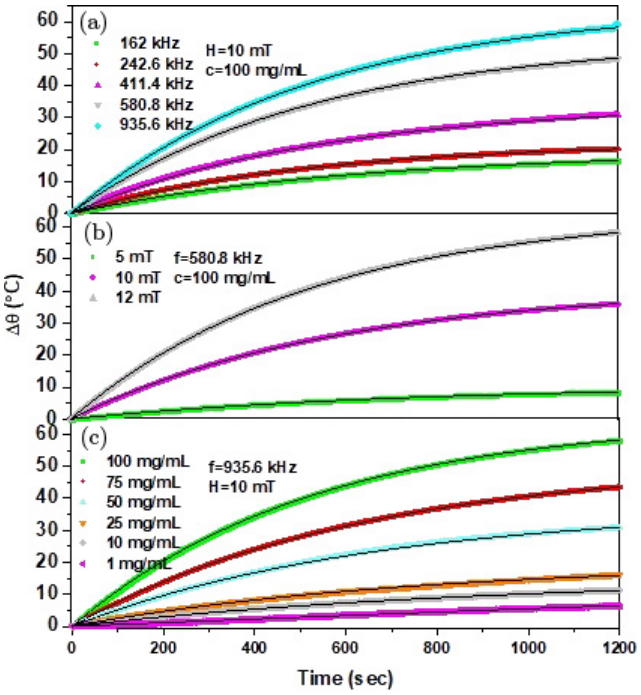

Fig. 9. $\Delta\theta$ versus time plots of PEG-coated Fe_3O_4 nanoparticles measured as a function of (a) Magnetic field frequency, (b) Magnetic field strength and (c) Nanoparticle concentration, which are fitted with box-Lucas model (Eq. (5)).

The heating efficiency of magnetic nanoparticles in hyperthermia applications is usually represented in the form of the SLP, which is described as the amount of heat generated by the unit mass of the magnetic nanoparticles in the material (W/g) at a given strength and frequency of the applied magnetic field.[27] SLP depends on the magnetic nanoparticle's properties, such as size, saturation magnetization (M_S), magnetic anisotropy and magnetic field parameters like strength and frequency.[28] SLP values are calculated by using the following equation[25]:

$$\text{SLP} = \frac{\rho}{x} c\Delta\theta_s k, \tag{6}$$

where ρ denotes the density of the medium (for water $\rho = 1.0$ g/mL), c is the specific heat of the medium (4.18 J/gK for water), $\Delta\theta_s$ denotes the initial slope of the temperature–time plot, k is kinetic parameter and x represents concentration of magnetic nanoparticles. SLP values of PEG-coated Fe_3O_4 nanoparticles measured as a function of magnetic field frequency, field strength and nanoparticle concentrations are also reported in Table 3. SLP value of PEG-coated Fe_3O_4 nanoparticles increases with frequency and field strength and

Table 3. Fitting parameters ($\Delta\theta_s$ and k) of empirical box-Lucas model obtained by fitting temperature ($\Delta\theta$) — Time profile of PEG-coated Fe_3O_4 nanoparticles with Eq. (5) and their magnetic hyperthermia efficiency determined in terms of SLP and intrinsic loss power (ILP) measured as a function of magnetic field frequency, field strength and nanoparticle concentration.

Frequency (kHz)	Magnetic field (mT)	Nanoparticle concentration (mg/mL)	$\Delta\theta_s$ (°C)	$k \times 10^{-5}$ (min^{-1})	SLP (W/g)	ILP ($Wg^{-1}/(fH^2)$)
162.0	10	100	19.4	160	1.04	0.10
242.6	10	100	22.2	195	1.99	0.13
411.4	10	100	34.5	181	2.30	0.08
580.8	10	100	54.1	179	2.87	0.07
935.6	10	100	65.0	187	4.54	0.07
580.8	5	100	10.5	136	0.60	0.06
580.8	10	100	54.1	179	2.87	0.07
580.8	12	100	65.0	189	5.13	0.09
935.6	10	1	6.1	91	24.13	0.04
935.6	10	10	15.5	107	6.92	0.12
935.6	10	25	20.0	133	4.43	0.07
935.6	10	50	37.0	151	4.66	0.07
935.6	10	75	51.3	158	4.51	0.07
935.6	10	100	65.0	187	4.54	0.07

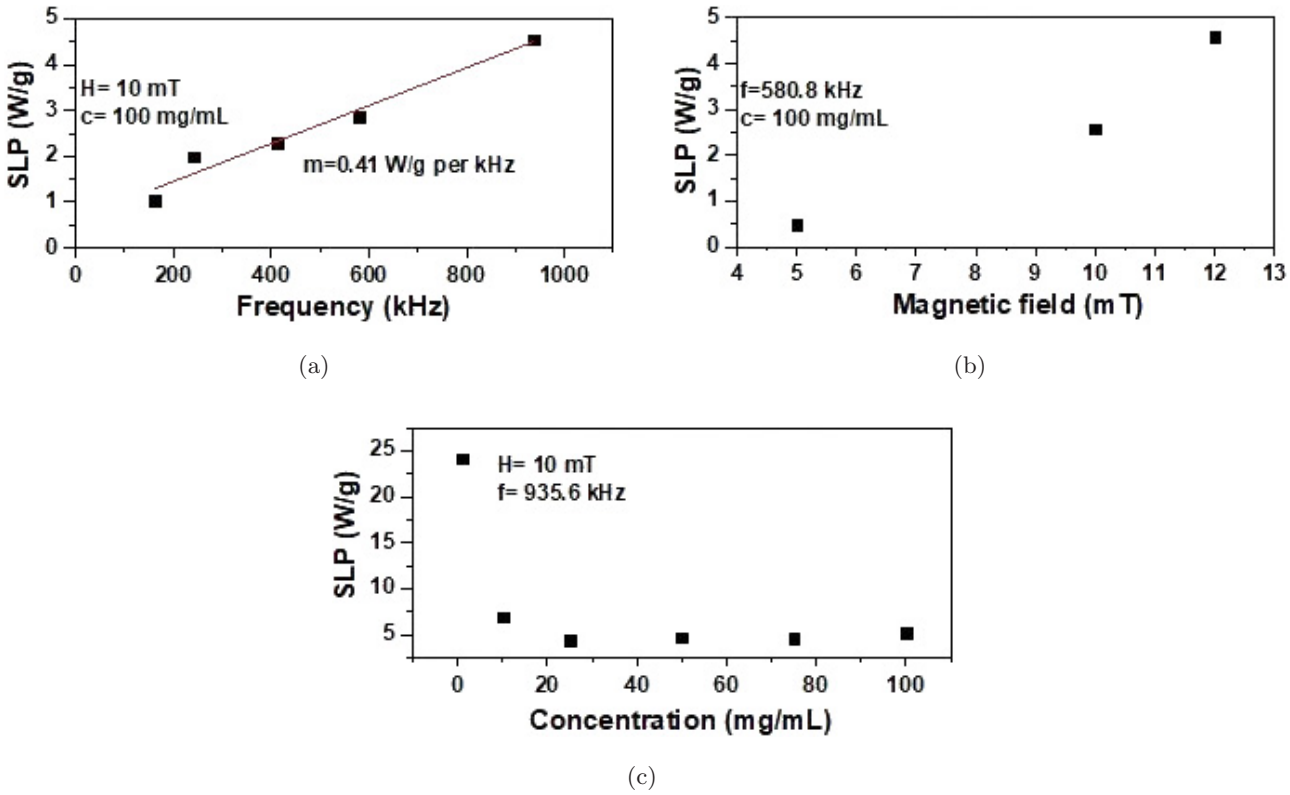

(a) (b) (c)

Fig. 10. Effect of magnetic field frequency field strength, and nanoparticle concentration on the SLP of PEG-coated Fe_3O_4.

decreases with nanoparticle concentration (Fig. 10). The slope is 0.41 W/g mL per 100 kHz when measured as a function of frequency. A similar trend was also reported previously by Kouzoudis *et al.*[25]

From the literature, it was found that interparticle interactions play a vital role and influence the SLP values of nanoparticle suspensions. With an increase in nanoparticle concentration, dipolar interactions between the nanoparticles increase, leading to the hindrance in Brownian motion. Hence, an increase in nanoparticle concentration resulted in lower SLP values.[25,28–31]

The heating capacity of the nanoparticles is also quantified by the intrinsic loss parameter (ILP)

$$\mathrm{ILP} = \frac{\mathrm{SLP}}{fH^2}. \tag{7}$$

Here, H is the applied external field, and f is the excitation frequency. In our study, the obtained ILP values are independent of frequency, magnetic field strength and concentration of nanoparticles, which is in line with past observations.[32,33] Thus, the ILP parameter can be used for a better comparison of the hyperthermia efficiency of magnetic nanoparticles.

4. Conclusions

PEG-coated Fe_3O_4 nanoparticles synthesized by the chemical coprecipitation method are superparamagnetic. The optimum conditions for magnetic hyperthermia of PEG-coated Fe_3O_4 nanoparticles are as follows: 965 kHz of field frequency, 10 mT field strength and 25 mg/mL of nanoparticle concentration. The heating efficiency of nanoparticles determined in terms of SLP increases with field strength and field frequency and decreases with nanoparticle concentration. This decrease in SLP of nanoparticles with their concentration can be ascribed to increased dipolar interactions between nanoparticles. PEG-coated Fe_3O_4 nanoparticles developed in this study produce the requisite temperature ($>42°C$) for the magnetic hyperthermia within the biologically safe limit of magnetic field frequency and field strength at a nanoparticle concentration of 25 mg/mL. Thus, PEG-coated Fe_3O_4 nanoparticles developed in this study are suitable for magnetic hyperthermia of cancer.

Acknowledgments

We would like to thank the Centre of Excellence in Emerging Materials (CEEMS) Thapar Institute of Engineering & Technology Patiala, Punjab and Department of Science and Technology (DST), India for financial support under DST-FIST Grant (No. SR/FST/PSII-53/2018).

ORCID

N. Srivastava https://orcid.org/0009-0003-8007-2724
M. Baranwal https://orcid.org/0000-0002-6581-9346
B. Chudasama https://orcid.org/0000-0002-4540-8785

References

1. Z. Behrouzkia, Z. Joveini, B. Keshavarzi, N. Eyvazzadeh and R. Z. Aghdam, *Oman Med. J.* **31**, 89 (2016), doi:10.5001/omj.2016.19.
2. G. Baronzio, G. Parmar, M. Ballerini and A. Szasz, *J. Integr. Oncol.* **3**, 1 (2014), doi:10.4172/2329-6771.1000115.
3. Y. Dou, K. Hynynen and C. Allen, *J Control Release* **249**, 63 (2017), doi:10.1016/j.jconrel.2017.01.025.
4. J. Jose *et al.*, *Environ. Sci. Pollut. Res.* **27**, 19214 (2020), doi:10.1007/s11356-019-07231-2.
5. I. M. Obaidat, V. Narayanaswamy, S. Alaabed, S. Sambasivam and C. V. V. Muralee Gopi, *Magnetochemistry* **5**, 67 (2019), doi:10.3390/magnetochemistry5040067.
6. H. Fatima, T. Charinpanitkul and K. S. Kim, *Nanomaterials* **11**, 1203 (2021), doi:10.3390/nano11051203.
7. P. Kaur, M. L. Aliru, A. S. Chadha, A. Asea and S. Krishnan, *Int. J. Hyperthermia* **32**, 76 (2016), doi:10.3109/02656736.2015.1120889.
8. P. Martinkova, M. Brtnicky, J. Kynicky and M. Pohanka, *Adv. Healthc. Mater* **7**, 1700932 (2018), doi:10.1002/adhm.201700932.
9. A. Rajan and N. K. Sahu, *J. Nanoparticle Res.* **22**, 1 (2020), doi:10.1007/s11051-020-05045-9.
10. J. Y. Park, P. Daksha, G. H. Lee, S. Woo and Y. Chang, *Nanotechnology* **19**, 1 (2008), doi:10.1088/0957-4484/19/36/365603.
11. N. Zhu, H. Ji, P. Yu, J. Niu, M. U. Farooq, M. W. Akram, I. O. Ugedo, H. Li and X. Niu, *Nanomaterials* **8**, 810 (2018), doi:10.3390/nano8100810.
12. C. Quinto, P. Mohindra, S. Tong and G. Bao, *Nanoscale* **7**, 12728 (2015), doi: 10.1039/c5nr02718g.
13. S. Prijic and G. Sersa, *Radiol. Oncol.* **45**, 1 (2011), doi:10.2478/v10019-011-0001-z.
14. I. Belyanina, O. Kolovskaya, S. Zamay, A. Gargaun, T. Zamay and A. Kichkailo, *Molecules* **22**, 975 (2017), doi:10.3390/molecules22060975.
15. A. Sudame, G. Kandasamy and D. Maity, *J. Nanosci. Nanotechnol.* **19**, 3991 (2019), doi:10.1166/jnn.2019.16326.
16. M. Vassallo, D. Martella, G. Barrera, F. Celegato, M. Coïsson, R. Ferrero and A. Manzin, *ACS Omega* **8**, 2143 (2023), doi:10.1021/acsomega.2c06244.
17. A. Rajan, M. Sharma and N. Sahu, *Sci. Rep.* **10**, 1 (2020), doi:10.1038/s41598-020-71703-6.
18. A. Tomitaka, T. Yamada and Y. Takemura, *J. Nanomater.* **2012**, 1 (2012), doi:10.1155/2012/480626.
19. R. V. Mehta, R. V. Upadhyay, S. W. Charles and C. N. Ramchand, *Biotechnol. Tech.* **11**, 493 (1997), doi:10.1023/A:1018457915380.
20. N. Andhariya, B. Chudasama, R. V. Mehta and R. V. Upadhyay, *J. Nanoparticle Res.* **13**, 1677 (2011), doi:10.1007/s11051-010-9921-6.

21. B. Chudasama, A. K. Vala, N. Andhariya, R. V. Upadhyay and R. V. Mehta, *Nano Res.* **2**, 955 (2009), doi:10.1007/s12274-009-9098-4.
22. C. Kurniawan *et al.*, *IOP Conf. Ser. Mater. Sci. Eng.* **202**, 012051 (2017), doi:10.1088/1757-899X/202/1/012051.
23. D. L. Zhao, P. Teng, Y. Xu, Q. S. Xia and J. T. Tang, *J. Alloys Compd.* **502**, 392 (2010), doi:10.1016/j.jallcom.2010.04.177.
24. N. Andhariya, R. Upadhyay, R. Mehta and B. Chudasama, *J. Nanoparticle Res.* **15**, 1 (2013), doi:10.1007/s11051-013-1416-9.
25. D. Kouzoudis, G. Samourgkanidis, A. Kolokithas-Ntoukas, G. Zoppellaro and K. Spiliotopoulos, *Front. Mater* **8**, 131 (2021), doi:10.3389/fmats.2021.638019.
26. R. Kumar, A. Chauhan, S. K. Jha and B. K. Kuanr, *J. Mater. Chem. B* **6**, 5385 (2018), doi:10.1039/C8TB01365A.
27. F. Soetaert, S. K. Kandala, A. Bakuzis and R. Ivkov, *Sci. Rep.* **7**, 6661 (2017), doi:10.1038/s41598-017-07088-w.
28. C. L. Dennis and R. Ivkov, *Int. J. Hyperth.* **29**, 715 (2013), doi:10.3109/02656736.2013.836758.
29. Y. Iqbal, H. Bae, I. Rhee and S. Hong, *J. Nanosci. Nanotechnol.* **16**, 11862 (2016), doi:10.1166/jnn.2016.13608.
30. V. Narayanaswamy *et al.*, *Molecules* **26**, 1 (2021), doi:10.3390/molecules26040796.
31. A. E. Deatsch and B. A. Evans, *Biophys. J.* **104**, 674a (2013), doi:10.1016/j.bpj.2012.11.3721.
32. G. R. Iglesias, Y. Jabalera, A. Peigneux, B. L. Checa Fernandez, A. V. Delgado and C. Jimenez-Lopez, *Pharmaceutics* **11**, 273 (2019), doi:10.3390/pharmaceutics11060273.
33. H. Xu and Y. Pan, *Nanomaterials* **9**, 1457 (2019), doi:10.3390/nano9101457.

Biointerphases

REVIEW ARTICLE | DECEMBER 11 2023

Advancement in magnetic hyperthermia-based targeted therapy for cancer treatment FREE

Neha Srivastava ; Bhupendra Chudasama; Manoj Baranwal

Biointerphases 18, 060801 (2022)
https://doi.org/10.1116/6.0003079

Biointerphases
A Journal of Biomaterials and Biological Interfaces

REVIEW

pubs.aip.org/avs/bip

Advancement in magnetic hyperthermia-based targeted therapy for cancer treatment

Cite as: Biointerphases 18, 060801 (2023); doi: 10.1116/6.0003079
Submitted: 20 August 2023 · Accepted: 14 November 2023 ·
Published Online: 11 December 2023

Neha Srivastava,[1] Bhupendra Chudasama,[2] and Manoj Baranwal[1,a)]

AFFILIATIONS

[1]Department of Biotechnology, Thapar Institute of Engineering and Technology, Patiala 147004, India
[2]School of Physics and Materials Science, Thapar Institute of Engineering and Technology, Patiala 147004, India

[a)]**Author to whom correspondence should be addressed:** manoj.baranwal@thapar.edu

ABSTRACT

Magnetic hyperthermia utilizing magnetic nanoparticles (MNPs) and an alternating magnetic field (AMF) represents a promising approach in the field of cancer treatment. Active targeting has emerged as a valuable strategy to enhance the effectiveness and specificity of drug delivery. Active targeting utilizes specific biomarkers that are predominantly found in abundance on cancer cells while being minimally expressed on healthy cells. Current comprehensive review provides an overview of several cancer-specific biomarkers, including human epidermal growth factor, transferrin, folate, luteinizing hormone-releasing hormone, integrin, cluster of differentiation (CD) receptors such as CD90, CD95, CD133, CD20, and CD44 also CXCR4 and vascular endothelial growth factor, these biomarkers bind to ligands present on the surface of MNPs, enabling precise targeting. Additionally, this review touches various combination therapies employed to combat cancer. Magnetic hyperthermia synergistically enhances the efficacy of conventional cancer treatments such as targeted chemotherapy, radiation therapy, gene therapy, and immunotherapy.

I. INTRODUCTION

Cancer is a global health issue characterized by uncontrolled cell growth and reduced apoptosis, leading to compromised immune function and mortality.[1,2] In 2020, GLOBOCAN reported 19.3 million new cases and 10 million deaths related to cancer.[3] Traditional cancer treatments, such as surgery, radiation therapy, chemotherapy, and hormone therapy, lack the ability to distinguish between cancerous and healthy cells.[4] Systemic chemotherapy may have limited effectiveness on tumor cells at the core due to inadequate drug exposure in that region.

In recent years, hyperthermia has emerged as a promising alternative therapy for cancer treatment. Hyperthermia involves localized or whole-body application of heat, typically raising the temperature to 40–45 °C specifically within cancerous cells, while minimizing damage to surrounding healthy tissue.[5,6] This selective effect is attributed to morphological and structural differences between tumor and healthy tissues. Tumors, with their leaky vasculature, exhibit limited heat dissipation and disrupted blood flow, whereas healthy tissues benefit from vasodilation, promoting better blood flow and heat conduction.

Hyperthermia has shown efficacy in killing cancer cells, particularly in the acidic and hypoxic environment of solid tumor cores. It also enhances blood flow within tumor regions. Different clinical methods are employed for hyperthermia, including local, regional, and whole-body approaches.[7,8] Local hyperthermia is suitable for solid tumors and utilizes external or intraluminal modalities to raise the temperature in superficial or deep-seated subcutaneous tumors, such as those in the rectum or esophagus. Thermal ablation, involving very high temperatures, leads to irreversible damage to cells. Various heat sources like radio waves, microwaves, ultrasound waves, and radiofrequency ablation are used in hyperthermia.[8,9] Regional hyperthermia involves applying low heat to large sections, such as organs, limbs, or hollow body spaces, often in conjunction with chemotherapy or radiation therapy. Techniques like regional perfusion, continuous hyperthermic peritoneal perfusion, or hyperthermic intraperitoneal chemotherapy (HIPEC), have been attempted. In perfusion techniques, blood is temporarily removed from the body, heated externally, and then reintroduced to raise internal temperatures. HIPEC, on the other hand, delivers heated chemotherapy drugs directly into the peritoneal cavity during surgery to treat peritoneum cancer.[9–11] Whole-body hyperthermia (WBH) involves raising the overall body temperature and can synergize with chemotherapy or radiation

therapy in the treatment of metastatic cancer. WBH is achieved using a hot water bath or radiant heat with ultraviolet radiation.

Traditional hyperthermia treatments using laser or microwave applicators can cause invasive damage to superficial tissues and result in discomfort during therapy. Additionally, their effectiveness in treating deep-seated tumors is limited. Magnetic nanoparticle-mediated hyperthermia has emerged as a promising approach to overcome these drawbacks.[12]

The field of nanotechnology has emerged as a promising platform for advancing cancer therapy.[13,14] Numerous studies have focused on the development of nanoparticles (NPs) with therapeutic capabilities, and magnetic nanoparticles (MNPs) have particularly garnered attention for their potential in cancer detection and treatment.[15] MNPs possess the ability to convert electromagnetic energy into heat, making them suitable for the applications of magnetic hyperthermia. Magnetic hyperthermia utilizes the heat generated by MNPs to target and destroy cancerous tissues. By exposing cancer cells to an elevated temperature achieved through magnetic energy losses, MNPs can induce apoptosis, leading to the elimination of tumor cells.[16,17] This innovative approach holds promise for the selective destruction of cancer cells through controlled heating using MNPs.

In addition to addressing the challenges of specificity in magnetic hyperthermia, there is a growing focus on targeted approaches to improve its effectiveness in cancer treatment. Active targeting strategies utilizing cancer specific ligands have emerged as a promising solution for the specific delivery of MNPs to tumor sites. These ligands facilitate the internalization of targeted MNPs through receptor-mediated endocytosis, enhancing their accumulation in cancer cells while minimizing uptake by healthy tissues.[18,19]

In recent years, targeted magnetic hyperthermia has gained attention as an adjuvant therapy to conventional cancer treatments.[6,20] Previous comprehensive reviews have provided valuable insights into magnetic nanoparticle hyperthermia and drug targeting methods.[21–23] This review aims to provide a summary of various cancer-specific biomarkers. Additionally, it highlights the current understanding of targeted magnetic hyperthermia and its role in the specific delivery of chemotherapeutic drugs to cancer sites. The review also summarizes the synergistic effects of magnetic hyperthermia when combined with other conventional cancer therapies such as radiation therapy, gene therapy, and immunotherapy in the treatment of cancer (Fig. 1).

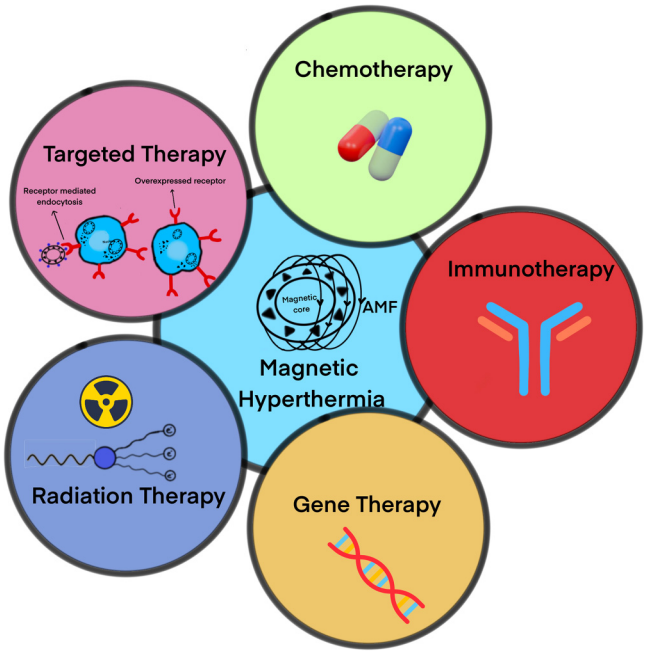

FIG. 1. Magnetic hyperthermia shows a synergistic effect while combining with various conventional cancer therapies such as targeted therapy, chemotherapy, radiation therapy, gene therapy, and immunotherapy.

II. MAGNETIC HYPERTHERMIA

Magnetic hyperthermia utilizes elevated temperatures produced by MNPs to eliminate cancerous tissues. MNPs can convert electromagnetic energy into heat, presenting the potential to eradicate tumor cells by heating them to their apoptosis threshold.[24] This technique relies on the application of an alternating magnetic field (AMF) to induce heat generation through the rotation of magnetic vectors or physical rotation of the NPs themselves.[25] The concept of magnetic hyperthermia was initially discovered by Gilchrist *et al.* in 1957,[26] who injected magnetic iron oxide nanoparticles (IONPs) (ranging from 20 to 100 nm in size) into lymphatic channels to heat cancer cells under an AMF.

By subjecting the NPs to a high-frequency magnetic field (typically 100–300 kHz), magnetic energy is dissipated as thermal energy through mechanisms such as hysteresis loss and relaxation processes. Hysteresis loss occurs mainly in multidomain NPs, where movement of domain walls under a magnetic field leads to heat loss. In single magnetic domain NPs (superparamagnetic nanoparticles), heat loss is predominantly caused by magnetic relaxation mechanisms, namely, neel and brownian relaxations.[27–29]

The heating potential of MNPs is commonly quantified in terms of watts per gram (W/g). The heat produced per unit volume depends on the specific absorption rate (SAR) product and the concentration of MNPs. SAR measures the hyperthermic response of the NPs, considering factors like the amplitude and frequency of the applied external field. The heat production is influenced by various characteristics of the NPs, including size, shape, composition, surface functionalization, saturation magnetization, magnetic susceptibility, and magnetic anisotropy. Size and shape particularly affect the magnetic anisotropy, which defines the maximum achievable SAR. Increasing magnetization/magnetic anisotropy and modifying the nanoparticle shape can enhance the relative heating efficiency.[30–33]

The desired temperature range for magnetic hyperthermia typically falls between 42 and 44 °C. Tumor cells, being hypoxic, are generally more sensitive to heat within this range compared to healthy cells. As the temperature of MNPs approaches the Curie temperature (T_c), they lose their magnetism and become nonmagnetic, resulting in a decrease in electromagnetic wave absorption and a subsequent decrease in temperature. Once the temperature

drops below T_c, the material regains its magnetism, causing the temperature to rise again until the Curie temperature is surpassed. This cyclic heating process occurs within the established Curie temperature range.[34]

Currently, IONPs are the most extensively studied MNPs for magnetic hyperthermia, primarily due to their low toxicity and well-known metabolic pathways.[35] IONPs demonstrate high biocompatibility, which can be attributed to their effective cellular uptake, excretion, and storage. Among the class of MNPs, IONPs are approved by the United States Food and Drug Administration for *in vivo* studies in humans. Surface functionalization of MNPs plays a crucial role in their biological applications. It ensures stability of their physicochemical properties in different mediums, accounting for factors such as *p*H changes, hydrophobicity/hydrophilicity, etc. Modifying the surface of MNPs is essential to prevent their engulfment by phagocytic immune cells like macrophages and neutrophils.[36]

According to Maity *et al.*,[37] the *in vitro* cell viability studies on human breast cancer cells (MCF-7) confirmed the cytocompatibility of triethylene glycol-coated magnetite NPs and demonstrated their efficient cellular uptake. Moreover, *in vitro* hyperthermia experiments revealed the potential of these for MNPs hyperthermia cancer treatment. Significantly, *in vivo* magnetic resonance imaging (MRI) studies displayed the promising potential of these NPs for clinical applications in MRI and thermotherapy.

In another study, the pluronic-coated NPs demonstrated biocompatibility with human cervical cancer cells (HeLa), showing no harmful effects. When exposed to a magnetic field strength of 16 kA/m (200 Oe) at a frequency of 210 kHz, these NPs exhibited optimal performance. Moreover, controlled heating effectively decreased the viability of HeLa cells and triggered apoptosis.[38] In a particular research investigation, the effects of manganese oxide perovskite NPs ($La_{0.56}(SrCa)_{0.22}MnO_3$) on HeLa cells were investigated. The study found that subjecting the cells to an AMF with a strength of 15 mT and a frequency of 100 kHz for 30 min led to cellular damage and subsequently triggered apoptotic cell death.[39] Therefore, surface reconstruction is necessary to minimize nanoparticle agglomeration in biological settings. Inorganic materials can be employed to achieve well-dispersed and uniformly coated nanostructures. Coating agents, such as surfactants, can alter the surface functionality, charge, reactivity, and dimensions of MNPs, enhancing their chemical stability and suitability for *in vivo* applications. Studies reported that retinoblastoma cells (Y79) display heightened susceptibility to thermal damage, consistent with the sensitivity observed in other cancer cells. The magnetic hyperthermia, utilizing dextran-coated iron NPs, selectively eradicates retinoblastoma cells in a manner contingent on dosage and duration *in vitro*, while preserving nontumor cells. This process induces apoptotic cell death in Y79 cells predominantly via the intrinsic pathway activated by TNF-α signaling. Given recent advancements in intravitreal chemotherapeutic injections for retinoblastoma management, magnetic hyperthermia employing dextran-coated iron NPs presents a promising therapeutic avenue.[40]

A. Magnetic hyperthermia combined with chemotherapy

Simultaneous application of magnetic hyperthermia and chemotherapy holds promising approach in anticancer therapy.[6] Various magnetic nanoparticle conjugates have been utilized in magnetic hyperthermia to effectively deliver chemotherapeutic drugs to the cancer site, as presented in Table I. In a study conducted by Christopher *et al.*,[41] they successfully designed phospholipid-polyethylene glycol-coated superparamagnetic IONPs to deliver doxorubicin (DOX), resulting in HeLa cancer cells apoptosis. Notably, these MNPs acted as dual-functionality platforms, serving as both drug carriers and heat generators when exposed to an AMF. Through *in vitro* analysis, it was found that the combined impact of DOX and superparamagnetic iron oxide nanoparticles (SPIONs) induced hyperthermia had a profound effect on inducing cell death in HeLa cells. Another innovative approach involved the development of multifunctional polymeric micelles that encapsulated SPIONs and the chemotherapeutic agent DOX, with drug release occurring through a pH-dependent mechanism.[50]

One advantage of multifunctional NPs is that the encapsulation of DOX and SPIONs within the hydrophobic micelle cores can prevent potential exposure of hydrophobic SPION surfaces

TABLE I. Magnetic nanoparticle conjugates exhibiting magnetic hyperthermia in different cancer cell lines.

Magnetic nanoparticle conjugates	Chemotherapeutic drug	Cancer cell lines	Reference
Phospholipid-polyethylene glycol-coated superparamagnetic iron oxide nanoparticles	Doxorubicin	Human cervical cancer cells	41
Polypyrrole-coated iron oxide nanoparticles	Doxorubicin	Human hepatocellular liver carcinoma cell	42
Superparamagnetic porous submicron vaterite particles	Doxorubicin	Murine colon carcinoma and Murine fibroblast	43
Cobalt- and manganese-doped iron oxide nanoparticles		Human ovarian carcinoma	44
Manganese-and zinc-doped ferrites	Doxorubicin	Human liver cancer cells	45
Pluronic-glycine-coated magnetic nanoparticles	Cinnamaldehyde	Human breast cancer cells	46
Polyamidoamine-based nanoparticles	Doxorubicin	Human cervical cancer cells	47
Ferucarbotran	Cisplastin	Human oral cancer cells	48
Mesosporous magnetic nanoassemblies	Doxorubicin	Mouse fibroblast & cervical cancer cells	49

and the adsorption of blood proteins, thus reducing nonspecific uptake by the reticuloendothelial system. In this context, polypyrrole-coated IONPs facilitated the delivery of DOX to tumor cells when an AMF was applied.[42] This magnetic core-shell nanocomposite served as a vehicle for magnetic hyperthermia-mediated chemotherapy. Biocompatible superparamagnetic porous submicron vaterite particles exhibited high drug loading capacity and demonstrated anticancer activities in murine colon carcinoma (CT26) and murine fibroblast (NIH3T3) cell lines upon exposure to an AMF.[43]

In another study, magnetic nanoconjugates, specifically PEG-PCL (poly (ethylene glycol)-b-poly(ε-caprolactone)) conjugated cobalt- and manganese-doped IONPs, were inhibit the growth of subcutaneous ovarian tumor in nude mice. This effect was observed after a single intravenous injection at a low dose (6 mg Fe/kg) in the presence of an AMF.[44] A magneto-thermally responsive nanocarrier/DOX called MTRN/DOX was used as a thermo-chemotherapeutic strategy for liver cancer (Huh-7). In this study, through magnetic targeting, MTRN/DOX can be effectively concentrated at the tumor site, resulting in enhanced uptake of DOX by Huh-7 cells and prolonged drug retention within the tumor. Furthermore, MTRN/DOX exhibited notable magnetothermal effects both *in vitro* and *in vivo*. Considering these findings, it is evident that MTRN/DOX possesses substantial anticancer properties. MTRN/DOX combined the magneto-thermal effect of Mn Zn ferrites MNPs with the temperature sensitivity of copolymer drug carriers.[45]

One of the studies highlights the effectiveness of magnetic targeting in concentrating nanocarriers precisely at the tumor site. This localization is facilitated by the utilization of an AMF, which not only heats the targeted area but also enables controlled release of the therapeutic drug. By employing this approach, they successfully achieved the spatial-temporal synchrony of thermo-chemotherapy.[51] Researchers also used external magnets near the target site for precise drug delivery with IONPs, ideal for small animal models like mice with skin tumors.[52] In another study, researchers utilized a dual targeting strategy, combining AMF with an external magnetic field, to efficiently transport MNPs across the blood-brain barrier for therapeutic delivery.[53] Pluronic-glycine-coated Fe_3O_4 MNPs conjugates exhibited targeted cytotoxicity and anti-cancer activity in breast cancer cells (MCF7 and MDAMB231) when tagged with cinnamaldehyde. The response to radiofrequency waves for magnetic hyperthermia therapy demonstrated dose-dependent cell killing.[46]

Coating MNPs with dendrimer macromolecules offers a promising alternative as it prevents aggregation and provides multiple surface functionalities. Studies have shown that polyamidoamine (PAMAM) dendrimers play various roles in biomedical applications, including drug delivery, biosensing, and magnetic resonance imaging. However, the degradation products of PAMAM exhibit significant toxicity, limiting their use in biological systems. To address this, peptide-coated dendrimer-based MNPs have been employed, displaying good potency for drug release on cancer cells. The effectiveness of the DOX-loaded PAMAM-based NPs was assessed using cancer cell lines such as HeLa cells. The synergistic effects of the DOX-loaded formulations in combination with alternating current magnetic field were also evaluated to assess their potential for combinatorial therapy against HeLa cells.[47]

Prior studies have shown that combining cisplatin with ferucarbotran (resovist)/AMF-induced hyperthermia boosts cisplatin's anticancer effects without changing the cell cycle, offering potential for oral cancer treatment (OSC-19 and HSC-3). This combination, already used clinically, has potential for early application, allowing reduced cisplatin dosage and minimizing side effects. Further research is needed for safety and efficacy in oral cancer patients.[48] The application of PEG modification on mesoporous $MgFe_2O_4$ magnetic nanoassemblies (MMNs) enhances their resistance to plasma protein adsorption, ensuring prolonged blood circulation. These MMNs exhibit exceptional colloidal stability in phosphate buffer saline and minimal cytotoxicity in mouse fibroblast (L929) and cervical cancer (HeLa) cells. Moreover, *in-vitro* studies confirm their potential as a versatile nanosystem for drug delivery and magnetic hyperthermia.[49]

B. Drug targeting methods

The successful application of MNPs conjugates as drug delivery systems relies on their targeted delivery to tumor sites.[54,55] The combination of magnetic hyperthermia and targeted chemotherapy exhibits a synergistic effect in cancer treatment. Two primary approaches, namely, passive and active targeting, are employed for effective MNP-based drug delivery. Both approaches aim to accumulate MNPs in metastatic and highly porous areas of the tumor, but they differ in the mechanisms of anchoring the MNPs at the tumor site.

Passive targeting, on the other hand, relies on the features of the nanoconjugates (e.g., size, circulation time) and the leaky vasculature of the tumor, which is a result of poor alignment of endothelial cells and defective lymphatic drainage in the hypoxic tumor environment. This phenomenon, known as the enhanced permeability and retention (EPR) effect, allows for easier retention of nanoparticle conjugates in tumor cells.[55] However, passive targeting is limited by the size constraints of tumor fenestrations, which can lead to unstable transport of NP conjugates in the bloodstream. Additionally, not all types of tumors exhibit the EPR effect. Active targeting serves as a supportive approach to passive targeting by enhancing the targeting capability of NPs and increasing their retention at the tumor site.[56] Hydrophilic groups on the surface of NPs enhance their circulation time and prevent uptake by the mononuclear phagocyte system.[5]

Active targeting of MNPs, in conjunction with hyperthermia under an AMF, offers a highly selective delivery of drugs to tumor sites through high-affinity binding between the nanoparticle surface and specific target structures in the tumor region. Active targeting takes advantage of the fact that tumor cells overexpress certain biological receptors on their surface compared to healthy cells. By conjugating MNPs with targeting ligands such as peptides, antibodies, or small organic molecules, active targeting facilitates the delivery of therapeutic agents.[5,54] These targeting ligands exhibit a higher affinity toward cell surface antigens (receptors) that are overexpressed on cancerous cells. The interaction between the targeting ligand and tumor biomarkers, either through ligandk-receptor or antigen-antibody interactions (Fig. 2), guides the NP

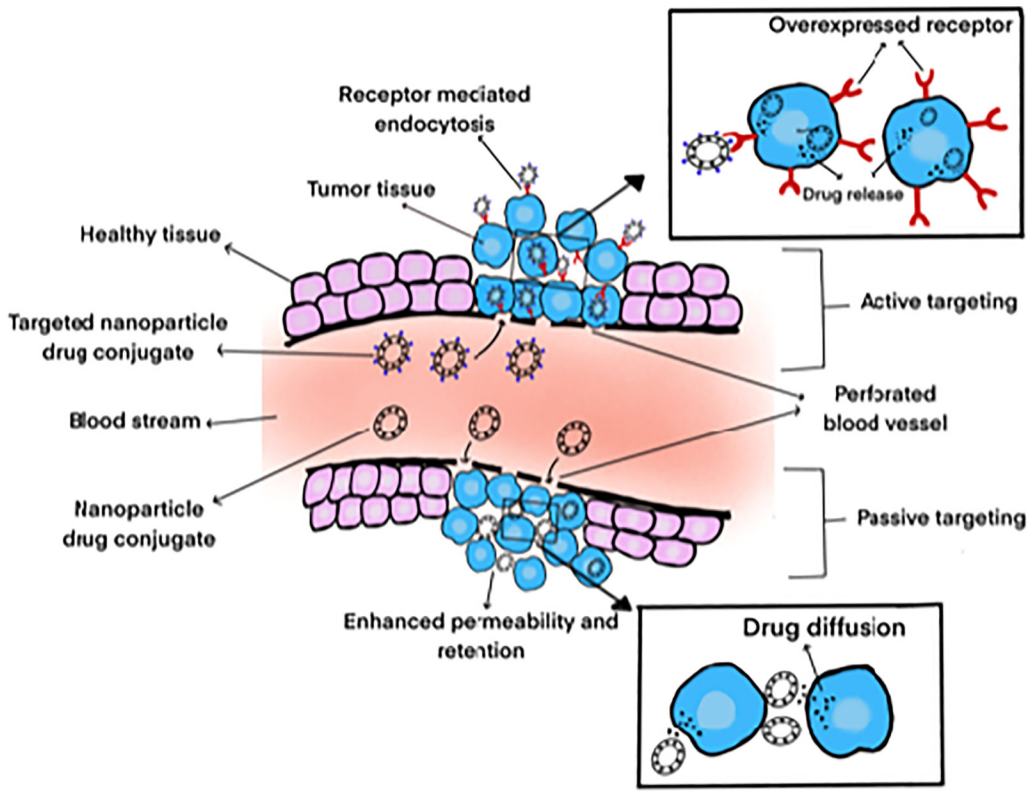

FIG. 2. Active and passive targeting approach.

conjugates to the tumor sites while avoiding nonspecific accumulation of the delivering agent.

These two targeting approaches differ in the mechanisms of NP retention at the tumor site. Compared to the passive approach, active targeting achieves a higher accumulation of NP-conjugated drugs at the tumor site through target-specific binding and internalization in specific cells. This reduces the undesired systemic exposure of cytotoxic drugs to healthy cells, thus improving the therapeutic outcome.

Active targeting operates through the process of receptor-mediated endocytosis,[4] enabling the binding between ligands on the surface of nanoparticle-drug conjugates and receptors that are overexpressed on tumor cells. This binding interaction facilitates the internalization of NPs toward the tumor site.[57] The binding of ligands to receptors triggers receptor activation and subsequent internalization of the ligand-receptor complex within a vesicle which is illustrated in Fig. 3. This vesicle then undergoes fusion with an endosome and subsequently with a lysosome. Within the lysosome, acidic enzymes with a *p*H range of 4.0–6.0 promote enzymatic degradation, leading to the release of the drug-conjugated nanoparticle at the tumor site.

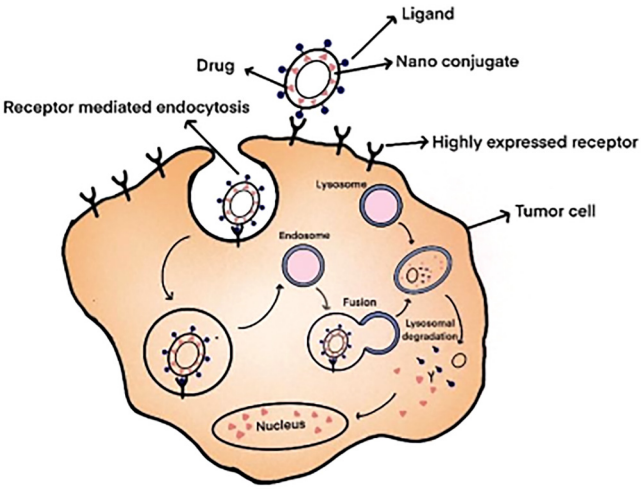

FIG. 3. Mechanism of receptor mediated endocytosis of nanoparticle-drug conjugate to the tumor site.

1. Targeted magnetic hyperthermia

Active targeting of nanoparticle drug conjugates utilizes various biological receptors, including human epidermal growth factor, transferrin, folate, luteinizing hormone-releasing hormone, integrin, CD20, CD44, CD95, VEGF, CXCR4, etc. to facilitate their delivery to the cancer site.[7–9] Table II presents the different biological receptors which were conjugated with MNPs to enhance the efficacy of cancer therapy in the presence of magnetic hyperthermia.

a. Integrin receptors. Integrins are a family of cell surface receptors involved in cell-to-extracellular matrix adhesion, and their interaction initiates signal transduction pathways related to cell growth, survival, division, and migration.[76] One notable example involves the use of arginine-glycine-aspartic acid (RGD) as a targeting ligand for integrin αvβ3, a marker of tumor angiogenesis. Recent studies have highlighted the enhanced efficacy of RGD targeted PEG-functionalized Mn-Zn ferrite NPs for active targeting in comparison to nontargeted magnetic nanocrystals. These targeted nanocrystals demonstrate improved retention at the tumor site and have been employed in MRI contrast imaging for diagnostic purposes. Additionally, they facilitate passive targeting through the enhanced permeability and retention (EPR) effect. Furthermore, these targeted nanocrystals exhibit a high heating potential, reaching 532 W/g, owing to the properties of Mn-Zn ferrite. In a mouse model of breast carcinoma (4T1), RAW264.7 macrophages, and HUVECs cell lines, the combination of targeted magnetic hyperthermia treatment and the application of an alternating current magnetic field at a strength of 2.58 kA/m and frequency of 390 kHz led to a significant elevation in temperature. This increase in temperature proved sufficient to induce apoptosis in tumor cells and hinder tumor angiogenesis. By administering repeated injections of magnetic nanoparticle complexes (MNCs), the tumor surface was consistently heated to approximately 43–44 °C.[58]

Upregulation of different types of integrins is observed in malignant cells, contributing to processes such as cell invasion, angiogenesis, and resistance to conventional cancer therapy.[77] Targeting integrins, therefore, represents a promising strategy for selectively killing cancer cells without harming healthy cells. The expression of αvβ3 integrin is particularly high in neoangiogenic blood vessels and glioblastoma (GBM) cells. By conjugating poly lactic-co-glycolic acid (PLGA)-coated SPIONs with the active moiety RGD and the drug paclitaxel (PTX), a potential targeting strategy for delivering PTX to the GBM site can be achieved in the presence of a magnetic field.[78]

TABLE II. Magnetic nanoparticles conjugated with different biological receptors used in magnetic hyperthermia against different cancer cell lines.

Magnetic nanoparticle conjugates	Receptor/antigen	Cancer cell lines	Reference
Mn-Zn ferrite nanoparticles	Integrin	RAW264.7 macrophage cells, Murine mammary carcinoma cells & Human umbilical vein endothelial cells	58
Superparamagnetic iron Oxide nanoparticles	CD44	Human and neck squamous cell carcinoma	59
Heat Shock Protein Inhibitor-loaded Silica-coated Fe_3O_4 nanoparticles	CD20	Lung cancer stem cells	60 and 61
Magnetite-based nanoparticles	CD133	Colorectal cancer cells	62
Magnetite nanoparticles	Folate receptor	Glioblastoma cells	63
Alginate-coated magnetite nanoparticles	Folate receptor	Lung cancer cells	64
Superparamagnetic Iron Oxide @poly (sodium styrene sulfonate)	Folate receptor	Pulmonary adenocarcinoma cells	65
(PLGA)-coated Superparamagnetic Iron Oxide Nanoparticles	Folate receptor, transferrin receptor	Breast and glial cancer cells	66
Holmium (III)doped Iron oxide nanoparticles	Human epithelial growth factor receptor 2	Breast cancer cells	67
Dextran spermine magnetic nanoparticles	Human epithelial growth factor receptor2	Breast cancer cells	68
Polyethylene glycol-coated magnetic nanoparticles	Luteinizing hormone-releasing hormone	Ovarian cancer cells	69
Chitosan-poly (methyl vinyl ether maleic acid) magnetic nanoparticles	Luteinizing hormone-releasing hormone	Breast cancer cells	70
Magnetite nanoparticles	CXCR4	Human acute T-cell leukemia	71
ZnCoFe nanocrystal	CXCR4	Glioblastoma cells	72
Zn^{+2} doped Superparamagnetic Iron Oxide Nanoparticles	Vascular endothelial growth factor	Liver cancer cells	73
Magnetic nanoparticles	CD95	Human cervical cancer cells	74
Magnetite iron oxide nanoparticles	L6 (antigen)	Breast cancer xenografts	75

b. Cluster of differentiation (CD) receptor. Targeted MNPs and magnetic hyperthermia have emerged as an important approach in the treatment of cancer stem cells (CSCs). CD44, a glycoprotein located on the cell surface and expressed in CSCs, is essential for various cellular processes including lymphocyte activation, hematopoiesis, and tumor metastasis. This transmembrane adhesion molecule is crucial for epithelial cell growth and the differentiation and activation of T and B lymphocytes during immune responses.[79]

CSCs are found in various tumor tissues, including head and neck squamous cell carcinoma (HNSCC). Hyaluronic acid (HA) is a known ligand for the CD44 receptor. Coating SPIONs with HA-PEG enhances biocompatibility and stability in biological applications. HA-PEG-coated SPIONs exhibit hyperthermia-mediated destruction of CSCs through active targeting in the presence of an AMF. These findings provide evidence for the treatment of CSCs through the utilization of targeted MNPs (CD44-targeted SPIONs) in combination with an AMF. The study demonstrates that this combined approach effectively triggers programmed cell death in CSCs, showcasing its potential as an effective therapeutic strategy for targeting and eliminating CSCs. Moreover, the application of magnetic hyperthermia demonstrated a significant inhibition of grafted human oral squamous cell carcinoma (Cal-27) tumor growth in mice. Together, these results highlight the potential of targeted magnetic nanoparticle therapy combined with AMF as a promising approach to combat CSCs and suppress tumor growth.[59]

Similarly, the CD20 targeted heat shock protein inhibitor-loaded silica-coated Fe_3O_4 NPs complex (CD20-HSPI&Fe_3O_4@SiNPs) demonstrates a heating potential of 69.7 W/g, enabling targeted drug delivery to tumor cells under an AMF.[60,61] They utilized the heat shock protein inhibitor (HSPI) as anticancer drug and tailored the silica shell with a CD20 antibody, specifically targeting human lung CSCs. This modification allowed receptor-mediated endocytosis, highlighting the effectiveness of CD20 receptor targeting in human lung CSCs. These findings highlight the potential of targeted MNPs and magnetic hyperthermia in enhancing the effectiveness of cancer treatments by specifically targeting CSCs and delivering therapeutic agents to tumor cells.

CD133, also known as prominin-1, is a prominent pentaspan membrane glycoprotein widely utilized as a biomarker for isolating CSCs. CSCs are a key factor contributing to tumor recurrence and resistance.[80] Extensive research suggests that CD133 may play a significant role in the tumorigenesis, metastasis, and chemoresistance of CSCs. The nanoparticle comprises a SPIONs-poly (sodium styrene sulfonate) core, encased in a layer-by-layer shell coated with irinotecan (CPT-11) and human serum albumin (HSA)/(CD133) monoclonal antibody conjugates. These NPs augment cellular uptake, enhancing the combined efficacy of hyperthermia and chemotherapy on CD133-expressing cancer cells. Additionally, they function as proficient T2-weighted MRI contrast agents for diagnosing colorectal cancer and CSCs. Notably, these NPs demonstrate superior synergistic anticancer effects compared to standalone chemotherapy or hyperthermia treatments, as evidenced in both *in vitro* and *in vivo* studies.[62]

c. Folate receptor (FR) and transferrin receptor (TFR). FR is involved in the intracellular transfer of tetrahydrofolate and has three functional isoforms in humans: hFR-α, hFR-β, and hFR-γ. Among these isoforms, hFR-α is commonly upregulated in various solid tumors, including those of the uterus, ovary, breast, cervix, kidney, and colon, making it an attractive target for immunotherapeutic approaches and cancer treatment. On the other hand, the hFR-β isoform is highly expressed on activated macrophages and serves as a biomarker for human inflammatory diseases.[81–83]

A synergistic approach combining active targeting and chemo-hyperthermia has been employed to deliver the drug temozolomide (TMZ) specifically to the site of GBM under the influence of an AMF. To achieve this, magnetite NPs conjugated with folic acid (FA) were utilized as the targeting moiety.[63] This complex exhibits a high SAR of 530 W/g, making it suitable for applications in magnetic hyperthermia. This innovative approach enables the precise delivery of TMZ to the GBM site, enhancing the effectiveness of treatment while minimizing potential side effects. In another study, scientists developed a multifunctional drug delivery system by incorporating the anticancer drug DOX and a targeting ligand, folate, onto alginate-coated Fe_3O_4 NPs. Folate was specifically attached to the NPs to enhance their tumor cell targeting and retention abilities. *In vivo* experiments demonstrated the significant efficacy of the combined treatment, particularly when the folate ligand was present, leading to improved survival outcomes in mice with lung cancer.[64]

The synergistic antitumor impact of combined chemotherapy and hyperthermia was markedly higher in pulmonary adenocarcinoma cells (A549 cells) than in human lung large cell carcinoma cells (NCI-H661 cells). This enhanced effect can be attributed to the core composition of SPIONs and poly (sodium styrene sulfonate) (PSS), augmented by a layer-by-layer coating of Cisplatin (cis-diamminedichloroplatinum (II) (CDDP), human serum albumin (HSA), or methotrexate (MTX) conjugate on the NPs (SPIO@PSS/CDDP/HSA−MTX). This design not only enhances nanoparticle uptake in folate receptor-expressing cells (A549 cells) but also intensifies the elimination of these cells following hyperthermia treatment.[65]

The transferrin receptor (TfR) is a glycoprotein involved in cellular iron distribution and exhibits a basal level of expression in healthy cells.[56] However, TfR, also known as CD71, is overexpressed in cancerous cells and plays a role in the signaling pathway of NF-κB, promoting cancer cell survival, mitochondrial respiration, and reactive oxygen species (ROS) generation, all of which contribute to tumor growth.[66] Due to their higher expression on cancerous cells, immature erythroid cells, and placenta compared to healthy cells, FR and TfR can be utilized for targeted drug delivery. Furthermore, the incorporation of poly (D,L-lactic-co-glycolic acid) (PLGA) NPs with dual-mode targeting and dual drug-loading holds great promise for cancer treatment.

Previous study specifically targeted the overexpressed folate receptor (FR) and transferrin receptor (TfR) in MCF-7 and glial cells (G1). The results of the research provide strong evidence that the combination of curcumin and 5-fluorouracil (5FU) within PLGA NPs leads to enhanced uptake, increased cellular accumulation, and improved cytotoxicity in cancer cells, including MCF-7 and G1 cells. Additionally, they explored the potential of magnetic hyperthermia therapy (MHT), which exhibited remarkable efficacy in the rapid destruction of cancer cells and the induction of

enhanced apoptosis. This synergistic effect was achieved through the combined treatment of MNPs and the dual-drug therapy of curcumin and 5FU.[66]

d. Human epithelial growth factor receptor 2 (HER2 receptor). The HER2 receptor is a transmembrane receptor with tyrosine kinase activity. It belongs to the epidermal growth factor receptor family and consists of 1255 amino acids, forming a 185 kD transmembrane glycoprotein.[84] In healthy cells, HER2 plays a crucial role in cell development. However, HER2 is overexpressed in various cancers, including breast, ovarian, and gastric cancers.[57] It can undergo homo or heterodimerization with other members of the epidermal growth factor receptor family, such as HER1 and HER3, leading to autophosphorylation of tyrosine residues. This, in turn, triggers downstream signaling pathways like MAPK, PI3K, and PKC, which promote cell proliferation, survival, differentiation, angiogenesis, and invasion in cancer cells.[85]

Targeting HER2 has been a focus of several chemotherapeutic approaches for the treatment of different types of cancer. Trastuzumab (herceptin), an FDA-approved monoclonal antibody, is a targeted anticancer drug that inhibits cancer cell proliferation by binding to HER2 receptors. By conjugating trastuzumab with Au-Fe_3O_4 nanoconjugates, it selectively targets HER2-positive gastric cancer cells, enabling effective delivery of oxaliplatin while minimizing chemotherapy side effects on healthy cells.[86] Similarly, trastuzumab-based targeted therapy allows for the delivery of holmium (III) doped IONP conjugates to HER2-positive breast cancer cells. These conjugates have high heating potential, making them suitable for magnetic hyperthermia applications under an AMF.[67] Studies have also demonstrated the use of the HER2 antibody as a targeting ligand in conjunction with dextranspermine MNPs. This approach induces magnetic hyperthermia-mediated cytotoxicity in breast cancer cells.[68]

In one of the studies, researchers successfully synthesized a novel therapeutic nanocarrier system by conjugating HER2 with PGFIO (fluorescent IONPs) and encapsulating gemcitabine within a poly(lactide-co-glycolide) matrix. This innovative approach combined targeted therapy with the use of magnetic hyperthermia for the treatment of pancreatic cancer. Furthermore, the study found that the HER-PGFIO nanocarrier system exhibited properties that regulated apoptosis and the cell cycle. The expression levels of Bcl-2 and cyclin D1 were notably reduced in both *in vitro* and *in vivo* analyses, further confirming the therapeutic efficacy of this nanocarrier system. Overall, the findings suggest that the HERPGFIO nanocarrier system, in conjunction with magnetic hyperthermia, holds great promise as a targeted and multifunctional therapeutic approach for pancreatic cancer treatment.[87]

e. Luteinizing hormone-releasing hormone (LHRH) receptor. LHRH, also referred to as gonadotropin-releasing hormone (GnRH), plays a crucial role in regulating reproductive functions. GnRH agonists, such as goserelin, triptorelin, buserelin, and leuprolide, are decapeptides (pGlu-His-Trp-Ser-Tyr-Gly-Leu-Arg-Pro-Gly-NH_2) that share a similar structure to native GnRH and exhibit high affinity for GnRH receptors. LHRH stimulates the release of luteinizing hormone and follicle-stimulating hormone from the pituitary gland.[88,89] These hormones, in turn, regulate the production of sex steroids in the gonads of both males and females. Overexpression of LHRH receptor has been observed in hormone-dependent cancers such as breast cancer endometrial cancer, ovarian cancer, and prostate cancer. Additionally, its overexpression has been detected in hormone-independent cancers such as pancreatic cancer, lung cancer, melanoma, and GBM.[90,91]

The studies have reported that drug-loaded LHRH-functionalized polyethylene glycol (PEG)-coated magnetic nano systems exhibit a high SAR value of 271 W/g, indicating their efficacy in magnetic hyperthermia treatment.[69] The utilization of synthesized nanocarrier based on IONPs proved to be a highly efficient vehicle for delivering DOX to A2780/AD multidrug resistant ovarian cancer cells. Furthermore, this nanocarrier demonstrated the remarkable capability to remotely induce mild hyperthermia (40 °C) in ovarian cancer cells when exposed to an AMF. This synergistic effect of mild hyperthermia, generated by IONPs in response to the AMF, significantly enhanced the cytotoxicity of DOX delivered by the nanocarrier to cancer cells. As a result, the developed IONP-based delivery system exhibits immense potential for effectively treating ovarian cancer through a combinatorial approach. Another study provides evidence supporting the potential application of LHRH-conjugated SPIONs as a remarkably sensitive MRI contrast agent in the detection of metastatic breast cancer cells. The targeted accumulation, improved delivery capabilities, and potential for precise drug delivery highlight the promising prospects of LHRH-conjugated magnetic IONPs in both the diagnosis and treatment of breast cancer metastases.[92] One of the studies demonstrated that the use of LHRH-targeted DOX-loaded NPs in combination with a magnetic field yielded the most significant inhibitory effect on cell growth, particularly in MCF-7 cells. These findings highlighted the promising potential of the layer-by-layer NPs [chitosan-poly (methyl vinyl ether maleic acid) (PMVMA)], which were designed to specifically target LHRH receptors. By utilizing a magnetic field to guide the NPs, they achieved dual tumor targeting in MCF-7 cells. This innovative approach has important implications as it could potentially lead to a reduction in the required dosage of DOX, thereby minimizing the adverse side effects associated with the drug.[70]

f. CXCR4 receptor. Another receptor such as CXCR4 is extensively used as a chemokine receptor and represents a crucial therapeutic target for most hematopoietic cell types including macrophages, monocytes, T and B lymphocytes, neutrophils, hematopoietic, endothelial progenitor, and stem cells in the blood or bone marrow, dendritic cells, Langerhans cells, vascular endothelial cells, neurons and neuronal stem cells, microglia and astrocytes, as well as embryonic stem cell. It serves as a coreceptor for several human diseases, including HIV-1 infection and different malignancies such as human acute T-cell leukemia. It is a member of the G-protein-coupled receptors superfamily, characterized by seven transmembrane domains.[93] One of the studies demonstrated an *in vitro* magnetic hyperthermia approach that completely eliminates the viability of human acute T-cell leukemia (Jurkat cells). This is accomplished by utilizing a combination of CXCR4-targeted and nontargeted MNPs.[71]

In other research studies, scientists have introduced a novel method for overcoming the blood-brain tumor barrier (BBTB) by modulating its permeability using redox-responsive nanocarriers

delivering fingolimod. Fingolimod regulates blood-brain barrier integrity and was encapsulated within polymeric nanocarriers. These carriers were surface-conjugated with Plerixafor (AMD3100) for recognizing CXCR4, a chemokine receptor highly expressed on tumor vessels and cells. The resulting nanocomplexes demonstrated efficient modulation of BBTB permeability. Additionally, codelivery of ZnCoFe nanocrystals and an HSP70 inhibitor, post-BBTB modulation, achieved synergistic treatment, utilizing magnetic hyperthermia effects in response to an alternating current magnetic field for the GBM site (GL261 and U87).[72]

g. Vascular endothelial growth factor (VEGF). VEGF, a homodimeric glycoprotein, plays a crucial role in angiogenesis, binding to VEGF receptor-1 and VEGF receptor-2 on vascular endothelial cells. In healthy individuals, it supports embryonic angiogenesis and adult wound healing. In cancer, VEGF is upregulated due to oncogene expression, various growth factors, and hypoxia, making it a central mediator of tumor-related angiogenesis.[94] Scientists have developed core-shell Zn^{2+} doped Zn-$CoFe_2O_4$@Zn-$MnFe_2O_4$ SPIONs (ZCMF) with precise magnetic hyperthermia properties. When modified with the VEGF antibody, these NPs (ZCMF-VEGF) exhibited enhanced uptake by liver cancer (HepG2) cells. Mild magnetic hyperthermia with ZCMF-VEGF effectively inhibited HepG2 cell growth by suppressing key proteins and activating innate immunity. In mouse models, targeted mild hyperthermia not only halted tumor growth but also prolonged survival, indicating its potential as a safe and promising treatment for liver cancer in the future.[73] Additionally, another study has shown that modifying NPs with a VEGFR-2-targeting peptide enhances their specificity for endometriosis. In mouse experiments, these targeted NPs efficiently accumulate in endometriotic lesions after a low-dose intravenous injection. When exposed to external AMF, they selectively elevate the temperature within lesions above 50 °C, completely eradicating them in a single treatment. Additionally, these NPs exhibit potential as MRI contrast agents for accurate detection of endometriotic tissue prior to AMF therapy.[95]

h. CD95. CD95(Fas/APO-1), a transmembrane receptor, plays a pivotal role in apoptosis induction within cancer cells. Upon activation by its ligand, CD95 recruits various proapoptotic factors, including caspase-8, to form the death-inducing signaling complex. This complex formation is vital for triggering the apoptotic cascade. Immune cells, particularly cytotoxic killer and natural killer cells, utilize CD95 ligand as one mechanism to eliminate cancer cells or virus-infected cells.[96] Additionally, Ch11 is monoclonal antibody developed to target Fas, a cell surface protein belonging to the tumor necrosis factor receptor family, which instigates cellular apoptosis, the programmed cell death process. In a research, scientists assessed the anticancer effects of magnetic hyperthermia in conjunction with the Ch11 antibody and cryptotanshinone, a blocker of antiapoptotic factors. The growth of HeLa cells was significantly reduced when treated with magnetic nanoparticle/antibody complexes in the presence of an AMF.[74]

i. L6, tumor-associated antigen. L6, a tumor-associated antigen belonging to the transmembrane-4 superfamily is highly expressed in multiple human cancers such as epithelial cell carcinomas but minimally in normal tissues. Its roles in cancer migration and angiogenesis are associated with poor prognosis, making it an attractive target for cancer therapies. It serves as a pivotal target for antibody-based therapies aimed at combating cancer.[97] In a particular study, magnetite IONPs combined with chimeric L6(ChL6), an antibody designed to target the tumor-associated antigen L6, displayed significant accumulation within tumors. Monoclonal antibody-guided IONPs, effectively targeted human breast cancer xenografts in mice. Additionally, *in vitro* analysis involving nanoparticle-induced heat through an AMF demonstrated a correlation with the delay in tumor growth.[75]

C. Magnetic hyperthermia combined with radiation therapy

It has been observed that radiation therapy and magnetic hyperthermia can potentiate each other's effects. The application of ionizing radiation in radiation therapy serves as a powerful tool to manage or eradicate tumor cells. By inflicting irreversible damage to the DNA of these cells, the therapy effectively disrupts the progression of the tumor, providing a crucial method in the treatment of cancer. Tumor cells generally exhibit higher metabolic activity compared to healthy cells. The translationally controlled tumor protein (TCTP) plays a crucial role in various cellular processes, including cell growth, apoptosis, DNA damage repair, and tumorigenesis. Targeting and suppressing TCTP can enhance the radiosensitivity of cancer cells, making it a potential therapeutic target for cancer treatment.[98]

In one of the studies, scientist has investigated the incorporation of actinium radio particles onto iron oxide nanoconjugates (225Ac@ Fe_3O_4), specifically targeting human epidermal growth factor receptor (HER)-2 positive ovarian cancer cells under an AMF.[99] The results demonstrated a more potent cytotoxic effect compared to using the magnetic field alone. The conjugates exhibited higher heating potential, indicated by a SAR value of 105 W/g, making them suitable for magnetic hyperthermia applications. Utilizing gadolinium-doped IONPs in magnetic field hyperthermia has been found to enhance the effectiveness of radiation therapy. This approach is capable of destroying oxygen-deprived cells that are resistant to radiation and inducing localized vascular necrosis specific to tumors.[100]

In another *in vivo* study, the combination therapy of magnetic hyperthermia and radiation showed improved control of lung metastasis and overall survival in mice. Magnetic hyperthermia facilitated tumor cell inhibition by utilizing the effects of radiation through the Bax protein, a crucial promoter of cell death. Additionally, it reduced the potential of radiotherapy to enhance the expression of matrix metalloproteinase-9, which is associated with breast cancer metastasis.[101]

IONPs have been found to induce the production of reactive oxygen species during radiation therapy. Radiation therapy itself increases the production of hydrogen peroxide, which is then followed by mitochondrial respiration. IONPs can act as catalysts, facilitating the conversion of hydrogen peroxide into highly reactive hydroxyl radicals. This synergistic effect enhances the cellular toxicity, leading to more effective treatment outcomes. Studies have shown that IONPs functionalized with cell penetrating peptides

(such as TAT) exhibit ROS-mediated cytotoxicity against A549 lung carcinoma cells when combined with radiation therapy.[102] In the metastatic triple negative murine mammary carcinoma model transfected with luciferin, 4T1-luc cells, combining magnetic iron oxide nanoparticle hyperthermia with radiotherapy and immune checkpoint inhibitors boosts local tumor control, eliminates cells, and attracts CD3+ T-lymphocytes, offering potential for reducing lung metastases. However, the addition of magnetic iron oxide nanoparticle hyperthermia has only a modest effect on lung metastases and no impact on overall survival, while combination therapy together could increase lung metastatic dissemination.[103]

In another study, researchers developed a nanoparticle-loaded micellar system for cancer treatment. By using hyaluronic acid-targeted Mn–Zn ferrite MNPs, they achieved specific targeting of tumor cells expressing CD44 such as A549 (a human lung adenocarcinoma cell line). These NPs, when exposed to an AMF, generated heat, enhancing the effects of radiation therapy. The experiments demonstrated successful targeting and enhanced therapeutic outcomes through apoptosis analysis.[104]

In recent research, core-shell NPs were engineered to provide targeted multimodal therapy for HER2-positive cancer, integrating radionuclide therapy and magnetic hyperthermia. The NPs, consisting of a magnetic core (Fe_3O_4) and a gold-198(radioactive) shell, were modified with a bifunctional PEG linker and trastuzumab monoclonal antibody. These functionalized NPs exhibited efficient heat conduction and specific binding to HER2-positive breast cancer cells (SKOV-3), suggesting promise for *in vivo* studies in combined therapy.[105]

While numerous preclinical studies have been conducted, only a limited number successfully progress to the pivotal third and final phase of clinical trials.[106] The world's first magnetic nanoparticle-based therapy, known as NanoTherm® therapy, has undergone extensive preclinical studies for the treatment of GBM and prostate cancer in Europe (MagForce Nanotechnologies AG, Berlin, Germany). Recently, clinical phase 2a has been completed to assess the efficacy of magnetic hyperthermia therapy alone or in combination with radiation therapy. This therapy utilizes a 15 nm wide iron oxide magnetic core under an AMF. Ongoing investigations aim to provide a comprehensive understanding of magnetic hyperthermia as a standalone treatment and as an adjuvant therapy for cancer treatment.[107–110] The NoCanTher project has reached an important milestone as it has commenced the final clinical trials for the treatment of advanced pancreatic ductal adenocarcinoma.[111] These trials signify a significant step forward in evaluating the effectiveness of the proposed treatment approach and bring hope for improved outcomes in patients with this challenging condition.

D. Magnetic hyperthermia combined with gene therapy

Gene therapy is an exciting new area that offers different ways to treat cancer. Gene therapy, a broad term covering various approaches, involves modifying cells using genetic material either in *in vitro* or *in vivo* to potentially achieve a cure. It is potentially better than chemotherapy, which lacks specificity and can cause unintended side effects.[112]

Gene therapy in combination with magnetic hyperthermia has emerged as a promising strategy for cancer treatment. The unique property of MNPs allows for the remote control of gene therapy through localized heating. Studies have indicated a correlation between heat-shock proteins (HSPs) and thermoresistance, as these proteins enable cells to withstand hyperthermia and other stress factors. HSPs function as chaperones and play a critical role in preventing the dissociation of denatured proteins after stress. They are also involved in ensuring the proper folding of newly synthesized proteins into their functional conformation. Heat-responsive genes, such as HSP40, HSP60, HSP70, and HSP90, are frequently utilized due to their ability to induce high levels of transgene expression both *in vitro* and *in vivo*.[113]

A novel system utilizing magnetic liposomes has been developed to deliver smart treatment to colorectal cancer cells, triggering the release of encapsulated chemotherapeutic drugs in response to a magnetic field.[114] liposomes, which consist of synthetic lipid bilayers, are highly biocompatible and biodegradable and serve as effective carriers for both hydrophilic and hydrophobic drugs. The use of CD90-targeted thermosensitive magnetoliposomes (TMs) encapsulating 17-AAG (CD90@17-AAG/TMs) has demonstrated efficient tumor cell eradication in the liver. Additionally, this approach enhances the sensitivity of magnetic hyperthermia. 17allylamino-1 demethoxgeldanamycin (17-AAG), an HSP90 inhibitor, is employed to overcome thermal resistance and promote apoptosis in cancer cells. Numerous publications have highlighted the potential of CD90, expressed by hepatic stem/progenitor cells during liver development, as a marker for human liver cancer stem-like cells and as a target for the diagnosis and therapy of hepatocellular carcinoma.[115]

Moreover, the silica-coated magnetic zinc-doped iron oxide (ZnFe2O4) nanoparticle has demonstrated efficient delivery and expression of a heat-inducible gene that encodes tumor necrosis factor (TNF)-related apoptosis inducing ligand (TRAIL) in adipose-derived mesenchymal stem cells (AD-MSCs) during magnetic hyperthermia treatment at a favorable temperature of 41 °C.[116] This study revealed that the AD-MSCs maintained their proliferation and differentiation capabilities while exhibiting specific expression of the ligand, resulting in significant apoptosis of ovarian cancer cells both *in vitro* and *in vivo*. Controlling therapeutic gene expression in tumors is crucial for effective gene therapy. Tumor-specific inducible promoters play a vital role in constructing viral and nonviral vectors to express therapeutic genes that repress cell proliferation and induce cell death. The αfetoprotein (AFP) promoter, widely used for suicide gene expression in hepatocellular carcinoma, has shown promising results in combination with magnetic nanoparticle carriers delivering the herpes simplex virus thymidine kinase/ganciclovir (HSV-TK/GCV) gene system, exhibiting high efficacy in hepatoma cell carcinoma. The AFP promoter and luciferase gene act as a tumor-specific promoter and reporter gene, respectively.[117]

In previous research, RNA interference (RNAi), a technique specifically reducing target gene expression, has found widespread applications in gene function studies and disease treatment. Small interfering RNA (siRNA) is a potent tool for this purpose, effectively reducing or silencing CXCR4 expression. Research focused on enhancing cellular uptake and reducing toxicity by refining fluorinated siRNA carriers on MNPs. Fluorination successfully

addressed the "PEG dilemma," overcoming challenges related to diminished cellular uptake and endosomal escape efficiency due to nanoparticle PEGylation. These carriers exhibited a transfection efficiency above 90%, further amplified in the presence of an external magnetic field.[118] Extensive investigation validated heightened CXCR4 expression in 4T1 breast cancer cells.[119] The use of fluorinated carriers significantly reduced CXCR4 expression on the cell membrane.

E. Magnetic hyperthermia combined with immunotherapy

Immunotherapy is becoming popular in cancer treatment because it is more precise and effective than traditional treatments. Modulating immune cells with drugs, proteins, or cells can enhance antitumoral responses, especially in immunosuppressive tumor environments. The main approaches to modulating tumor activity with immunotherapy involve boosting immune cell activation, as seen with cancer vaccines, or correcting dysfunctional immune pathways within the tumor microenvironment, achieved through checkpoint inhibition. Magnetic systems provide better control over drug transport, release, and dosing, minimizing side effects and boosting effectiveness in immunotherapies.[120]

Magnetic hyperthermia has a significant impact on the tumor immune microenvironment, which can be leveraged for immunotherapy. Immunotherapy reactivates the body's immune system to combat and eliminate tumor cells, offering promising results. Unlike conventional methods, immunotherapy uses cytokines, chemokines, and immune cells to reshape the tumor microenvironment, ensuring powerful effects and reducing the risk of recurrence.[121] Studies suggest that hyperthermia can activate specific immune cells and enhance the presence of apoptotic compounds in the bloodstream.[9–11] Macrophage colony-stimulating factor 1 (M-CSF1 or CSF1) is an immunosuppressor that is highly expressed in dendritic cells, neutrophils, and myeloid-derived suppressor cells, leading to tumor metastasis and the destruction of cytotoxic T lymphocytes, thereby reducing cancer patients' survival. To overcome this, scientists have proposed a synergistic approach combining an MCSF1 receptor inhibitor (BLZ945) with magnetic hyperthermia treatment. They have developed magnetic liposomes conjugated with cell-penetrating peptides to facilitate the targeted delivery of BLZ945 to the tumor site, generating immune responses under a low-power applied AMF.[122]

Researchers have also explored immunotherapy approaches to assess therapeutic effects in mouse models. Interleukin-2 (IL-2) stimulates the proliferation of T cells, induces the generation of natural killer (NK) cells and cytotoxic T lymphocytes (CTLs), and promotes the synthesis of immunoglobulin produced by B cells.[123,124] IL-2 has been used in antigen-presenting cell-based tumor vaccines, and its clinical use has been reported in patients with metastatic renal cell carcinoma and malignant melanoma.[125–127] However, a study revealed that IL-2 alone had a poor antitumor effect on lung cancer, as there was no substantial increase in the expression of CD4 or CD8 in tumors injected with IL-2, and tumor growth was not significantly suppressed. To overcome this limitation, IL-2 treatment combined with magnetic fluid hyperthermia (MFH) has been employed to improve the therapeutic effect on lung cancer.[128] In one of the studies conducted using magnetic hyperthermia combined with immunomodulatory agents to address B16-F10 melanoma in a mouse model. The application of magnetic hyperthermia induced tumor cell demise in the B16-F10 melanoma mouse model and escalated inflammatory responses. Administration of an anti-inflammatory inhibitor, glycyrrhizin, mitigated inflammation and decelerated tumor regrowth. The synergistic approach of employing magnetic hyperthermia alongside immunomodulators resulted in the comprehensive regression of tumors, particularly evident in 80% of actively growing 5-mm B16-F10 tumors.[129]

III. CONCLUSION

Current review presented a comprehensive overview of various biomarkers that can be utilized to enhance the efficacy of cancer treatments through targeted magnetic hyperthermia. By binding to ligands on the surface of magnetic nanoparticle conjugates, these biomarkers enable the NPs to specifically adhere to target sites when exposed to AMF. Currently, there is limited research on targeted magnetic hyperthermia for CSCs, which pose significant challenges to traditional cancer therapies due to their self-renewal capacity, tumor recurrence, and metastasis. Among the biomarkers discussed, CD44, CD90, and CD20 are found to be overexpressed on the surface of various CSCs. The binding of these biomarkers to their corresponding ligands on MNPs facilitates immune escape of cancer cells and subsequent destruction of these cells with minimal side effects. Future studies are focused on identifying additional biological markers that can further enhance the targeting capability of MNPs, improving their overall effectiveness and specificity while minimizing toxicity to healthy tissues. The review also highlights the advantages of dual-targeted and dual drug-loaded magnetic nanoparticle conjugates in combating cancer cells. Also, magnetic hyperthermia has the potential to elicit anticancer immunity by targeting immunosuppressor proteins, leading to tumor cell necrosis and apoptosis. This magnetic hyperthermia-mediated immunotherapy represents a promising approach to overcome tumor recurrence and metastasis. Therefore, future research efforts should focus on the development of multidisciplinary synergistic therapies in the field of cancer treatment.

ACKNOWLEDGMENTS

We would like to thank the scientific community and Centre of Excellence in Emerging Materials (CEEMS) Thapar Institute of Engineering & Technology Patiala, Punjab.

AUTHOR DECLARATIONS

Conflict of Interest

No author has a conflict of interest in this study.

Ethics Approval

Ethics approval is not required.

Author Contributions

Neha Srivastava: Conceptualization (equal); Investigation (equal); Supervision (equal); Writing – original draft (equal); Writing –

review & editing (equal). **Bhupendra Chudasama:** Conceptualization (equal); Supervision (lead); Writing – original draft (lead); Writing – review & editing (lead). **Manoj Baranwal:** Conceptualization (equal); Supervision (equal); Writing – original draft (equal); Writing – review & editing (equal).

DATA AVAILABILITY

Data sharing is not applicable to this article as no new data were created or analyzed in this study.

REFERENCES

[1]R. S. Wong, J. Exp. Clin. Cancer Res. **30**, 1 (2011).
[2]O. Warburg, J. Cancer Res. **9**, 148 (1925).
[3]H. Sung, J. Ferlay, R. L. Siegel, M. Laversanne, I. Soerjomataram, A. Jemal, and F. Bray, CA: Cancer J. Clin. **71**, 209 (2021).
[4]A. T. Malik, Tahir Butt, S. Zahid, F. Zahid, S. Waquar, M. Rasool, and A. M. Qazi, J. Nanotechnol. **2017**, 1.
[5]P. Ramalingam, D. S. Prabakaran, K. Sivalingam, V. Nallal, M. Razia, M. Patel, and D. Krishnamoorthy, Emerg. Nanomater. Adv. Technol. **10**, 83 (2022).
[6]D. Chang, M. Lim, J. A. Goos, R. Qiao, Y. Y. Ng, F. M. Mansfeld, and M. Kavallaris, Front. Pharmacol. **9**, 831 (2018).
[7]Z. Behrouzkia, Z. Joveini, B. Keshavarzi, N. Eyvazzadeh, and R. Z. Aghdam, Oman Med. J. **31**, 89 (2016).
[8]G. Baronzio, G. Parmar, M. Ballerini, A. Szasz, M. Baronzio, and V. Cassutti, J. Integr. Oncol. **03**, 2 (2014).
[9]S. Jha, P. K. Sharma, and R. Malviya, Achiev. Life Sci. **10**, 161 (2016).
[10]M. Sethi and S. K. Chakarvarti, Int. J. PharmTech Res. **8**, 292 (2015).
[11]M. H. Falk and R. D. Issels, Int. J. Hyperthermia **17**, 1 (2001).
[12]S. Dürr, C. Janko, S. Lyer, P. Tripal, M. Schwarz, J. Zaloga, and C. Alexiou, Nanotechnol. Rev. **2**, 395 (2013).
[13]D. Peer, J. M. Karp, S. Hong, O. C. Farokhzad, R. Margalit, and R. Langer, Nat. Nanotechnol. **2**, 751 (2007).
[14]Z. Li, E. Ye, R. Lakshminarayanan, and X. J. Loh, Small **12**, 4782 (2016).
[15]J. H. Lee, J. T. Jang, J. S. Choi, S. H. Moon, S. H. Noh, J. W. Kim, and J. Cheon, Nat. Nanotechnol. **6**, 418 (2011).
[16]C. Guibert, V. Dupuis, V. Peyre, and J. Fresnais, J. Phys. Chem. C **119**, 28148 (2015).
[17]D. Yoo, H. Jeong, S. H. Noh, J. H. Lee, and J. Cheon, Angew Chem. Int. Ed. **125**, 13285 (2013).
[18]A. G. Niculescu and A. M. Grumezescu, Int. J. Mol. Sci. **23**, 5253 (2022).
[19]S. Purushotham and R. V. Ramanujan, Acta Biomater. **6**, 502 (2010).
[20]X. Liu, Y. Zhang, Y. Wang, W. Zhu, G. Li, X. Ma, and X. J. Liang, Theranostics **10**, 3793 (2020).
[21]R. K. Jani and G. Krupa, J. Drug Deliv. Ther. **9**, 408 (2019).
[22]A. J. Giustini, A. A. Petryk, S. M. Cassim, J. A. Tate, I. Baker, and P. J. Hoopes, Nano Life **01**, 17 (2010).
[23]J. Yoo, C. Park, G. Yi, D. Lee, and H. Koo, Cancers **11**, 640 (2019).
[24]J. F. Liu, B. Jang, D. Issadore, and A. Tsourkas, Wiley Interdiscip. Rev. Nanomed. Nanobiotechnol. **11**, e1571 (2019).
[25]A. J. Cole, V. C. Yang, and A. E. David, Trends Biotechnol. **29**, 323 (2011).
[26]R. K. Gilchrist, R. Medal, W. D. Shorey, R. C. Hanselman, J. C. Parrott, and C. B. Taylor, Ann. Surg. **146**, 596 (1957).
[27]A. Yadollahpour, S. A. Hosseini, and A. Yadollahpour, Int. J. Pharm. Res. Allied Sci. **5**, 242 (2016).
[28]H. Gavilán, S. K. Avugadda, T. Fernández-Cabada, N. Soni, M. Cassani, B. T. Mai, and T. Pellegrino, Chem. Soc. Rev. **50**, 11614 (2021).
[29]A. Rajan and N. K. Sahu, J. Nanopart. Res. **22**, 1 (2020).
[30]I. M. Obaidat, V. Narayanaswamy, S. Alaabed, S. Sambasivam, and C. V. Muralee Gopi, Magnetochemistry **5**, 67 (2019).
[31]Z. Shaterabadi, G. Nabiyouni, and M. Soleymani, Prog. Biophys. Mol. Biol. **133**, 9 (2018).
[32]R. Gupta, T. Kaur, A. Chauhan, R. Kumar, B. K. Kuanr, and D. Sharma, Biomater. Adv. **139**, 213021 (2022).
[33]X. Yu, R. Yang, C. Wu, B. Liu, and W. Zhang, Sci. Rep. **12**, 16055 (2022).
[34]R. Sharma and C. J. Chen, J. Nanopart. Res. **11**, 671 (2009).
[35]P. H. L. Tran, T. T. D. Tran, T. V. Vo, and B. J. Lee, Arch. Pharm. Res. **35**, 2045 (2012).
[36]F. Y. Cheng, C. H. Su, Y. S. Yang, C. S. Yeh, C. Y. Tsai, C. L. Wu, and D. B. Shieh, Biomaterials **26**, 729 (2005).
[37]D. Maity, P. Chandrasekharan, C. T. Yang, K. H. Chuang, B. Shuter, J. M. Xue, and S. S. Feng, Nanomedicine **5**, 1571 (2010).
[38]A. Tomitaka, T. Yamada, and Y. Takemura, J. Nanomater. **2012**, 1.
[39]A. Villanueva, P. De La Presa, J. M. Alonso, T. Rueda, A. Martinez, P. Crespo, and G. Rivero, J. Phys. Chem. C **114**, 1976 (2010).
[40]H. Demirci, N. Slimani, M. Pawar, R. E. Kumon, P. Vaishnava, and C. G. Besirli, Transl. Vis. Sci. Technol. **8**, 18 (2019).
[41]C. A. Quinto, P. Mohindra, S. Tong, and G. Bao, Nanoscale **7**, 12728 (2015).
[42]J. Zhou, J. Li, X. Ding, J. Liu, Z. Luo, Y. Liu, and K. Cai, Nanotechnology **26**, 425101 (2015).
[43]G. Choukrani, B. Maharjan, C. H. Park, C. S. Kim, and A. R. K. Sasikala, Mater. Sci. Eng. C **106**, 110226 (2020).
[44]H. A. Albarqi, L. H. Wong, C. Schumann, F. Y. Sabei, T. Korzun, X. Li, and O. Taratula, ACS Nano **13**, 6383 (2019).
[45]M. Li, W. Bu, J. Ren, J. Li, L. Deng, M. Gao, and P. Wang, Theranostics **8**, 693 (2018).
[46]K. D. Wani, B. S. Kadu, P. Mansara, P. Gupta, A. V. Deore, R. C. Chikate, and R. Kaul-Ghanekar, PloS One **9**, e107315 (2014).
[47]S. Nigam and D. Bahadur, Colloids Surf. B **155**, 182 (2017).
[48]I. Sato, M. Umemura, K. Mitsudo, M. Kioi, H. Nakashima, T. Iwai, and Y. Ishikawa, J. Physiol. Sci. **64**, 177 (2014).
[49]S. Kumar, A. Daverey, N. K. Sahu, and D. Bahadur, J. Mater. Chem. B **1**, 3652 (2013).
[50]N. Nasongkla, E. Bey, J. Ren, H. Ai, C. Khemtong, J. S. Guthi, and J. Gao, Nano Lett. **6**, 2427 (2006).
[51]P. Wust, U. Gneveckow, P. Wust, U. Gneveckow, M. Johannsen, D. Böhmer, and A. Jordan, Int. J. Hyperthermia **22**, 673 (2006).
[52]Q. T. Shubhra, Med. Rev. **11** (2023).
[53]R. Gupta, A. Chauhan, T. Kaur, B. K. Kuanr, and D. Sharma, Nanoscale **14**, 17589 (2022).
[54]K. Loomis, K. McNeeley, and R. V. Bellamkonda, Soft Matter. **7**, 839 (2011).
[55]M. Wu and S. Huang, Mol. Clin. Oncol. **7**, 738 (2017).
[56]M. F. Attia, N. Anton, J. Wallyn, Z. Omran, and T. F. Vandamme, J. Pharm. Pharmacol. **71**, 1185 (2019).
[57]J. D. Byrne, T. Betancourt, and L. Brannon-Peppas, Adv. Drug Deliv. Rev. **60**, 1615 (2008).
[58]J. Xie, C. Yan, Y. Yan, L. Chen, L. Song, F. Zang, and Y. Zhang, Nanoscale **8**, 16902 (2016).
[59]Z. Su, D. Liu, L. Chen, J. Zhang, L. Ru, Z. Chen, and X. Wang, Int. J. Nanomed. **14**, 7549 (2019).
[60]D. Liu, Y. Hong, Y. Li, C. Hu, T. C. Yip, W. K. Yu, and M. Yang, Theranostics **10**, 1181 (2020).
[61]W. Zhao, Y. Li, and X. Zhang, Cancer Transl. Med. **3**, 87 (2017).
[62]S. J. Yang, S. Y. Tseng, C. H. Wang, T. H. Young, K. C. Chen, and M. J. Shieh, Nanomedicine **15**, 2543 (2020).
[63]S. E. Minaei, S. Khoei, S. Khoee, F. Vafashoar, and V. P. Mahabadi, Mater. Sci. Eng. C **101**, 575 (2019).
[64]P. T. Ha, T. T. H. Le, T. Q. Bui, H. N. Pham, A. S. Ho, and L. T. Nguyen, New J. Chem. **43**, 5404 (2019).
[65]S. J. Yang, C. H. Huang, C. H. Wang, M. J. Shieh, and K. C. Chen, Int. J. Nanomed. **15**, 10331 (2020).
[66]S. Balasubramanian, A. R. Girija, Y. Nagaoka, S. Iwai, M. Suzuki, V. Kizhikkilot, and S. D. Nair, Int. J. Nanomed. **9**, 437 (2014).

[67]W. Gawęda, M. Osial, M. Żuk, M. Pękała, A. Bilewicz, and P. Krysinski, Nanomaterials **10**, 288 (2020).
[68]R. Avazzadeh, E. Vasheghani-Farahani, M. Soleimani, S. Amanpour, and M. Sadegh, Prog. Biomater. **6**, 75 (2017).
[69]O. Taratula, R. K. Dani, C. Schumann, H. Xu, A. Wang, H. Song, and O. Taratula, Int. J. Pharm. **458**, 169 (2013).
[70]J. Varshosaz, F. Hassanzadeh, H. S. Aliabadi, F. R. Khoraskani, M. Mirian, and B. Behdadfar, Int. J. Biol. Macromol. **93**, 1192 (2016).
[71]V. Vilas-Boas, B. Espina, Y. V. Kolen'ko, M. Banobre-Lopez, J. A. Duarte, V. C. Martins, and F. D. Carvalho, Biointerphases **13**, 011005 (2018).
[72]H. Wu, L. Liu, M. Ma, and Y. Zhang, J. Control. Release **355**, 248 (2023).
[73]J. Pan, Y. Xu, Q. Wu, P. Hu, and J. Shi, J. Am. Chem. Soc. **143**, 8116 (2021).
[74]S. Ota, N. Yamazaki, A. Tomitaka, T. Yamada, and Y. Takemura, Nanomaterials **4**, 319 (2014).
[75]S. J. DeNardo, G. L. Denardo, A. Natarajan, L. A. Miers, A. R. Foreman, and C. Gruettner, J. Nucl. Med. **48**, 1338 (2007).
[76]R. Bazak, M. Houri, S. El Achy, S. Kamel, and T. Refaat, J. Cancer Res. Clin. Oncol. **141**, 769 (2015).
[77]P. H. Wu, A. E. Opadele, Y. Onodera, and J. M. Nam, Cancers **11**, 1783 (2019).
[78]L. P. Ganipineni, B. Ucakar, N. Joudiou, R. Riva, C. Jérôme, B. Gallez, and V. Préat, J. Drug Target. **27**, 614 (2019).
[79]J. A. P. Gomes, R. Amankwah, A. Powell-Richards, and H. S. Dua, Br. J. Ophthalmol. **88**, 821 (2004).
[80]Z. Li, Exp. Hematol. Oncol. **2**, 1 (2013).
[81]Y. S. Yi, Immune Netw. **16**, 337 (2016).
[82]M. D. A. Salazar and M. Ratnam, Cancer Metastasis Rev. **26**, 141 (2007).
[83]S. K. Kottarath, M. Bhat, C. Verma, S. Bhattacharya, A. Kaul, U. Kumar, and A. K. Dinda, J. Drug Deliv. Sci. Technol. **60**, 101946 (2020).
[84]W. Tai, R. Mahato, and K. Cheng, J. Control. Release **146**, 264 (2010).
[85]N. Iqbal and N. Iqbal, Mol. Biol. Int. **2014**, 1 (2014).
[86]D. Liu, X. Li, C. Chen, C. Li, C. Zhou, W. Zhang, and L. Chen, Oncol. Lett. **15**, 8079 (2018).
[87]L. R. Jaidev, D. R. Chellappan, D. V. Bhavsar, R. Ranganathan, B. Sivanantham, A. Subramanian, and S. Sethuraman, Acta Biomater. **49**, 422 (2017).
[88]A. V. Schally, A. Arimura, and A. J. Kastin, Science **179**, 341 (1973).
[89]M. Huerta-Reyes, G. Maya-Núñez, M. A. Pérez-Solis, E. López-Muñoz, N. Guillén, J. C. Olivo-Marin, and A. Aguilar-Rojas, Front. Oncol. **9**, 943 (2019).
[90]M. Venturelli, G. Guaitoli, C. Omarini, and L. Moscetti, Breast Cancer **10**, 39 (2018).
[91]X. Li, O. Taratula, O. Taratula, C. Schumann, and T. Minko, Mini. Rev. Med. Chem. **17**, 258 (2017).
[92]C. Leuschner, C. S. Kumar, W. Hansel, W. Soboyejo, J. Zhou, and J. Hormes, Breast. Cancer Res. Treat. **99**, 163 (2006).
[93]W. T. Choi, Y. Yang, Y. Xu, and J. An, Curr. Top. Med. Chem. **14**, 1574 (2014).
[94]P. Carmeliet, Oncology **69**, 4 (2005).
[95]Y. Park, A. A. Demessie, A. Luo, O. R. Taratula, A. S. Moses, P. Do, and O. Taratula, Small **18**, 2107808 (2022).
[96]M. E. Peter, A. Hadji, A. E. Murmann, S. Brockway, W. Putzbach, A. Pattanayak, and P. Ceppi, Cell Death Differ. **22**, 549 (2015).
[97]Y. P. Sher, K. M. Chai, W. C. Chen, K. Y. Shen, I. H. Chen, M. H. Lee, and S. J. Liu, Vaccines **8**, 620 (2020).
[98]J. Jung, J. S. Lee, Y. S. Lee, and K. Lee, Cancers **11**, 386 (2019).
[99]E. Cędrowska, M. Pruszyński, W. Gawęda, M. Żuk, P. Krysiński, F. Bruchertseifer, and A. Bilewicz, Molecules **25**, 1025 (2020).
[100]P. S. Jiang, H. Y. Tsai, P. Drake, F. N. Wang, and C. S. Chiang, Int. J. Hyperthermia **33**, 770 (2017).
[101]H. Wang, X. Li, X. Xi, B. Hu, L. Zhao, Y. Liao, and J. Tang, Int. J. Hyperthermia **27**, 563 (2011).
[102]A. K. Hauser, M. I. Mitov, E. F. Daley, R. C. McGarry, K. W. Anderson, and J. Z. Hilt, Biomaterials **105**, 127 (2016).
[103]A. L. Oei, P. Korangath, K. Mulka, M. Helenius, J. B. Coulter, J. Stewart, and R. Ivkov, Int. J. Hyperthermia **36**, 47 (2019).
[104]Y. Wang, L. Zou, Z. Qiang, J. Jiang, Z. Zhu, and J. Ren, ACS Biomater. Sci. Eng. **6**, 3550 (2020).
[105]M. Żuk, R. Podgórski, A. Ruszczyńska, T. Ciach, A. Majkowska-Pilip, A. Bilewicz, and P. Krysiński, Pharmaceutics **14**, 1680 (2022).
[106]J. V. Nuzhina, A. A. Shtil, A. Y. Prilepskii, and V. V. Vinogradov, J. Drug Deliv. Sci. Technol. **54**, 101282 (2019).
[107]D. Egea Benavente, J. G. Ovejero, M. D. P. Morales, and D. F. Barber, Cancers **13**, 4583 (2021).
[108]M. Johannsen, U. Gneveckow, B. Thiesen, K. Taymoorian, C. H. Cho, N. Waldöfner, and P. Wust, Eur. Urol. **52**, 1653 (2007).
[109]M. Johannsen, U. Gneveckow, K. Taymoorian, B. Thiesen, N. Waldöfner, R. Scholz, and S. A. Loening, Int. J. Hyperthermia **23**, 315 (2007).
[110]K. Maier-Hauff, F. Ulrich, D. Nestler, H. Niehoff, P. Wust, B. Thiesen, and A. Jordan, J. Neurooncol. **103**, 317 (2011).
[111]M. Johannsen, U. Gneveckow, L. Eckelt, A. Feussner, N. Waldöfner, R. Scholz, and A. Jordan, Int. J. Hyperthermia **21**, 637 (2005).
[112]S. K. Das, M. E. Menezes, S. Bhatia, X. Y. Wang, L. Emdad, D. Sarkar, and P. B. Fisher, J. Cell. Physiol. **230**, 259 (2015).
[113]I. Rubia-Rodríguez, A. Santana-Otero, S. Spassov, E. Tombácz, C. Johansson, P. De La Presa, and D. Ortega, Materials **14**, 706 (2021).
[114]S. Chatterjee and T. F. Burns, Int. J. Mol. Sci. **18**, 1978 (2017).
[115]A. Hardiansyah, L. Y. Huang, M. C. Yang, T. Y. Liu, S. C. Tsai, C. Y. Yang, and C. H. Lin, Nanoscale Res. Lett. **9**, 497 (2014).
[116]R. Yang, Q. Tang, F. Miao, Y. An, M. Li, Y. Han, and R. Chen, Int. J. Nanomed. **10**, 7345 (2015).
[117]P. T. Yin, S. Shah, N. J. Pasquale, O. B. Garbuzenko, T. Minko, and K. B. Lee, Biomaterials **81**, 46 (2016).
[118]Y. Cao, S. Zhang, M. Ma, and Y. Zhang, Nanomaterials **12**, 1692 (2022).
[119]Z. Wang, Z. Chang, M. Lu, D. Shao, J. Yue, D. Yang, and W. F. Dong, Biomaterials **154**, 147 (2018).
[120]C. Liu, M. Yang, D. Zhang, M. Chen, and D. Zhu, Front. Immunol. **13**, 961805 (2022).
[121]N. B. Day, W. C. Wixson, and C. W. Shields IV, Acta Pharm. Sin. B **11**, 2172 (2021).
[122]Y. Fang, Y. He, C. Wu, M. Zhang, Z. Gu, J. Zhang, and Y. Huang, Theranostics **11**, 6860 (2021).
[123]M. Beyer, Oncoimmunology **1**, 1181 (2012).
[124]C. Quintarelli, B. Savoldo, and G. Dotti, Immunother. Cancer **651**, 119 (2010).
[125]J. Y. Yang, X. Li, L. Gao, Z. H. Teng, and W. C. Liu, Exp. Ther. Med. **4**, 655 (2012).
[126]S. A. Rosenberg, Sci. Transl. Med. **4**, 127 (2012).
[127]E. Ellebaek, L. Engell-Noerregaard, T. Z. Iversen, T. M. Froesig, S. Munir, S. R. Hadrup, and I. M. Svane, Cancer Immunol. Immunother. **61**, 1791 (2012).
[128]R. Hu, S. Ma, X. Ke, H. Jiang, D. Wei, and W. Wang, Biomed. Rep. **4**, 59 (2016).
[129]A. Nishikawa, Y. Suzuki, M. Kaneko, and A. Ito, Cancer Immunol. Immunother. **72**, 1493 (2023).